Dioxygen Activation at Mononuclear Nonheme Iron Active Sites: Enzymes, Models, and Intermediates

Miquel Costas,[†] Mark P. Mehn,[‡] Michael P. Jensen,[‡] and Lawrence Que, Jr.*[,‡]

Departament de Quimica, Universitat de Girona, 17071, Girona, Spain, and Department of Chemistry and Center for Metals in Biocatalysis, University of Minnesota, Minneapolis, Minnesota 55455

Received August 15, 2003

Contents

1. Introduction

There have been significant advances in our understanding of mononuclear nonheme iron oxygenases since our 1996 *Chemical Reviews* article,[1] promoted in large part by the many crystal structures that have been solved for enzymes in this class, the development of sophisticated spectroscopic and computational approaches to probe these nonheme sites, and the discovery of a number of functional biomimetic systems that shed light on how iron centers in such active sites carry out the activation of dioxygen to effect a diverse range of oxidative transformations. Pertinent recent reviews on this topic include those by Nordlund focusing on the structures of nonheme iron enzymes with oxygen/nitrogen coordination[2] and by Solomon focusing on insights derived from spectroscopic and computational methods.[3,4] In this review, we compile and analyze the relevant information obtained mainly in the past 10 years from structural biology, mechanistic enzymology, physical methods, and synthetic chemistry to demonstrate the powerful synergy among these approaches in enhancing our comprehension of how the iron centers in these enzymes function in dioxygen activation.

* To whom correspondence should be addressed. Phone: (612) 625-0389. Fax: (612) 624-7029. E-mail: que@chem.umn.edu.
[†] Universitat de Girona.
[‡] University of Minnesota.

2. Iron(III) Dioxygenases: Enzymes That Function by Substrate Activation

2.1. Intradiol-Cleaving Catechol Dioxygenases

Bacterial catechol dioxygenases are enzymes found in a diverse range of soil bacteria and are responsible for the last step in the biodegradation of aromatic molecules in the environment. These enzymes convert dihydroxybenzenes into nonaromatic, acyclic compounds, which are then utilized as carbon sources for cell growth.[1,3,5−10] Catechol dioxygenases catalyze the oxidative cleavage of an aromatic double bond in a catechol molecule, inserting both oxygen atoms from an O_2 molecule into the product. Depending on the position of the cleaved double bond relative to the hydroxyl groups, catechol dioxygenases can be split into two families: the intradiol-cleaving catechol dioxygenases, which cleave the carbon−carbon bond of the enediol moiety, and the extradiol-cleaving catechol dioxygenases, which cleave adjacent to the enediol (Figure 1). Although these enzymes share similar substrates, the intradiol- and extradiol-cleaving enzymes exhibit near exclusivity in their oxidative cleavage products, suggesting that there are two different mechanisms for cleavage. Furthermore, intradiol-cleaving catechol dioxygenases use an $[Fe^{III}(His)_2(Tyr)_2]$ active site, while extradiol-cleaving catechol dioxygenases contain a $[M^{II}(His)_2(Asp/Glu)]$ active site,[1,6,7] typically iron(II) but manganese(II) in a few cases.[11−14]

Because of the rich spectroscopic properties of the iron(III) ion, intradiol-cleaving enzymes represent the first and most thoroughly studied subclass of nonheme iron oxygenases. Within this subclass, the most extensively investigated is protocatechuate (3,4-dihydroxybenzoate) 3,4-dioxygenase (3,4-PCD). Crystallographic information is available for a number of complexes of 3,4-PCD from *Pseudomonas putida*, including the as-isolated state,[15,16] several enzyme−

10.1021/cr020628n CCC: $48.50
Published on Web 01/28/2004

From left to right: Mark Mehn, Miquel Costas, Larry Que, and Mike Jensen in front of the Frank Gehry-designed Weisman Art Museum on the University of Minnesota Twin Cities campus.

Miquel Costas was born in Vigo, Spain, in 1971. He pursued graduate studies with Professor Antoni Llobet at the Universitat de Girona (Ph.D., 1999). Part of his Ph.D. work was performed at Texas A&M, under the supervision of the late Professor Sir Derek H. R. Barton, and at the University of Basel with Professor Andreas Zuberbühler. He then moved to the University of Minnesota to carry out postdoctoral work with Professor Que. He returned to the University of Girona in 2003, where he currently holds an appointment as an Associate Professor of Inorganic Chemistry. His research interests are in metal-catalyzed organic transformations with special interest in bio-inspired oxidation catalysis.

Mark P. Mehn was born in 1975 in Berlin, WI. He received a B.S. in chemistry and mathematics from the University of Wisconsin–Stevens Point in 1997, and completed his Ph.D. on models for nonheme iron oxygenases in 2003, under Professor Que at the University of Minnesota. He is currently a postdoctoral associate with Professor Jonas Peters at Caltech.

Michael P. Jensen was born in Missoula, MT, in 1965 and grew up in suburban Portland, OR. He attended Caltech (B.S., 1987) and then did graduate work at Northwestern University with Professor Duward F. Shriver (Ph.D., 1992). Following an NIH postdoctoral fellowship with Professor Jack Halpern at the University of Chicago, he joined Dennis Riley's group at Monsanto Corporate Research in 1995. He has since returned to academic work, presently holding a postdoctoral appointment with Professor Que at the University of Minnesota. His research interests lie in the general area of physical inorganic chemistry, with emphasis on mechanisms of bioorganometallic reactions.

Lawrence Que, Jr., was born in 1949 in Manila. He attended Ateneo de Manila University (B.S., 1969) and pursued graduate studies with Professor Louis H. Pignolet at the University of Minnesota (Ph.D., 1973). Following postdoctoral appointments with Professors Richard H. Holm at MIT, and Eckard Münck at the University of Minnesota, he joined the faculty of Cornell University. In 1983, he returned to the University of Minnesota, where he is presently the 3M/Alumni Distinguished Professor of Chemistry and serves as Co-Director of the Center for Metals in Biocatalysis as well as Chief Editor of the *Journal of Biological Inorganic Chemistry*. His research interests focus on the mechanisms of dioxygen activation by nonheme iron enzymes and on the design and synthesis of iron complexes that mimic enzyme function, stabilize key oxidizing intermediates, or serve as bio-inspired green oxidation catalysts.

substrate complexes,[17,18] and many complexes with inhibitors.[19] Crystal structures for the related catechol 1,2-dioxygenase from *Acinetobacter* sp. ADP1 in its as-isolated and substrate-bound forms have also been solved.[20] The crystal structure of as-isolated 3,4-PCD reveals a trigonal bipyramidal iron center[15,16] with four endogenous protein ligands, namely His460, His462, Tyr408, and Tyr447 (Figure 2A). The fifth coordination position, situated in the trigonal plane, is occupied by a solvent-derived ligand, identified to be hydroxide on the basis of EXAFS analysis and

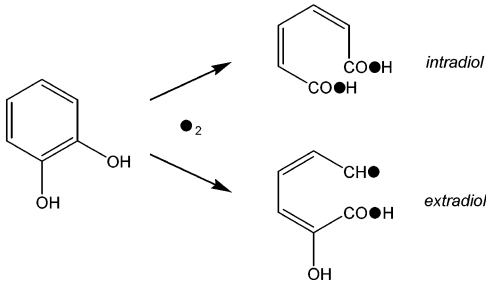

Figure 1. Intradiol versus extradiol cleavage reaction.

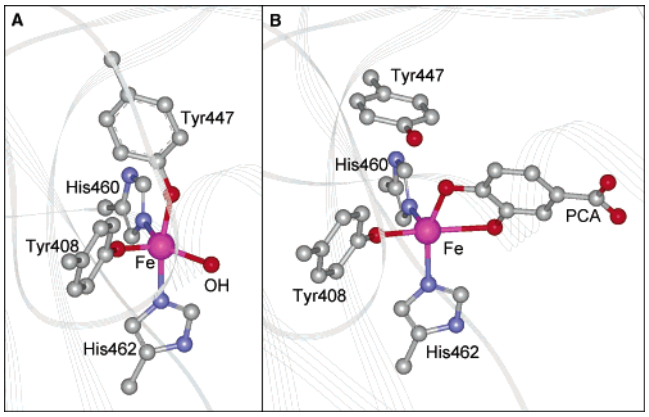

Figure 2. Active sites of (A) as-isolated 3,4-PCD (2PCD-.pdb) and (B) its enzyme substrate complex (3PCA.pdb).

thus giving rise to a charge-neutral iron(III) active site.[21]

The structure of the enzyme−substrate complex of 3,4-PCD reveals that substrate binding to the iron center results in the displacement of the hydroxide and the axial Tyr447 residue.[17,18] The catechol donates both its protons to the displaced ligands and chelates to the metal center as a dianionic ligand (Figure 2B). The two Fe−$O_{catecholate}$ bonds are trans to His460 and Tyr408, respectively, and differ by at least 0.2 Å in length, presumably due to the distinct trans effects exerted by the histidine and tyrosinate groups. This asymmetric chelation is proposed as a key feature of the catalytic mechanism.

When the crystallographic information is combined with the wealth of pre-existing spectroscopic data, a clear picture emerges of the enzyme active site during catalysis to validate the substrate activation mechanism proposed nearly 30 years ago (Figure 3).[22] This novel mechanism was postulated on the basis of spectroscopic data that showed the metal center retaining its iron(III) character throughout the catalytic cycle.[23−25] The lack of spectroscopic evidence for the participation of the iron(II) oxidation state strongly suggested that O_2 does not first bind to the metal center but instead must attack a different site. Support for this notion derived from the lack of reactivity of the enzyme−substrate complex with the O_2 surrogate NO, unless the metal center was first reduced by added reductant.[26,27] These observations led to the proposal that the role of the iron(III) center is the activation of the catechol substrate for direct interaction with O_2.[22,28,29] According to the proposed mechanism in Figure 3, the first step is the binding of the catecholate substrate to the iron(III) center, displacing the hydroxide and the axial Tyr447 resi-

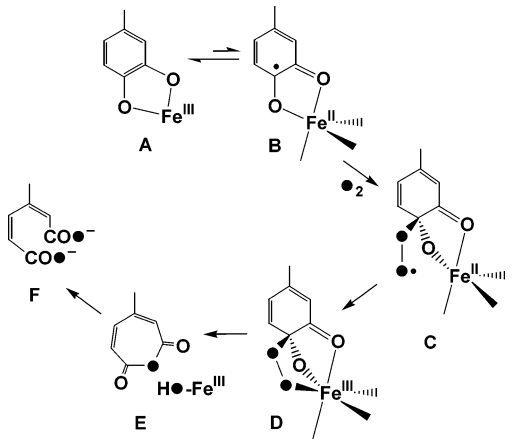

Figure 3. Proposed reaction mechanism for intradiol-cleaving catechol dioxygenases.

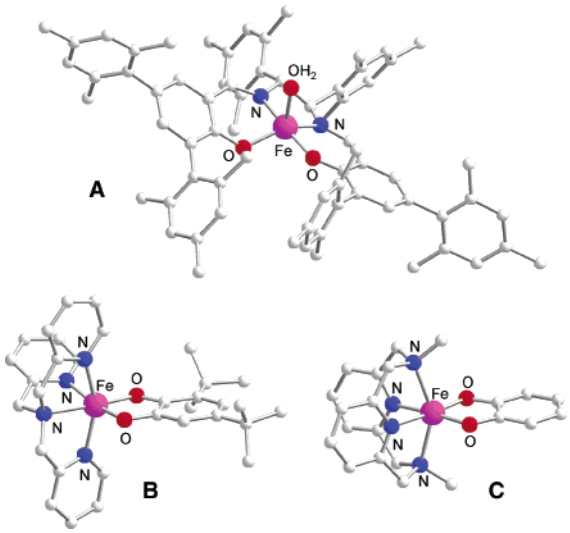

Figure 4. Key model complexes for intradiol-cleaving catechol dioxygenases: (A) $[Fe^{III}(Mes_6\text{-SALEN})(OH_2)]^+$, (B) $[Fe^{III}(TPA)(DBC)]^+$, and (C) $[Fe^{III}(L\text{-}N_4Me_2)(catecholate)]^+$.

due to generate a square pyramidal [Fe(His)$_2$(Tyr)-(κ^2-catecholate)] complex. The covalency of the iron-(III)−catecholate interaction introduces semiquinonate radical character to bound substrate and makes it susceptible to O_2 attack, generating a transient alkylperoxoiron(III) intermediate. Alkylperoxo intermediate D then undergoes a Criegee-type rearrangement to form muconic anhydride E, and the Fe^{III}−OH species thus formed acts as the nucleophile to convert the anhydride into the ring-opened product F.

Bioinorganic chemists have been quite successful in developing model complexes that mimic the structure, function, and spectroscopy of these enzymes.[30] Models for the as-isolated 3,4-PCD active site have relied on the use of tetradentate ligand structures corresponding to the endogenous His_2Tyr_2 donor set.[31−35] Particularly impressive is a recent effort by Fujii,[36] who has synthesized the complex [Fe(Mes_6-SALEN)(OH_2)](ClO_4), where Mes_6-SALEN is a sterically bulky version of the previously much used SALEN ligand, bis-(3,5-dimesitylsalicylidene)-1,2-dimesitylethylenediamine (Figure 4A). The steric interactions introduced by the bulky mesityl groups presumably destabilize the usually preferred planar topology of the salen ligand and allow the metal center to adopt a more trigonal bipyramidal geometry (τ = 0.48), like that found in the 3,4-PCD active site (τ = 0.44).[16] Thus, the axial Fe−$O_{phenolate}$ bond is longer than the equatorial Fe−$O_{phenolate}$ bond, giving rise to two distinct phenolate-to-iron(III) charge-transfer bands and two different ν_{C-O} features in its Raman spectrum, as observed for 3,4-PCD.[37] The aqua complex could be titrated with base to form the corresponding hydroxo complex, with an estimated pK_a of 7 in THF/H_2O. Interestingly, the hydroxo complex remains mononuclear, as the steric bulk of the mesityl substituents prevents formation of the (μ-oxo)diiron(III) complex that is the thermodynamic sink for many Fe(SALEN) derivatives. This complex thus serves as the best structural and spectroscopic model to date of the as-isolated 3,4-PCD active site.

Despite their structural correspondence to the active site of 3,4-PCD, catecholate complexes with phenolates in the ligand set display rather disappointing catecholate oxidation reactivity.[31−33,35,38] The rates of oxidation are low, and the main product obtained in the reaction is typically the two-electron oxidation product benzoquinone. This poor behavior may be ascribed to the low Lewis acidity of the metal ion in this ligand environment (vide infra).

The first functional models for catechol dioxygenases that yielded significant fractions of oxidative cleavage products were reported by Funabiki,[39,40] who employed a combination of $FeCl_2$, pyridine, and bipyridine to elicit the desired reactivity. Interestingly, both intradiol and extradiol cleavage products were produced. Unfortunately, due to the use of mono- and bidentate ligands, it has been difficult to establish the precise chemical composition of the cleavage catalyst. Subsequently, tetradentate ligands were used to synthesize discreet [Fe^{III}(L)(catecholate)] complexes (Figure 5, Table 1), and many of these have been structurally characterized (Figure 4). These complexes react with O_2 to afford intradiol cleavage products in high yield. It is clear that muconic anhydride E (Figure 3) must be the common intermediate that is formed, which is then easily ring-opened by available nucleophiles like hydroxide or amines in the reaction mixture to afford the products observed.

Following the initial observations of Weller and Weser,[41] Que and co-workers carried out the first systematic study of such functional models for intradiol-cleaving catechol dioxygenases (Table 1).[28,29,38,42,43] The functional groups on the tetradentate tripods were systematically varied from phenolate to carboxylate to pyridine to alter the electron-donating properties of the ligand, which in turn modulated the Lewis acidity of the iron(III) center. The changing Lewis acidity of the metal center could be conveniently followed by the positions of the two catecholate LMCT bands in the UV−vis−NIR spectra of the complexes.[44] Increasing the Lewis acidity of the iron center led to a red shift of these transition maxima, indicating that the metal acceptor (t_{2g}) orbitals decreased in energy to approach the ligand donor orbitals in energy. The more red-shifted the catecholate LMCT band, the faster the reaction of the

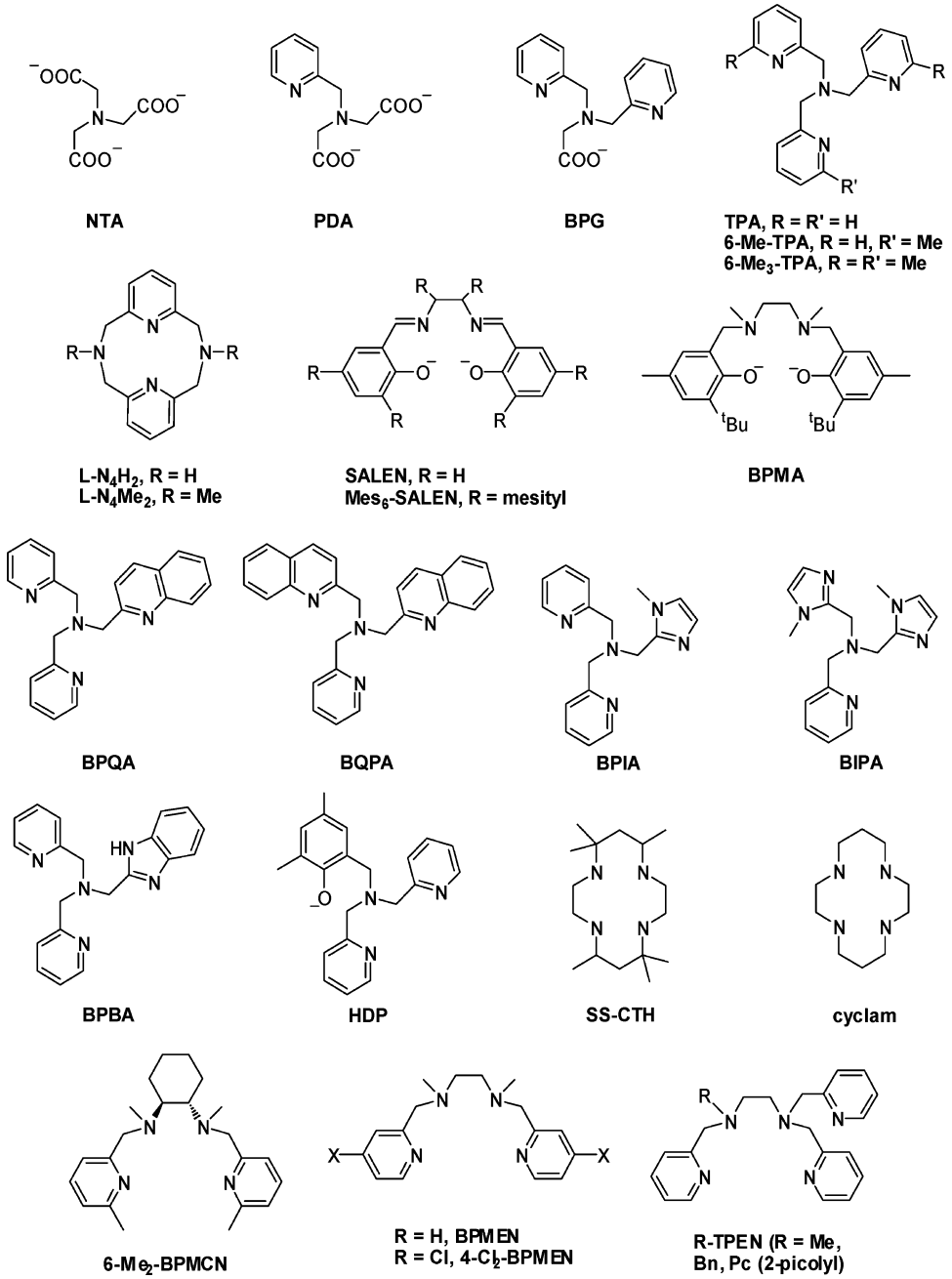

Figure 5. Ligands used for functional models for the intradiol-cleaving catechol dioxygenases.

complex with O_2 and the higher the yield of the intradiol cleavage product.

From this series of [Fe(L)(catecholate)] complexes was obtained the first insight into the substrate activation reaction mechanism for the intradiol-cleaving catechol dioxygenases. The red shifts of the LMCT bands in the more reactive complexes suggested that the Lewis acidity of the iron(III) center was a major factor in promoting reactivity. However, the Lewis acidity of the metal center by itself was not sufficient, since the Ga^{III} analogue of the most reactive Fe^{III}TPA complex showed no activity;[28] this observation suggested that the metal ion should be redox active as well. It has been proposed that a Lewis acidic and redox-active metal center can enhance the reactivity of the bound catecholate by increasing its radical character. The increased radical character can be demonstrated by NMR spectroscopy from the observation of upfield shifts of the catecholate protons in the more reactive complexes; these unusual, upfield shifts have been ascribed to the increasing semiquinonate character of the bound catecholate as a result of an increased covalency in the metal−catecholate interaction. This is not surprising since the triplet ground state of O_2 is kinetically inert toward substrates that contain a closed-shell electronic structure but is an excellent trap for species with radical character.[45] Since the semiquinonate state is responsible for the interaction with O_2, the lower the energy difference between the iron(III)−catecholate ground state and the iron(II)−semiquinonate excited state, the more they can mix, and consequently, the higher the reaction rate. The observed trend strongly suggests that more Lewis acidic centers have more (semiquinonato)iron(II) character.

Table 1. Biomimetic Iron(III) Complexes That Carry Out Intradiol Cleavage of 3,5-Di-*tert*-butylcatechol

complex	λ_{max}, nm (solvent)	k_{obs}, O_2 (M^{-1} s^{-1}), (solvent)	ref
$[Fe(BPMA)(DBC)]^-$		n.r.[a]	35
$[Fe(salen)(DBC)]^-$	637 (DMF)	(4−6 days)	38
[Fe(HDP)(DBC)]	476, 726 (DMF)	0.0033 (DMF)	28
$[Fe(NTA)(DBC)]^{2-}$	408, 622 (CH_3CN)	0.037 (DMF)	28
$[Fe(PDA)(DBC)]^-$	444, 688 (CH_3CN)	0.043 (DMF)	28
[Fe(BPG)(DBC)]	488, 764 (CH_3CN)	0.18 (DMF)	28
$[Fe(TPA)(DBC)]^+$	568, 883 (CH_3CN)	15 (DMF)	29
$[Fe(BPIA)(DBC)]^+$	558, 865 (CH_3OH)	4.3 (CH_3OH)	51
$[Fe(BQPA)(DBC)]^+$	582, 957 (DMF)	0.13 (DMF)	52
$[Fe(6\text{-}Me_2\text{-}BPMCN)(DBC)]^+$	598, 950 (MeCN)	$<10^{-6}$ (CH_3CN)	55
$[Fe(6\text{-}Me_3\text{-}TPA)(DBC)]^+$	600, 1020 (MeCN)	7.8×10^{-5} (CH_3CN)	55
$[Fe(6\text{-}Me_2\text{-}TPA)(DBC)]^+$	583, 962 (MeCN)	0.09 (DMF)	61
$[Fe(Me\text{-}TPEN)(DBC)]^+$	560, 935 (DMF)	0.28 (DMF)	52
$[Fe(BPMEN)(DBC)]^+$	550, 925 (DMF)	0.026 (DMF)	52
$[Fe(4\text{-}Cl_2\text{-}BPMEN)(DBC)]^+$	557, 941 (DMF)	0.16 (DMF)	52
$[Fe(L\text{-}N_4Me_2)(DBC)]^+$	553, 784 (CH_3CN)	0.38 (CH_3CN)	54
$[Fe(L\text{-}N_4H_2)(DBC)]^+$	553, 744 (MeOH), 546, 753 (MeCN)	8.6 (MeOH), 48 (MeCN)	56
$[Fe(cyclam)(DBC)]^+$	500, 769 (CH_3CN)	n.r.	62
$[Fe(SS\text{-}CTH)(DBC)]^+$	529, 833 (CH_3CN)	n.r.	62

[a] n.r. = no reaction.

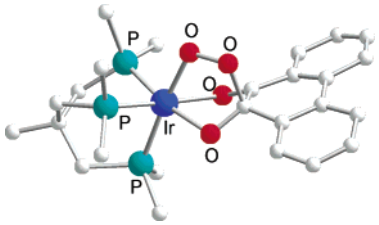

Figure 6. Crystal structure of the O_2 adduct of $[Ir(triphos)(phenanthrene\text{-}9,10\text{-}diolate)]^+$.

Studies of the O_2 reactivity of Rh^{III} and Ir^{III} catecholate complexes with phosphine ligands support the mechanistic notions discussed above, despite the non-biomimetic nature of the metal centers and ligands used.[46−49] Formation of O_2 adducts to these diamagnetic but coordinatively unsaturated d^6 complexes was observed, and crystal structures of key intermediates were obtained. The reaction of $[Rh^{III}(triphos)(DBC)]^+$ (triphos = $CH_3C(CH_2PPh_2)_3$; DBC = 3,5-di-*tert*-butylcatecholate dianion) with O_2 forms a reversible diamagnetic adduct formulated as $[Rh^{III}(triphos)(DBSQ)(O_2^-)]$ (DBSQ = 3,5-di-*tert*-butylcatecholate semiquinone anion); it is proposed that the dioxygen moiety is bound as a superoxide and the catechol has been oxidized to the semiquinone oxidation state, which corresponds to structure C in Figure 3.[46] However, crystal structures of the adducts to $[Ir^{III}(triphos)(catecholate)]^+$ (Figure 6) and $[Rh^{III}(PPh_3)_2(catecholate)(Cl)]$ complexes show the bound O_2 going one step further in the mechanism by attacking the bound catecholate to form a tridentate alkylperoxo species ligated to the metal center, analogous to D in Figure 3.[47,49]

A number of other complexes have been synthesized and investigated subsequent to the systematic study by Que and co-workers (Table 1).[33,35,50−55] In general, the results support the mechanistic hypothesis, although there is not necessarily a one-to-one correlation between the energy of the LMCT bands and reactivity due to differences in the nature of the pendant ligands and the topologies of tetradentate ligands employed. For example, steric shielding of the complex results in lower reaction rates; $[Fe^{III}(TPA)(DBC)]^+$ reacts with O_2 >10^5 times faster than the analogous 6-methyl-substituted complex $[Fe^{III}(6\text{-}Me_3\text{-}TPA)(DBC)]^+$. Considerations about the spin state of the iron center and the asymmetry between the Fe−O_{cat} bonds have also been recently raised.[52,56] Clarification of these reactivity factors requires further in-depth study. These studies have also shown that catecholates besides $DBCH_2$ ($DBCH_2$ = 3,5-di-*tert*-butylcatechol) can be oxidized, albeit at expectedly slower rates.[50,55,56]

While most of the model complexes prepared thus far have been investigated only under conditions of stoichiometric oxidation, the few complexes studied in the presence of excess substrate have been found to exhibit catalytic behavior. The first example, reported by Weller and Weser,[41] consisted of the Fe^{III}-(NTA) complex in a pH 9 borate buffer (to inhibit the $2e^-$ oxidation of DBC to its quinone form). Although the oxidative cleavage reaction required days, a good yield of the intradiol cleavage product was obtained. Faster-reacting systems, identified more recently, carry out the oxidative cleavage of $DBCH_2$ in the presence of 1% iron catalyst. Krüger and co-workers found that $[Fe(L\text{-}N_4Me_2)(CH_3CN)_2]^{3+}$ (Figure 4C) converted 54% of the $DBCH_2$ into muconic anhydride after 30 h,[54] while Krebs and co-workers reported that $[Fe(BPIA)(CH_3CN)_2]^{2+}$ afforded 80% yield of the intradiol-cleaved anhydride in 12 h.[51] Girerd and co-workers removed the *N*-methyl groups of Kruger's $L\text{-}N_4Me_2$ ligand and elicited catalytic rates 2 orders of magnitude faster but obtained a 1:1 mixture of intradiol and extradiol cleavage products.[56] The relationship between intradiol and extradiol cleavage mechanisms will be addressed in section 3.1.

Funabiki and co-workers recently recognized potential environmental applications for these model reactions. Using the fast-reacting Fe(TPA) complex),[29] they demonstrated that the catalyst was even capable of cleaving otherwise inert chorocatechol substrates (Figure 7).[57] This reaction in fact models

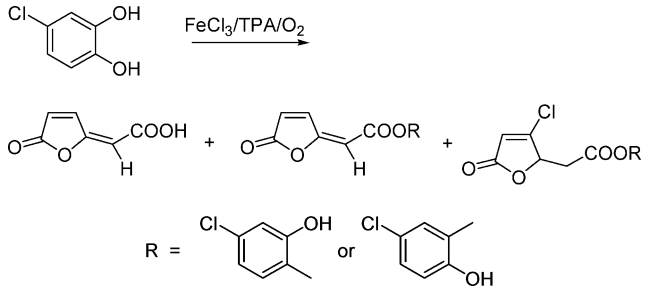

Figure 7. Biomimetic cleavage of chlorocatechols.

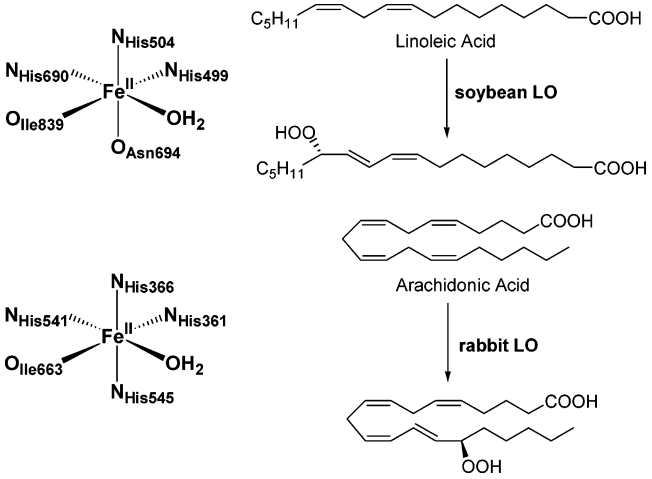

Figure 8. Active sites of soybean and rabbit lipoxygenases and the respective reactions they catalyze.

the chemistry of chlorocatechol dioxygenases, intradiol-cleaving enzymes closely related to 3,4-PCD but less well characterized.[58,59] Funabiki also introduced sulfonate groups into the TPA ligand to afford water-soluble iron catalysts that oxidatively cleave a range of water-soluble catechol substrates such as chlorocatechols and protocatechuic acid.[57,60] However, addition of excess TPA ligand is required for these reactions, and detailed structural characterization of these metal complexes is lacking. Further studies would be required in order to have a full understanding of this highly active system.

2.2. Lipoxygenases

Lipoxygenases (LOs) are mononuclear nonheme iron-containing enzymes, found in animals and plants, which catalyze the regiospecific and stereospecific dioxygenation of 1,4-diene units in fatty acids to the corresponding hydroperoxides (Figure 8).[3,63−65] Plant LOs generally act on linoleic acids, which are involved in growth regulation and wound repair. Human LOs, on the other hand, catalyze the peroxidation of arachidonic acid in the biosynthesis of leukotrienes and lipoxins, compounds that have implications in a number of inflammatory diseases as well as cancer growth regulation.[66−68]

X-ray structures of several soybean lipoxygenases in the as-isolated iron(II) state reveal a high-spin metal(II) center with a distorted octahedral geometry.[69−73] There are five amino acid ligands, the imidazole N atoms of three histidine residues, a carboxylate oxygen of the C-terminal isoleucine, and the carbonyl oxygen of the amide of a weakly bound

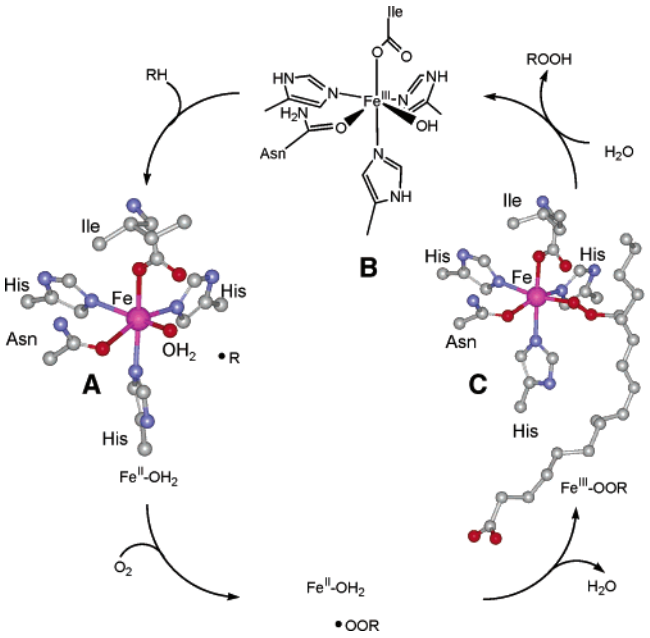

Figure 9. Proposed lipoxygenase reaction cycle (as-isolated soybean LO (1F8N.pdb) and Fe(III)-OOR intermediate (1IK3.pdb)).

(3 Å) aspargine, and the sixth site is occupied by a solvent molecule (Figure 9A). Rabbit LO differs from the soybean enzymes in that the aspargine residue is replaced by a fourth, more strongly bound histidine (Figure 8).[74] Sequence homology suggests that other mammalian enzymes have similar active sites. The imidazole-rich active sites found in LOs give rise to a high $Fe^{III/II}$ redox potential, estimated to be ~0.6 V vs NHE in soybean lipoxygenase,[75] which is proposed to be crucial for the catalytic role of the iron center in this enzyme.

As for the intradiol-cleaving catechol dioxygenases, it is the iron(III) form of LOs that is catalytically active.[76,77] The as-isolated iron(II) form is activated solely by oxidation with the fatty acid hydroperoxide product.[78] A typical reaction profile of the as-isolated enzyme and substrate in the presence of air shows an initial lag phase with no activity. This phase is then followed by an increase in enzyme activity as the fatty acid hydroperoxide, formed by nonenzymatic autoxidation of the substrate, oxidizes the iron(II) enzyme to its active iron(III) form.[79] Active LO has a high-spin six-coordinate iron(III) metal center that is characterized by an $S = {}^5/_2$ EPR signal, which is axial in the soybean enzyme ($g \approx 6$) but rhombic ($g = 4.3$) in the rabbit enzyme.[78,80] This difference has been attributed to the substitution of the weak Asn amide ligand in the former with a much stronger His ligand in the latter, a conclusion supported by site-directed mutagenesis experiments.[80] Active LO exhibits a yellow chromophore ($\lambda_{max} = 350$ nm, $\epsilon = 2000$ M^{-1} cm^{-1}) that arises from a hydroxo-to-iron(III) charge-transfer transition.[78] The presence of a hydroxide at the sixth coordination site (Figure 9B) is unequivocally established by the observation of a short Fe−O distance (1.9 Å) from EXAFS analysis that can be attributed to the Fe^{III}−OH bond.[81]

A purple chromophore ($\lambda_{max} = 585$ nm, $\epsilon = 1300$ M^{-1} cm^{-1}) forms when active LO reacts with O_2 and

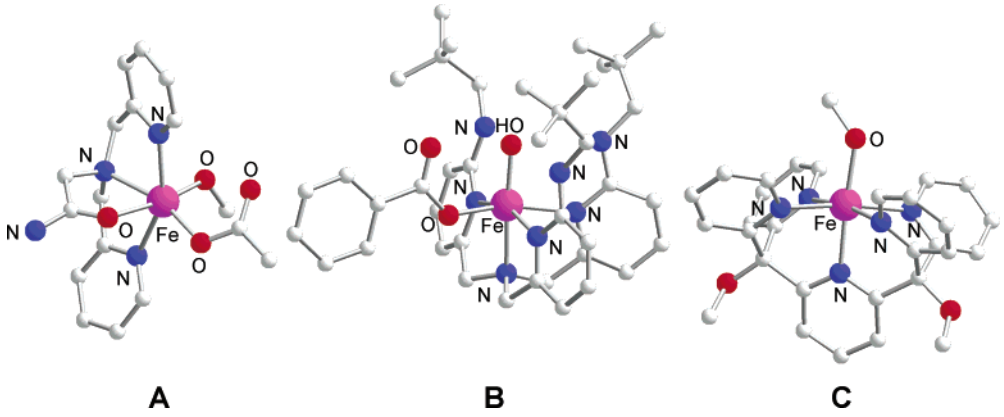

Figure 10. Structures of (A) $[Fe^{II}(BPGm)(O_2CCH_3)(CH_3OH)]^+$, (B) $[Fe^{III}(TNPA)(OH)(O_2CR)]^+$, and (C) $[Fe^{III}(PY5)(OCH_3)]^{2+}$.

substrate or with an excess of the hydroperoxide product.[65] The crystal structure of this purple metastable species of soybean lipoxygenase-3 has been recently solved,[82] showing that the site for the exogenous ligand is now occupied by an end-on-coordinated alkylperoxo moiety (Figure 9C). This species is thermally unstable and photolabile[65,76] and represents a catalytically competent intermediate,[82] which releases the fatty acid hydroperoxide product to regenerate the active Fe(III)−hydroxide form and the fatty acid hydroperoxide.

Three structural features particular to the bioinorganic chemistry of lipoxygenase have been modeled by synthetic complexes. The first feature is the coordination of Asn amide carbonyl oxygen, which is quite unusual for the bio-coordination chemistry of iron. The complex $[Fe^{II}(BPGm)(O_2CCH_3)(CH_3OH)](BPh_4)$ (BPGm = *N*-bis(2-pyridylmethyl)glycinamide) was synthesized for this purpose. Its structure reveals an iron coordination sphere with three N ligands, a carboxylate oxygen, an amide carbonyl oxygen, and a methanol molecule (Figure 10A),[83] a ligand combination in good correspondence to that found in soybean LO. The amide carbonyl oxygen has an $Fe-O_{amide}$ bond length of 2.185(6) Å, much shorter than the distance found in the enzyme and comparable to the corresponding $Fe-N_{py}$ bond distance in $[Fe^{II}(TPA)(O_2C^tBu)(CH_3OH)](BPh_4)$. This result suggests that the much longer $Fe-O_{Asn}$ distance found in the soybean enzyme is a result of protein structure constraints.

The second novel structural feature of lipoxygenase iron chemistry is the $Fe^{III}-OH$ unit, postulated to be the agent that cleaves the doubly allylic C−H bond of the substrate. Modeling this catalytically more relevant $Fe^{III}-OH$ species is a challenge, due to the strong tendency of this unit to form oxo-bridged dimers.[84] Ogo et al. succeeded by incorporating sterically bulky neopentylamino groups onto the 6-positions of the pendant pyridines of the TPA framework and obtained crystals of $[Fe^{III}(TNPA)(OH)(O_2CR)]ClO_4$ (TNPA = tris(6-neopentylamino-2-pyridylmethyl)amine) (Figure 10B).[85,86] Steric shielding of the hydroxide group, as well as H-bonding interactions with amine N−H groups from the ligand, accounts for the stability of this molecule. The Fe−OH distance of 1.873(5) Å found for the synthetic complex compares well with that of active soybean LO determined by EXAFS analysis.[81]

The third novel structural feature is the $Fe^{III}-OOR$ purple intermediate.[82] Until it was recently established by the crystal structure of the enzyme−product complex, the speculation that the purple chromophore obtained upon addition of excess product to the enzyme was an $Fe^{III}-OOR$ complex was principally supported by model studies. This notion was first illustrated in the reaction of $[Fe^{II}(6\text{-}Me_3\text{-}TPA)(\kappa^2\text{-}O_2CPh)]BPh_4$ with excess ^{t}BuOOH to form a transient pink chromophore (λ_{max} = 510 nm, ϵ = 2300 M^{-1} cm^{-1}).[87] The chromophore was identified to be an alkylperoxo-to-iron(III) charge-transfer transition by resonance Raman spectroscopy (see section 5.1), and the intermediate was formulated as $[Fe^{III}(6\text{-}Me_3\text{-}TPA)(OO^tBu)(O_2CPh)]^+$ on the basis of its electrospray mass spectrum.[88]

The $[Fe^{II}(6\text{-}Me_3\text{-}TPA)(\kappa^2\text{-}O_2CPh)]BPh_4$ complex in fact follows the sequence of transformations at the LO metal center as outlined in Figure 9, making it a good spectroscopic model for LO.[88] Like the enzyme, it is air stable and reacts with half an equivalent of ^{t}BuOOH at −40 °C to form a yellow chromophore. The yellow chromophore was identified by EPR and electrospray mass spectrometry to be $[Fe^{III}(6\text{-}Me_3\text{-}TPA)(OH)(O_2CPh)]^+$. Further addition of ^{t}BuOOH afforded the metastable pink $[Fe^{III}(6\text{-}Me_3\text{-}TPA)(OO^tBu)(O_2CPh)]^+$ intermediate. The decay kinetics of the latter was investigated by systematic variation of para substituents on the benzoate. It was found that the rate of decay of the intermediate increases with the electron-withdrawing capability of the para substituent, consistent with irreversible Fe−OOR bond homolysis to generate an alkylperoxyl radical and Fe^{II}, as proposed by DFT calculations.[89]

The most intriguing step of the lipoxygenase mechanism is the cleavage of a doubly allylic C−H bond on the fatty acid substrate by the yellow $Fe^{III}-OH$ species. Kinetic studies of this transformation have revealed an unusually large KIE of greater than 50, indicating that C−H bond cleavage is the rate-determining step above 32 °C and that the reaction proceeds through a quantum-mechanical tunneling pathway.[90−93] DFT calculations describe this process as a proton-coupled electron transfer (PCET), with the doubly allylic proton being extracted from the substrate by the $Fe^{III}-OH$ moiety, followed by or coincident with electron transfer from the substrate anion to the iron(III) center.[94] This C−H bond cleavage step is akin to those associated with higher-

valent iron−oxo species such as those in cytochrome P450 and methane monooxygenase in the hydroxylation of alkane substrates, except that the metal center is iron(III) and the C−H bond is much weaker.

Model compounds demonstrate that the C−H activation step proposed in the LO mechanism is quite plausible.[95−97] Stack and co-workers prepared [Fe^{II}(PY5)(CH_3OH)]($OTf)_2$ (PY5 = 2,6-bis-((2-pyridyl)-methoxymethane)pyridine), an air stable, high-spin iron(II) complex with a remarkably high $Fe^{III/II}$ redox potential (0.930 V vs SHE).[95,97] One-electron oxidation afforded [Fe^{III}(PY5)(OCH_3)]($OTf)_2$, whose X-ray structure (Figure 10C) reveals a rather short (1.78 Å) Fe−OCH_3 bond, consistent with multiple bond character and reminiscent of the short Fe−O bond distance (1.88 Å) found in soybean LO.[81] This complex oxidizes hydrocarbons with weak C−H bonds (BDE (bond dissociation energy) = 75−88 kcal mol^{-1}), concomitant with its reduction. Kinetic studies demonstrate that the reaction proceeds via a rate-determining bimolecular collision between the iron(III) complex and the substrate with primary kinetic isotope effects (up to 6.5 for the oxidation of toluene at 295 K in MeOH). Furthermore, a linear correlation is obtained in a plot of log k_{reac} vs substrate BDE but not for a plot of log k_{reac} vs substrate pK_a, strongly favoring a hydrogen atom abstraction mechanism.

Hydrogen abstraction reactions by organic radicals,[98,99] transition metal complexes,[96,100,101] and metal−oxo complexes in particular[98,102,103] generally follow the Evans−Polanyi relationship, which states that, in these types of reactions, the change in entropy is independent of the reagents and that there is a linear correlation between the activation energy and the enthalpy of the reaction. Therefore, for a particular H-abstracting species, the logarithm of the reaction rate will be directly related to the substrate C−H BDE. For the particular case of [Fe^{III}(PY5)(OMe)]-($OTf)_2$, a thermodynamic cycle can be established from which the O−H bond strength of the methanol ligand on the iron(II) complex can be estimated to be 83.5 ± 2.0 kcal mol^{-1}.[97] A similar analysis of the O−H BDE in the Fe^{II}−OH_2 form of LO gives a remarkably similar 85 kcal mol^{-1}, which matches the value obtained by DFT calculations (85.3 kcal/mol), assuming that both the Fe^{II}−OH_2 and the Fe^{III}−OH forms of the enzyme are six-coordinate.[94] In conclusion, oxidation of substrates containing weak C−H bonds (BDE = 75−88 kcal mol^{-1}) by [Fe^{III}(PY5)-(OMe)]($OTf)_2$ via a H-abstraction mechanism takes place because the reaction is either exothermic or only slightly endothermic (provided a second irreversible reaction such as radical−radical coupling follows).

Parallel to Stack's studies, Mayer and co-workers prepared [Fe^{III}(Hbim)(H_2bim)$_2$]($ClO_4)_2$ (H_2bim = 2,2′-bis-imidazoline) and showed its ability to react with substrates containing weak C−H bonds via a hydrogen abstraction mechanism.[96,99,104] The hydrogen acceptor in this complex is an N atom on an imidazolinate ligand, and a thermodynamic cycle could be proposed from which the N−H bond strength of 76 ± 2 kcal mol^{-1} could be calculated. Formation of this bond constitutes the driving force for the hydrogen atom abstractions. These two examples provide strong support for the hypothesis that oxidation of *cis*,*cis*-1,4-pentadiene-containing fatty acids by LOs is initiated via H-atom abstraction by an Fe^{III}−OH species corresponding to Figure 9B in a mechanism that requires no high-valent iron intermediate. One key feature of the enzyme reaction not yet modeled is the high kinetic isotopic effect observed in the enzyme, despite the striking similarity in thermodynamic driving force between the enzyme and some of the model compounds.

3. Iron(II) Enzymes with the 2-His-1-Carboxylate Facial Triad Motif

Great strides have been made in the past 10 years toward our understanding of mononuclear nonheme iron(II) enzymes. Fueling interest is the ever increasing number of crystal structures available for this class of enzymes, which is clearly emerging as a diverse collection of metalloenzymes that activate dioxygen with a common structural motif (Table 2). The iron(II) center in these enzymes is invariably coordinated by three protein residues, two His and one Asp or Glu, constituting one face of an octahedron, a recurring motif referred to as the 2-His-1-carboxylate facial triad.[105,106] Among these enzymes are dioxygenases involved in the biodegradation of aromatic molecules that catalyze oxidative ring cleavage or arene *cis*-dihydroxylation, a superfamily of enzymes that require an α-keto acid as cosubstrate, and pterin-dependent hydroxylases. Sequence comparisons show that the 2-His-1-carboxylate triad is conserved within each group (or subgroup), but the sequence motifs differ from each other. This strongly suggests convergent evolution toward a particularly favored metal binding site that is useful for promoting a variety of reactions.

The 2-His-1-carboxylate facial triad serves as an excellent monoanionic three-pronged platform for binding divalent metal ions (Figure 11). The three remaining sites on the opposite face of the octahedron are consequently available for exogenous ligands. In the as-isolated enzymes, these sites are usually occupied by solvent molecules but can accommodate both substrate (or cosubstrate) and O_2 in later steps of the catalytic cycle. Despite the many different transformations catalyzed, a general mechanistic pattern at the iron(II) center has emerged from spectroscopic and crystallographic studies of the various enzymes in this superfamily (Figure 11).[3,4,106] The iron(II) center is typically six-coordinate at the start of the catalytic cycle and relatively unreactive toward O_2. Subsequent substrate and/or cofactor binding to the active site makes the metal center five-coordinate and increases its affinity for O_2. O_2 binding then initiates the oxidative mechanism specific for each subclass. In other words, the metal center becomes poised to bind O_2 only when substrate and cofactor(s) are present in the active site, thereby promoting strong coupling between the reduction of O_2 and the oxidation of substrate. This structural motif thus allows the metal center to activate both substrate and O_2 and bring them into close proximity for subsequent reaction, thereby accounting in large part for its versatility.[105,106] As will be illustrated in

Table 2. Iron Enzymes with a Crystallographically Established 2-His-1-Carboxylate Facial Triad

	PDB file no	metal ligands[a]	ref
Extradiol Catechol Dioxygenases: $HX_{55(8)}HX_{50(2)}E$			
BphC	1DHY, 1HAN	H145, H209, E260	122, 123
2,3-CTD	1MPY	H153, H214, E265	124
HPCD		H155, H214, E267	125
MndD (Mn)		H155, H214, E267	125
LigAB	1BOU	H12, H61, E242	126
homogentisate 1,2-dioxygenase	1EY2	H335, E341, H371	127
α-Keto Acid-Dependent Enzymes: $HX(D/E)X_nH$			
DAOCS	1RXF	H183, D185, H243	128
clavaminate synthase	1DS1	H144, E146, H279	129
proline 3-hydroxylase	1E5S	H107, D109, H158	130
TauD	1GQW, 1OTJ	H99, D101, H255	131, 132
anthocyanidin synthase	1GP4	H232, D234, H288	133
Asn hydroxylase (FIH)	1MZF	H199, D201, H279	134, 135
carbapenam synthase	1NX4	H101, D103, H251	136
HPP dioxygenase	1CJX	H161, H240, E322	137
isopenicillin N synthase	1IPS	H214, D216, H270	138
Pterin-Dependent Enzymes: $HX_4HX_{40(1)}E$			
phenylalanine hydroxylase	2PAH, 1PHZ	H285, H290, E330	139, 140
	1LTV	H138, H143, E184	141
tyrosine hydroxylase	1TOH	H331, H336, E376	142
tryptophan hydroxylase	1MLW	H272, H277, E317	143
Rieske Dioxygenases: $HX_4HX_{148}D$			
naphthalene dioxygenase	1NDO	H208, H213, D362	144

[a] Sequence motif listed for each subclass reflects the dominant sequence pattern found.

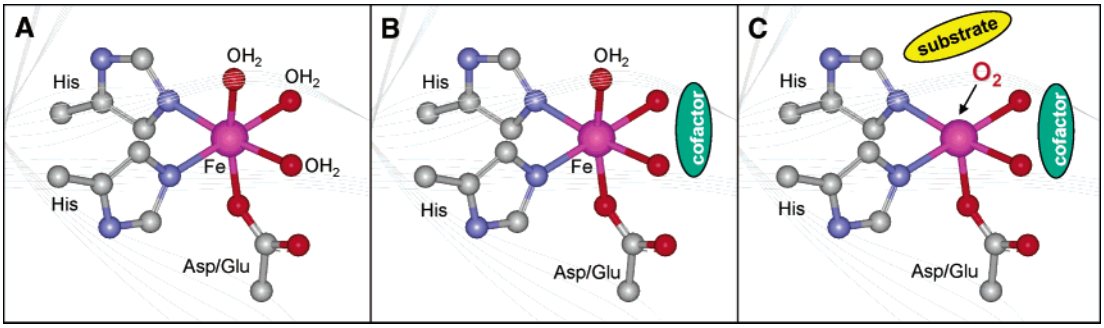

Figure 11. Mechanistic paradigm for dioxygen activation proposed by Solomon[3,4] for nonheme iron(II) enzymes with a 2-His-1-carboxylate facial triad motif, as exemplified by the active site of DAOCS (1RXF.pdb).

the examples discussed below, the coordination flexibility afforded by this site translates into a mechanistic diversity unparalleled by any other metalloenzyme class.

Many polydentate ligand frameworks have been used to mimic the 2-His-1-carboxylate facial triad in structural and functional models (Figure 12). Prominent among these is the $Tp^{R,R'}$ ligand, well explored initially by Kitajima in the early 1990s.[107] Its C_3 symmetry, facial topology, and monoanionic nature make it an attractive and convenient ligand to use for such studies. Iron(II) complexes have been shown to bind O_2[108] and model the chemistry of the extradiol-cleaving dioxygenases[109] and the α-keto acid-dependent enzymes.[110−112] The related C_3-symmetric but neutral R_3TACN ligand can also be used in similar applications.[55,113,114] Despite their tetradentate framework, neutral TPA and BPMCN ligands have also been very useful in the development of structural and functional models of the extradiol-cleaving dioxygenases,[55,115] the α-keto acid-dependent enzymes,[116] and the Rieske dioxygenases.[117−119] Details of these studies will be discussed in subsequent sections. Finally, efforts have been initiated to explore the coordination chemistry of monoanionic *N*,*N*,*O*-heteroscorpionate ligands that more closely resemble the 2-His-1-carboxylate facial triad, and the first iron(II) complexes have recently been reported.[120,121]

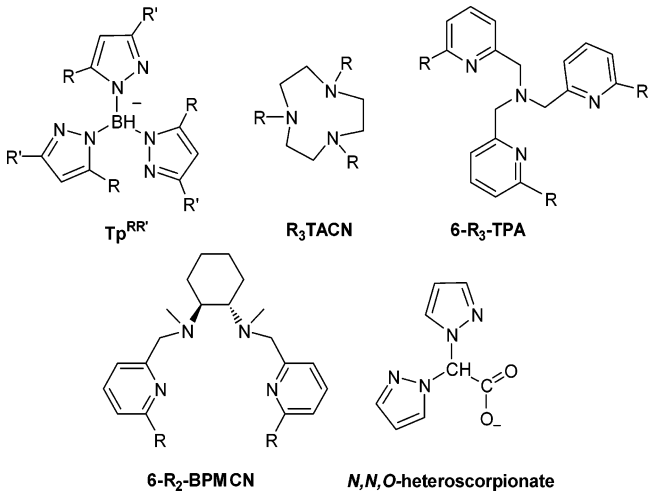

Figure 12. Ligands used to model iron(II) enzymes with the 2-His-1-carboxylate facial triad.

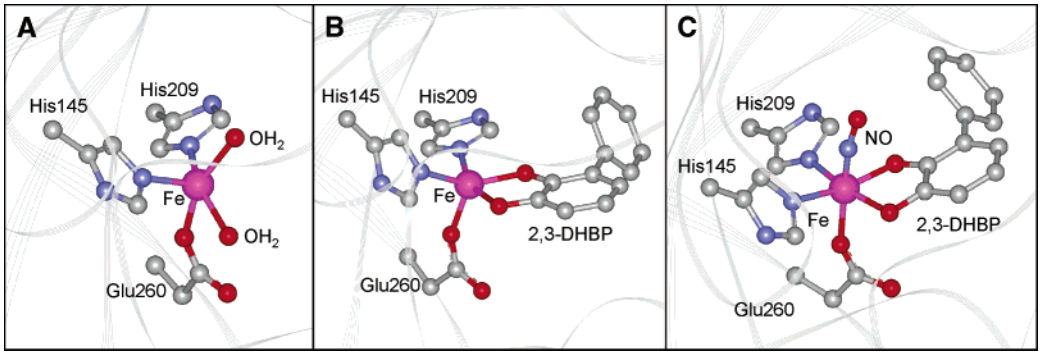

Figure 13. Active site structures of (A) as-isolated BphC (1KW3.pdb), (B) its enzyme−substrate complex (1KW6.pdb), and (C) its ternary E·S·NO adduct (1KW8.pdb).

3.1. Extradiol-Cleaving Catechol Dioxygenases

The extradiol cleavage of dihydroxybenzenes represents the more common pathway for the biodegradation of aromatic molecules in the soil. While the intradiol-cleaving enzymes utilize an iron(III) active site, the extradiol-cleaving enzymes typically use iron(II) (or manganese(II) in a few examples). Sequence comparisons classify the enzymes in this category into three subclasses,[145] but crystallographic data for representative proteins of each subclass show the metal center to be in a square pyramidal active site with a 2-His-1-carboxylate facial triad (Figure 13).

Steady-state kinetic studies have revealed that extradiol-cleaving enzymes utilize an ordered mechanism with substrate binding prior to O_2 activation.[6] Indeed, the coordination of the substrate appears to serve as a trigger and significantly increase the affinity of the metal center for O_2, as demonstrated by NO binding data.[146] Crystallographic studies on 2,3-dihydroxybiphenyl 1,2-dioxygenase (BphC), 3,4-dihydroxyphenylacetate 2,3-dioxygenase (HPCD), and protocatechuate 4,5-dioxygenase (LigAB) all demonstrate that substrate binding results in the displacement of the two water ligands to form a square pyramidal metal center poised to bind O_2.[125,126,147−149] In the BphC structure, one oxygen atom of the bidentate catecholate occupies the vacant position present in the as-isolated enzyme, while the other occupies the site trans to His210, leaving the site trans to Glu260 vacant (Figure 13B). Spectroscopic studies[150] and high-resolution crystallography[125,126,147−149] indicate that the catechol binds in an asymmetric fashion to the iron(II) center with Fe−O_{cat} bond lengths that differ by 0.2−0.4 Å. These structural parameters are in excellent agreement with those reported for synthetic iron(II)−monoanionic catecholate complexes (Figure 14A), and on the basis of this comparison, it has been proposed that the catechol binds to the iron(II) center as a monoanion.[55,115,150,151] The monoanionic nature of the catechol substrate in extradiol dioxygenases is in sharp contrast with the dianionic catecholate character commonly found in iron(III) complexes.[1,6] This difference is understandable on the basis of the differing Lewis acidities of the metal center in its divalent and trivalent oxidation states. O_2 binding is thus expected to occur at the vacant site trans to Glu260 (Figure 13B), and this notion is supported by a third BphC structure (Figure 13C) that shows the binding of the O_2 surrogate NO in a nearly linear fashion at this site.

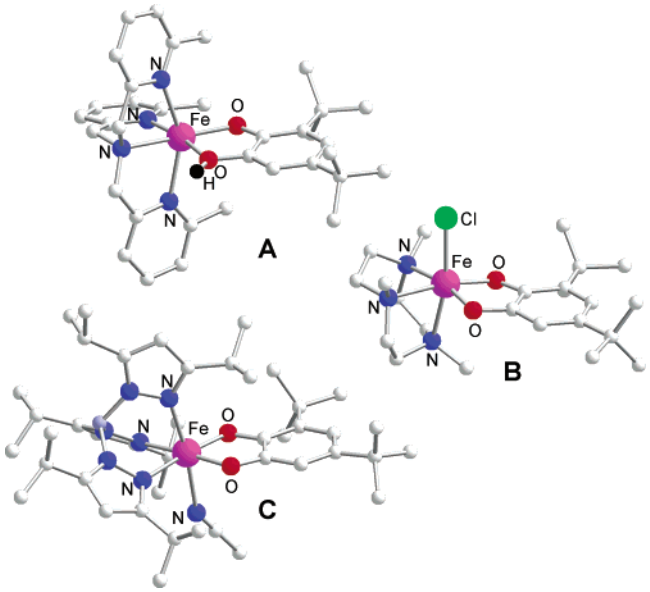

Figure 14. Model compounds for extradiol-cleaving catechol dioxygenases: structural model $[Fe^{II}(6\text{-}Me_3\text{-}TPA)(DBCH)]^+$ (A) and functional models $[Fe^{III}(Me_3TACN)(DBC)(Cl)]$ (B) and $[Fe^{III}(Tp^{iPr_2})(DBC)(NCCH_3)]$ (C).

The 3,4-dihydroxyphenylacetate 2,3-dioxygenases from *Brevibacterium fuscum* and *Arthrobacter globoformis* represent an interesting pair of enzymes.[125] These two enzymes have 82% sequence identity[12,152] but have distinct metal ion requirements: the *B. fuscum* enzyme (HPCD) has iron(II) in the active site, while the *A. globoformis* enzyme (MndD) requires manganese(II). While there is no current insight into the reasons for the different metal ion requirements, it is clear that both enzymes can catalyze extradiol cleavage of the same substrate. The recently solved crystal structures of the two enzymes show nearly congruent first and second coordination spheres about the metal centers. This apparent Fe/Mn substitution is reminiscent of the situation for Fe and Mn superoxide dismutases (SODs), which also have very similar active site structures.[153−155] However, there are second coordination sphere differences for the latter pair, and it is possible to replace Fe for Mn in MnSOD and Mn for Fe in FeSOD in some cases but not yet for the dioxygenases.

Table 3. Biomimetic Complexes That Carry Out Extradiol Cleavage of Catechols

	% intradiol	% extradiol	% quinone	ref
$FeCl_2$/bpy/py/$DBCH_2$ (1:3:23:4 in THF)	21	~10	52	40
$FeCl_2$/TACN/catechol/pyridine (1:1:1:3 in CH_3OH)	7.5	50	n.r.	114, 164
$FeCl_2$/TACN/3-methylcatechol/pyridine (1:1:1:3 in CH_3OH)		*a*	n.r.	114
$[Fe^{III}(TACN)(DBC)(Cl)]/CH_3CN$		35	65	62
$[Fe^{III}(cyclam)(DBC)]^+/CH_3CN$				62
$[Fe^{III}(TACN)(DBC)(Cl)]/CH_2Cl_2 + Ag^+$		3	82	113
$[Fe^{III}(TACN)(DBC)(Cl)]/CH_2Cl_2 + Ag^+ +$ 4-picoline		98		113
$[Fe^{III}(Me_3TACN)(DBC)(Cl)]/CH_2Cl_2 + Ag^+$		97		165
$[Fe^{III}(Tp^{iPr_2})(DBC)]$/toluene	33	67		109
$[Fe^{III}(Tp^{tBu,iPr})(DBC)]$/toluene				109
$[Fe^{III}(BnBPA)(DBC)(Cl)]/CH_2Cl_2 + Ag^+$	25	72		165
$[Fe^{III}(L\text{-}N_4H_2)(DBC)]^+/CH_3OH$	~50	~50		56
$[Fe^{III}(6\text{-}Me_2\text{-}BPMCN)(DBC)]^+/CH_3CN$	78	12		55
$[Fe^{III}(6\text{-}Me_2\text{-}TPA)(DBC)]^+/CH_3CN$	70(5)	18(2)		61, 166
$[Fe^{III}(6\text{-}Me_3\text{-}TPA)(DBC)]^+/CH_3CN$	89	3		55
other tetradentate ligand complexes	84−99			see Table 1

[a] Only extradiol products observed but not quantified.

Substrate binding to the metal centers of HPCD and MndD is also found to be asymmetric, supporting the postulate of a monoanionic catecholate.[125] As observed for BphC, it is the oxygen atom adjacent to the C−C bond that is cleaved that is associated with the shorter metal−oxygen bond and presumably the one that is ionized. The substrate analogue 4-nitrocatechol (4-NCH_2) has proven useful as a colorimetric probe to indicate the ionization state of the substrate in the extradiol dioxygenase active site.[151,156,157] Thus, 4-NC binding to catechol 2,3-dioxygenase, HPCD, and MndD showed an increasing dianionic character. This order correlated inversely with the rate of extradiol cleavage of 4-NC, supporting the notion that binding a monoanionic substrate is crucial for extradiol cleavage.

In contrast to their intradiol counterparts, model complexes capable of eliciting extradiol dioxygenase activity are fewer in number (Table 3). The iron(II)−hydrogencatecholate complexes, mentioned earlier as excellent structural models for the monoanionic catecholate binding,[55,115] react readily with O_2 to afford the corresponding iron(III)−catecholate complexes. Since the iron(II) complexes all have a bidentate hydrogencatecholate and a tetradentate supporting ligand, the metal centers are coordinatively saturated, so the lack of an available coordination site for O_2 probably renders the complexes susceptible to one-electron oxidation by an outer-sphere mechanism.

Funabiki and co-workers discovered the first functional mimics of iron-containing extradiol dioxygenases.[39,40,158−163] Oxygenation of a mixture of $FeCl_2 \cdot 4H_2O$ or $FeCl_3$, 3,5-di-*tert*-butylcatechol ($DBCH_2$), and pyridine derivatives in organic solvents afforded intradiol and extradiol cleavage products, together with 3,5-di-*tert*-butylbenzoquinone. Extradiol cleavage products were favored by using $FeCl_2 \cdot 4H_2O$ and $DBCH_2$ in aqueous THF. Unfortunately, these pioneering efforts were hampered by the presence of a complex mixture of iron species in solution, making a mechanistic interpretation difficult to achieve.

Along a similar vein, Bugg and co-workers explored the oxygenation of catechols in methanol by a mixture of $FeCl_2$ or $FeCl_3$, TACN (TACN = 1,4,7-triazacyclononane), and pyridine.[114,164] Under these conditions, catechol was converted in 50% yield to 2-hydroxymuconic semi-aldehyde methyl ester, the authentic extradiol cleavage product of catechol 2,3-dioxygenase. A 7:1 extradiol:intradiol selectivity was found for $Fe^{II}Cl_2$/TACN, compared to 2:1 for $Fe^{III}Cl_3$/TACN, emphasizing the importance of iron(II) for promoting extradiol cleavage. No cleavage reaction was elicited by using other metal halides such as $MnCl_2$, $CoCl_2$, and CuCl, replacing one N by an O atom in the TACN ligand, or changing the number of carbon atoms on the macrocycle. One equivalent of pyridine or use of the monoanionic monosodium catecholate was necessary for activity in the $FeCl_2$/TACN system, strongly suggesting that the catechol binds as a monoanion. In addition, pyridine was required for high extradiol:intradiol selectivity. The oxidation state specificity displayed by these systems, the apparently required monoanionic nature of the catecholate substrate, and the tridentate facially coordinating structure of the ligand are characteristics reminiscent of the extradiol-cleaving dioxygenases.

Extradiol cleavage has also been observed with isolated and characterized $[Fe^{III}(L)(DBC)]$ complexes. The first example was provided by Dei et al., who found that $[Fe^{III}(TACN)(DBC)(Cl)]$ reacted with O_2 to generate products derived from the extradiol cleavage of DBC in 35% overall yield.[62] (Interestingly, the corresponding cyclam complex is unreactive toward O_2.) The two products observed, 3,5-di-*tert*-butyl-2-pyrone and 4,6-di-*tert*-butyl-2-pyrone (Figure 15), presumably derive from loss of CO from the seven-membered-ring 3,5-diene-α-ketolactone intermediates. Ito and Que found that the addition of $AgBF_4$ and pyridine made this reaction almost quantitative.[113] The addition of the silver salt removes the Cl ligand and generates an available coordination site in the complex for O_2 binding. In the absence of pyridine, 3,5-di-*tert*-butyl-1,2-benzoquinone is formed quantitatively, but the addition of pyridine to the reaction mixture appears to suppress this pathway and directs the catechol oxidation almost quantitatively toward extradiol cleavage. The replacement of TACN with Me_3TACN (Figure 14B, Me_3TACN = 1,4,7-trimethyl-1,4,7-triazacyclononane) made the

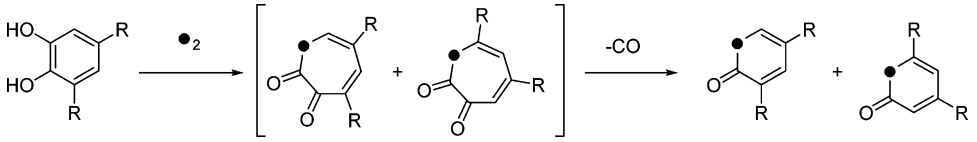

Figure 15. Extradiol cleavage products observed in model $DBCH_2$ oxidations.

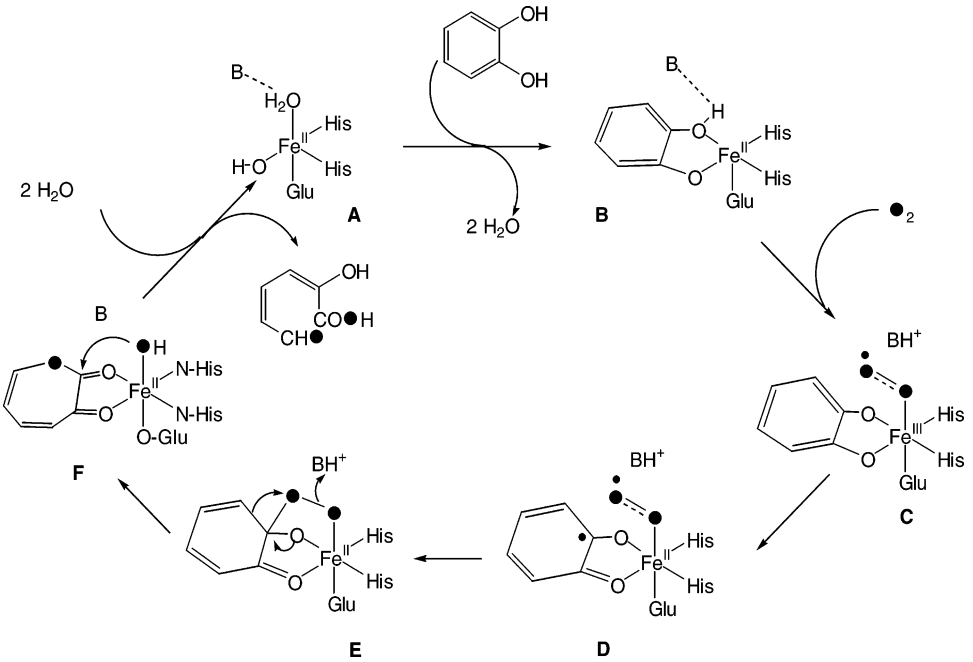

Figure 16. Proposed mechanism for the extradiol-cleaving catechol dioxygenases.

addition of pyridine unnecessary, and extradiol cleavage products were obtained in 97% yield.[165]

The use of other tridentate ligands emphasizes the importance of the facial topology for eliciting extradiol cleavage. The use of Tp^{iPr_2} (Tp^{iPr_2} = hydridotris(3,5-diisopropyl-1-pyrazolyl)borate) afforded an [Fe^{III}(L)-(DBC)] complex (Figure 14C) that reacts with O_2 to afford extradiol cleavage products in 67% yield.[109] The corresponding $Tp^{iPr,tBu}$ complex ($Tp^{iPr,tBu}$ = hydridotris(3-*tert*-butyl-5-isopropyl-1-pyrazolyl)borate), however, did not react at all with O_2, probably due to the extreme steric congestion around the iron center. The complex with the meridional tridentate ligand TPY (TPY = 2,2′:6′,2″-terpyridine), on the other hand, mainly affords quinone (78%) and intradiol-cleaving products (20%).[165] It has been proposed that facially coordinated tridentate ligands promote the extradiol cleavage pathway by allowing the substrate and O_2 to bind on the opposite face of the metal coordination sphere, thereby bringing them into close proximity for reaction.

There are, however, examples of iron complexes of tetradentate ligands that elicit extradiol cleavage. [Fe^{III}(6-Me_3-TPA)(DBC)]$^+$ and [Fe^{III}(6-Me_2-BPMCN)-(DBC)]$^+$, complexes obtained from the one-electron oxidation of their iron(II) hydrogencatecholate precursors, react with O_2 and undergo oxidative cleavage.[55,115] Although the major product in the two reactions results from intradiol cleavage, there are measurable amounts of extradiol products (3% and 12%, respectively). It is conjectured that the steric hindrance introduced by the 6-Me substitution may cause one pendant arm to dissociate and form a five-coordinate species that is responsible for the extradiol cleavage. This rationale probably cannot apply to [Fe-(L-N_4H_2)(DBC)]$^+$ (L-N_4H_2 = 2,11-diaza[3,3](2,6)-pyridinophane), which reacts with O_2 to yield a roughly 1:1 mixture of intradiol and extradiol products.[56] In this example, the proposed conversion of the tetradentate ligand to a tridentate form is difficult to envision due to the macrocyclic nature of the ligand. This dramatic difference in the cleavage preferences between structurally similar catalysts strongly suggests that there are subtle factors yet to be identified that modulate the oxidative cleavage mechanism. Furthermore, the isolated iron catecholate complexes thus far that elicit extradiol cleavage all have iron(III) centers, and there are no examples of well-defined iron(II) catecholate complexes that carry out this transformation.

To date, little is known of the mechanistic steps subsequent to O_2 binding, as the binding of catechol to the divalent metal center is the last observable step in the catalytic cycle of the enzyme and no O_2 adduct has so far been detected. NO has been used as an O_2 surrogate to great advantage to support the likelihood of a ternary E·S·O_2 complex,[146,150,167] but how the electrons flow from substrate to O_2 is a matter of speculation at this point. The structural and spectroscopic data accumulated so far have led to the proposed mechanism in Figure 16.[1]

The first step of the reaction involves the displacement of two water molecules from the enzyme resting state (Figure 16A) by substrate to form a five-coordinate iron(II) species with a chelated monoanionic catecholate (Figure 16B). This change in ligation

would be expected to result in a decrease in the redox potential of the metal center that primes it to react with O_2. The ternary enzyme−substrate−O_2 complex (Figure 16C) thus formed consists of the 2-His-1-carboxylate triad on one face of the metal octahedron and, on the opposite face, a bidentate monoanionic catecholate and O_2. This arrangement juxtaposes the two substrate molecules into the proper orientation for reaction. O_2 binding to the iron(II) center then results in one-electron transfer from metal to O_2, forming an iron(III)−superoxide complex (Figure 16C, by analogy to the formation of the Fe−NO adduct), and another one-electron transfer from substrate to metal, forming a semiquinonatoiron(II)−superoxide species (Figure 16D).

There is a conserved His residue in the second coordination sphere that may serve as the base depicted in the proposed mechanism. Indeed, His194 is found in the structures of BphC to be quite mobile.[168] In the as-isolated enzyme it is hydrogen bonded to the water ligand trans to Glu260 and then interacts strongly with the HO group of the bound monoanionic substrate in the E·S complex. In the ternary complex, it is 3 Å away from the oxygen atom of the bound NO. His194 is thus postulated to act as a base to remove the remaining proton of the bound monoanionic substrate as O_2 binds and in turn serve as an acid to stabilize the charge on the incipient superoxide in the E·S·O_2 adduct. Later in the cycle it is suggested that this residue acts as an acid to facilitate O−O bond lysis in the ring cleavage step and protonate the incipient oxide that becomes the hydroxide ligand needed to hydrolyze the lactone.

Evidence for the development of a radical species on the catecholate substrate in the mechanism is provided by experiments on the enzyme 3-(2′,3′-dihydroxyphenyl)propionate 1′,2′-dioxygenase (MhpB).[169] Bugg and co-workers used a substrate analogue containing a cyclopropyl side chain as a radical probe and found that the substituents on the cyclopropyl group underwent substantial epimerization in the course of enzyme-catalyzed extradiol cleavage. The formation of a semiquinonate radical (Figure 16D) during the catalytic cycle would promote reversible cyclopropyl ring opening that rationalizes the observed epimerization.

The next step of the mechanism is the nucleophilic attack of the incipient superoxide on the aromatic ring that generates an alkylperoxo intermediate (Figure 16E), which in turn undergoes a Criegee rearrangement to generate a seven-membered α-oxolactone ring (Figure 16F) that is hydrolyzed to afford product. Two sites of superoxide attack are possible. Earlier mechanistic postulates of Lipscomb and Que favored attack at C3 (versus C2 as shown in Figure 16E) as a way to explain the different regiospecificities characteristic of intradiol and extradiol dioxygenases (Figure 1).[1] However, the subsequently available crystal structure information on enzyme−substrate complexes clearly indicated that such an attack is implausible,[125,147−149] since it would entail a substantial structural change within the active site for C3 to form a bond with the metal-bound superoxide. The geometry of the metal−catecholate unit, on the other hand, is set up for attack at C2 to generate an alkylperoxo intermediate that resembles that proposed for the intradiol-cleaving enzymes (Figure 3D). With a common alkylperoxo species, how then can the regiospecificity of ring cleavage be rationalized?

Bugg has proposed that the regiospecificity of the cleavage may derive from the different orientations of the peroxo group.[10] Rearrangement of the alkylperoxo intermediate (Figure 16E) by acyl migration would afford the intradiol product, while alkenyl migration gives rise to the extradiol product. There are precedents for both alkenyl and acyl migration in organic hydroperoxo species, and the choice of mechanism may be dictated by stereoelectronic factors.[170−176] An axial orientation for the peroxo group favors alkenyl migration, while an equatorial orientation favors acyl migration. Bugg and co-workers tested this model by preparing a series of substrate analogues where the putative OOH group was replaced by a CH_2OH, and the 1-hydroxocyclohexadien-2-one moiety was replaced by a 1-hydroxocyclohexan-2-one ring.[177] Only substrate analogues with the proximal hydroxymethyl group placed in an axial orientation relative to the cyclohexanone ring exhibited competitive inhibition of the MhpB enzyme.

More recently, Deeth and Bugg reported DFT calculations on probable extradiol cleavage pathways and found an interesting new twist in the peroxide decomposition mechanism (Figure 17).[178] Their calculations suggest that the intervening peroxo species that is stable enough to be crystallized in the Ir^{III} complex[47] (Figure 6) is only a transition state in the Fe^{II} case and undergoes heterolytic cleavage to form an epoxide at the C−C bond that is cleaved prior to lactone formation. Experiments will have to be designed to test this intriguing idea.

Even more recently, Groce and Lipscomb reported the unexpected but instructive observation that the ring cleavage specificity of HPCD can be dramatically altered by mutation of the second sphere H200 residue (Figure 18).[179] The native substrate 3,4-dihydroxyphenylacetate is cleaved by the H200F mutant enzyme in the expected proximal extradiol fashion (i.e., at the C2−C3 bond) under saturating conditions but at 1% the rate of the wild-type HPCD. However, the substrate analogue 2,3-dihydroxybenzoate is cleaved by the wild-type enzyme in a distal extradiol fashion (i.e., at the C3−C4 bond) and by the H200F mutant, quite surprisingly, in an intradiol fashion (i.e., at the C2−C3 bond). These remarkable results show that an iron(III) center is not required for intradiol cleavage and that an iron(II) center coordinated to a 2-His-1-carboxylate facial triad can catalyze either intradiol or extradiol cleavage. Thus, earlier assumed determinants of cleavage specificity, such as metal oxidation state or ligand environment, now appear to be less important than the geometry of the ternary E·S·O_2 adduct. Given the cleavage patterns observed, O_2 attack at C-3 of either substrate would give rise to peroxo intermediates that rationalize all three products. It is clear that our understanding of enzymatic catechol cleavage will

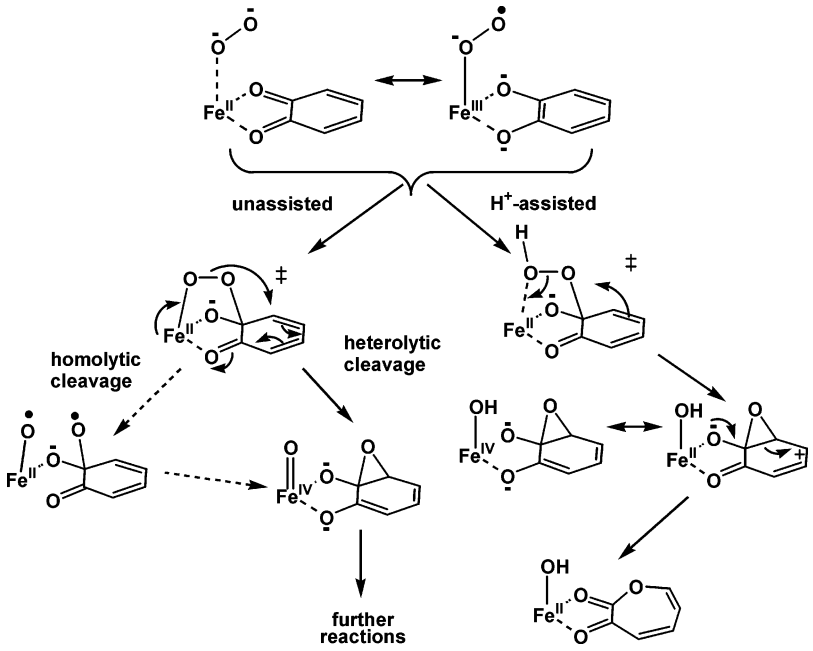

Figure 17. New twists in the extradiol cleavage mechanism proposed by Deeth and Bugg. Reprinted with permission from ref 178. Copyright 2003 Society of Biological Inorganic Chemistry.

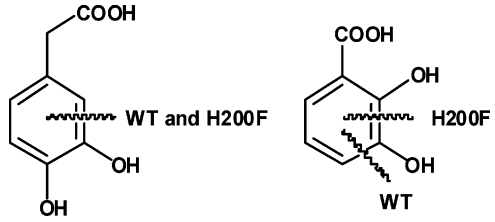

Figure 18. Ring cleavage specificity observed for WT HPCD and its H200F mutant.

deepen with further investigations into this intriguing set of observations.

To date, all the structurally well-characterized biomimetic extradiol-cleaving systems are iron(III) complexes. The fact that oxidative cleavage is regiospecific in many cases and quantitative in some strongly suggests that a divalent metal oxidation is not absolutely required for this chemistry. However, the proposed mechanism in Figure 16 must be adapted for the biomimetic iron(III) complexes to reflect the oxidation state difference between these complexes and the enzymes. Que and co-workers have proposed a mechanism for these five-coordinate iron(III)−catecholate complexes that starts out like the intradiol cleavage mechanism (Figure 3), with radical character being introduced into the bound catecholate as a result of the covalency of the iron(III)−catecholate interaction. But, instead of O_2 attacking the substrate, it attacks the metal center due to the availability of a binding site to form an iron(III)−semiquinone−superoxide adduct. This adduct is analogous to species 16D except for the trivalent metal oxidation state and proceeds to the extradiol cleavage product.

Our current understanding of how extradiol dioxygenases work is less well developed than for its intradiol counterparts. Our ability to elicit extradiol cleavage with biomimetic complexes demonstrates that the oxidative cleavage chemistry is accessible with appropriate ligand design. The lack of well-characterized functional divalent models is clearly a drawback at this stage, but the intriguing observations of Bugg and Funabiki suggesting that iron(II) centers may be better effectors of extradiol cleavage should serve as a compelling rationale for future work aimed at obtaining structurally characterized functional models with iron(II) and manganese(II) centers.

3.2. Enzyme-Catalyzed Oxidations Accompanied by the Oxidative Decarboxylation of α-Keto Carboxylates

Enzymes that require an α-keto acid as a cosubstrate constitute the largest and most diverse family of mononuclear nonheme iron enzymes, catalyzing many pivotal metabolic transformations.[180−182] Substrate oxidation, typically involving but not limited to functionalization of an unactivated C−H bond, occurs concomitantly with the oxidative decarboxylation of an α-keto carboxylate, such as 2-oxoglutarate (2-OG). For the hydroxylation reactions, one atom of dioxygen is incorporated into the product, while the other atom ends up on the carboxylate derived from the keto acid, i.e.,

$$\mathrm{R{-}H + R'COCOOH + \bullet_2 \rightarrow R{-}\bullet H + R'CO\bullet H + CO_2}$$

So these enzymes, like the extradiol-cleaving enzymes discussed in the preceding section, can be classified as dioxygenases, but the elements of the labeled dioxygen are often found in two different products in this intermolecular variant of a dioxygenase reaction (Figure 19A−G). While these isotopic labeling results are typical of the hydroxylation reactions, other oxidative processes such as cyclization, ring expansion, and desaturation reactions result in only one of the atoms of dioxygen being

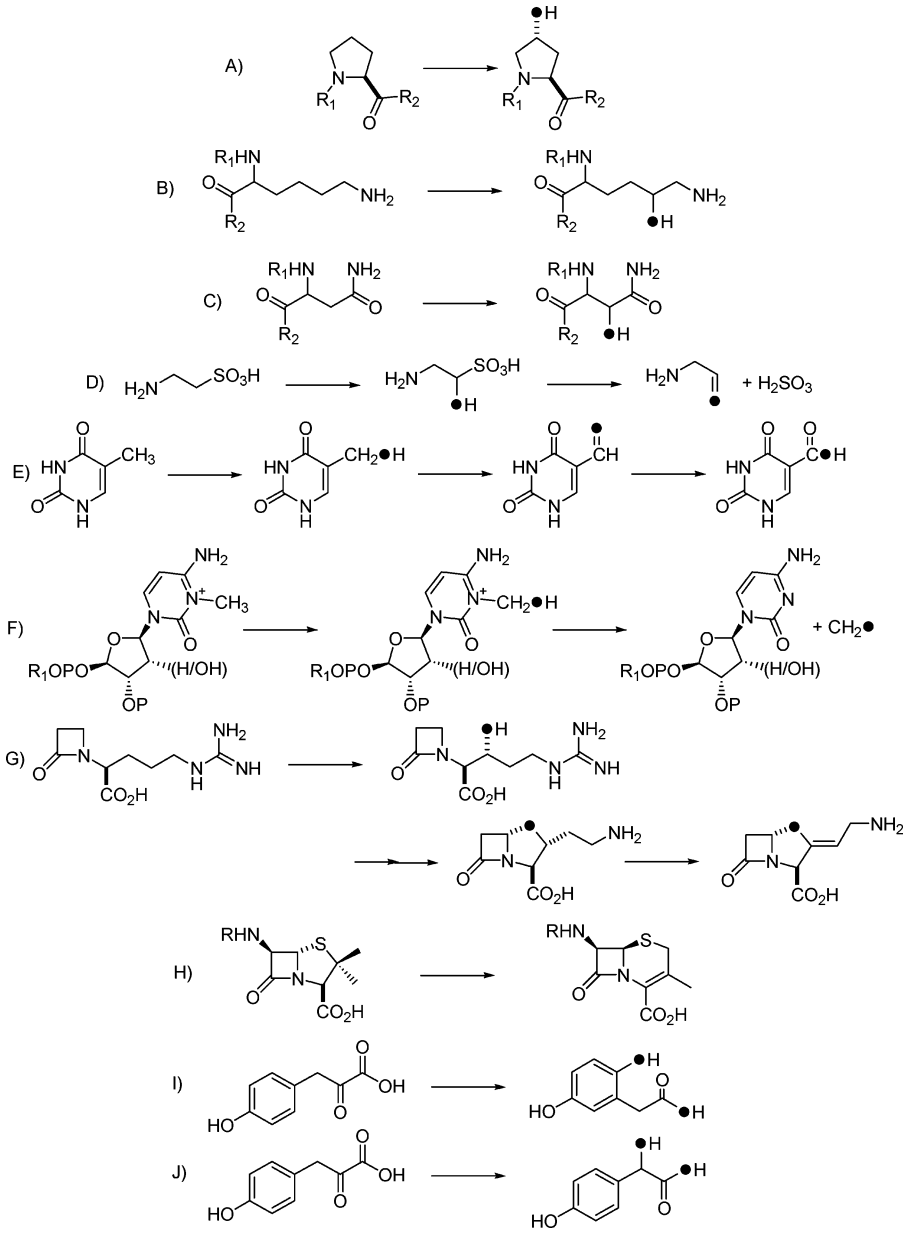

Figure 19. Some reactions catalyzed by α-keto acid-dependent enzymes: (A) prolyl 4-hydroxylase, (B) lysyl hydroxylase, (C) asparagine hydroxylase, (D) taurine/2-OG dioxygenase (TauD), (E) thymine hydroxylase, (F) RNA and DNA repairing N-demethylase (AlkB), (G) clavaminate synthase 2 (CAS), (H) deacetoxycephalosporin C synthase (DAOCS), (I) 4-hydroxyphenylpyruvate (HPP) dioxygenase, and (J) 4-hydroxymandelate synthase.

incorporated into the succinate byproduct and the other being liberated as water. For example, the primary substrate undergoes a two-electron oxidation without oxygen incorporation to form a ring, as in Figure 19G, or to expand a five-membered ring to a six-membered one, as in Figure 19H. Figure 19I,J shows novel reactions in tyrosine catabolism in which the primary substrate in fact also possesses an α-keto acid functionality. In reaction 19I, oxidative decarboxylation of the α-keto carboxylate is accompanied by hydroxylation of the phenyl ring as well as a 1,2-alkyl shift, while in reaction 19J, hydroxylation of the benzylic carbon occurs instead.

α-Keto acid-dependent enzymes are found in microorganisms, plants, and animals and play vital roles in pathways of environmental, pharmaceutical, and biological significance. For instance, the bacterial enzyme TfdA hydroxylates the broadleaf herbicide 2,4-dichlorophenoxyacetate in the first step in its biodegradation;[183,184] AlkB demethylates 1-methyladenine and 3-methylcytosine in the repair of single-stranded DNA and RNA (Figure 19F);[185−187] clavaminic acid synthase (CAS) catalyzes three distinct steps in the synthesis of the β-lactamase inhibitor clavulanic acid (Figure 19G);[188] and deacetoxycephalosporin C synthase (DAOCS) catalyzes the ring expansion of the thiazolidine ring of the penicillin N nucleus to afford deacetoxycephalosporin C (Figure 19H).[189,190] These enzymes also appear in microbes that use alternative energy sources, such as sulfonates and hypophosphites. For example, taurine/2-OG dioxygenase (TauD) enables *E. coli* to use the aliphatic sulfonate taurine as a sulfur source during periods of sulfate starvation (Figure 19D),[191] and hypophosphite/2-OG dioxygenase (HtxA) allows microbes to oxidize phosphite and hypophosphite.[192]

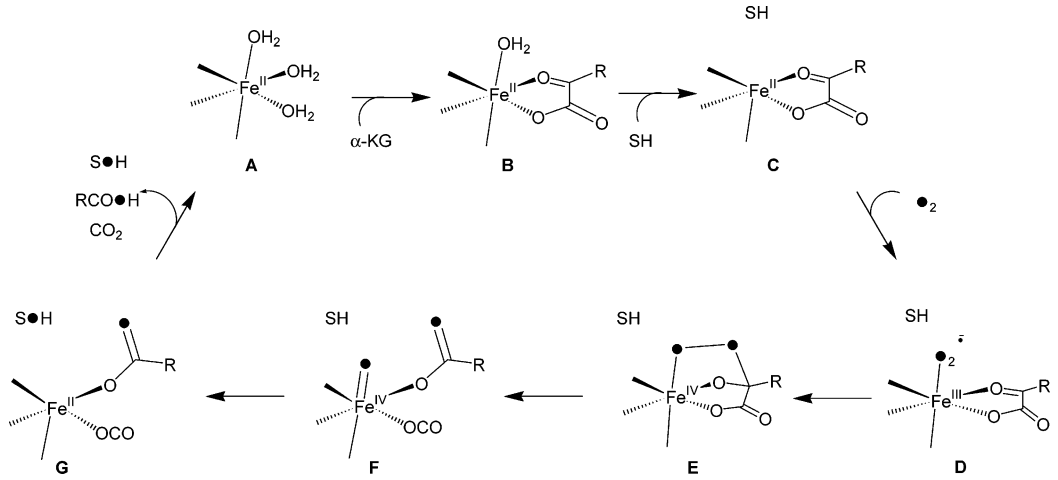

Figure 20. Proposed reaction mechanism for α-keto acid-dependent enzymes.

Mutations in α-keto acid-dependent oxygenases have also been linked to certain disease states. The mammalian HPP dioxygenase has been linked to conditions of tyrosinaemia type III and hawksinuria related to the buildup of metabolites of tyrosine.[181,193] Prolyl 3-hydroxylase, prolyl 4-hydroxylase, and lysyl hydroxylase are responsible for the post-translational modification of procollagen, which is crucial to the formation of fibrous tissues,[182] while recent reports show prolyl (HIF-1) and asparaginyl hydroxylases (FIH-1) to be linked to oxygen sensing in cells.[194−196] Under conditions of low oxygen tension (hypoxia), hypoxia inducible factor (HIF) promotes increased expression of (a) erythropoietin, a precursor to red blood cells; (b) vascular endothelial growth factor, a vasodilator and key component in the growth of new blood vessels; (c) certain glycolytic enzymes, leading to the liberation of energy rich compounds; and (d) tyrosine hydroxylase (vide infra), the rate-determining step in the synthesis of adrenaline. At normal oxygen concentrations, proline hydroxylation leads to ubiquitination and degradation of HIF, while asparagine hydroxylation inhibits interaction of HIF with transcriptional coactivators, thereby exerting a second level of control over gene expression. Disruption of the signaling cascade in which HIF-1 and FIH-1 participate can affect the onset and development of cancerous tumors and ischemia.[197,198] This, coupled with the observation of an α-keto acid-dependent enzyme in a virus that initiates DNA replication,[199] has led to a proliferation of interest in the relationship of structure to function in α-keto acid-dependent dioxygenases, not only on therapeutic grounds but also for etiological reasons.

Despite the vast array of distinct transformations these enzymes carry out, the members of this family in general require 1 equiv of iron(II), an α-keto acid, dioxygen, and ascorbate for full activity. Crystal structures of a number of different 2-oxoglutarate-dependent enzymes show the double-stranded β-helix (or jellyroll) as a common architecture for this superfamily,[128−131,133−136] suggesting a close evolutionary relationship among the three branches of the family identified by sequence comparisons.[200,201] While many of these enzymes show minimal sequence identity, there is a high degree of sequence homology. There is a conserved set of residues with the motif HX(D/E)X_mHX_n(R/K)XS (where $m = 50-70$ and $n = 10$, $m = 138-207$ and $n = 10-13$, or $m = 72-101$ and $n = 10$ for the three subsets). The HX(D/E)X_mH set of residues provides the common 2-His-1-carboxylate facial triad that binds the high-spin iron(II) center (Figure 11, Table 2),[105] while the (R/K)XS residues serve to bind the anionic C-5 carboxylate of 2-oxoglutarate.

Several enzymes in this class have substrates with a built-in α-keto acid function and thus do not require 2-oxoglutarate as a cosubstrate. These enzymes appear to have different topologies from enzymes utilizing 2-oxoglutarate and include HPP dioxygenase and 4-hydroxymandelate synthase, which utilize the same substrate but catalyze different transformations (Figure 19I,J). The crystal structure of HPP dioxygenase also reveals a 2-His-1-carboxylate active site but within a $\beta\alpha\beta\beta\beta\alpha$ scaffold[137] that is more closely related to those observed in catechol 2,3-dioxygenase, fosfomycin resistance protein, bleomycin resistance protein, and human glyoxylase I (which are part of the vicinal oxygen chelate superfamily).[202,203] 4-Hydroxymandelate synthase and HPP dioxygenase exhibit 43% sequence similarity and 34% identity.[204] A third member of this subset is α-ketoisocaproate dioxygenase, which is involved in leucine metabolism.[205]

The accumulated data allow a common mechanism to be proposed for α-keto acid-dependent iron oxygenases (Figure 20).[1,3,182,206] The iron(II) center in the resting enzyme is sequestered by the 2-His-1-carboxylate facial triad, with three water molecules completing the coordination sphere (Figure 11A). The six-coordinate nature of the iron center has also been established in frozen solution by XAS for TfdA[207] and DAOCS[208] and by CD analysis for CAS.[209]

Steady-state kinetic studies on prolyl 4-hydroxylase,[210,211] thymine hydroxylase,[212] lysyl hydroxylase,[213] deacetoxyvindoline hydroxylase,[214] and HPP dioxygenase[215,216] support an ordered binding mechanism in which α-keto carboxylate binding occurs prior to binding of either dioxygen or substrate. The binding of the α-keto carboxylate leads to a six-coordinate iron(II) center with a bidentate α-keto carboxylate, which displaces two of the water molecules from the metal center (Figures 20B and 21A).[111,128,129,133,136] The equatorial plane of the dis-

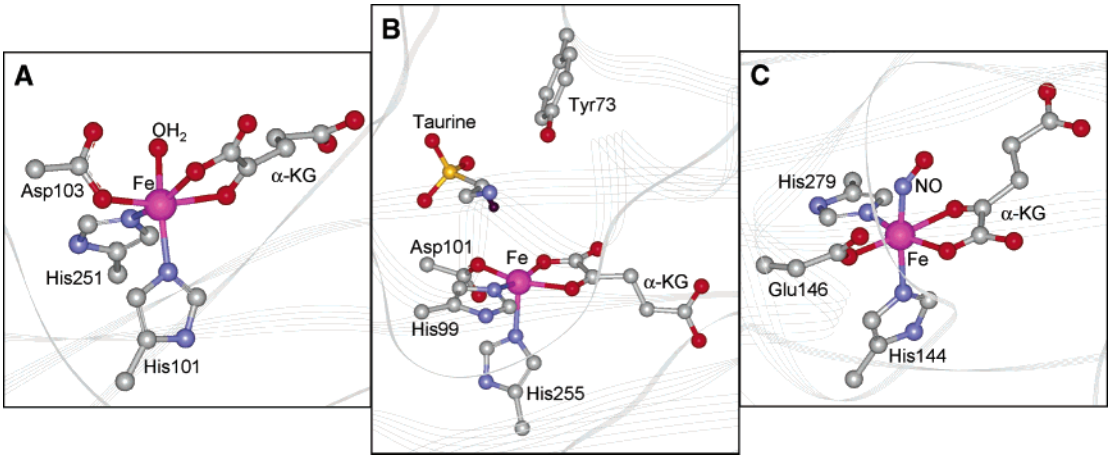

Figure 21. Crystallographically observed stages in the catalytic cycle of α-keto acid-dependent enzymes, as the binary complex (1NX4.pdb), ternary complex (1GQW.pdb), and the NO adduct of the ternary complex (1GVG.pdb).

torted octahedron is composed of the nearly planar five-membered ring of the chelated α-keto carboxylate as well as a histidine and a carboxylate of the facial triad, with the α-keto group bound trans to the aspartate or glutamate residue. Apical sites are occupied by the remaining histidine residue and one water molecule, which appears to have a hydrogen-bonding interaction with the carboxylate residue (Figure 21A). The chelation of the α-keto carboxylate to the iron(II) center observed crystallographically gives rise to several characteristic low-intensity metal-to-ligand charge-transfer bands in the visible region that serve as a useful probe for optical,[217] MCD and CD,[218−220] and resonance Raman experiments.[111] These studies, carried out mainly on CAS and TauD, support the notion that the metal center is six-coordinate at this stage of the mechanism.

Consensus on the next step in the catalytic mechanism has not been reached. Steady-state kinetic studies on prolyl hydroxylase suggest that oxygen binding occurs prior to substrate binding,[210,211] but spectroscopic studies of CAS and TauD[111,217−220] indicate the opposite sequence, i.e., substrate binding prior to O_2. Indeed, the latter studies show that substrate binding results in the formation of a coordinatively unsaturated iron(II) center, presumably by loss of the remaining water ligand, that primes the metal center for oxygen binding and activation (Figure 20C). Crystal structures of the ternary enzyme−2-OG−substrate complexes of CAS and TauD (Figure 21B)[129,131] (but not of anthocyanidin synthase[133]) support the proposed substrate-induced conversion from a six-coordinate to a five-coordinate metal center. Substrate binding may induce a shift of the carboxylate residue, removing the hydrogen-bonding interaction with the water ligand in the binary complex and facilitating its departure.

In these three structures of ternary enzyme−2-OG−substrate complexes, the putative site for O_2 binding is trans to the apical His residue. Though no O_2 adducts have been observed, a structure with the O_2 surrogate NO has been determined for CAS (Figure 21C), where the nitrosyl is bound trans to a histidine residue.[221] However, this histidine residue was originally trans to the carboxylate of the α-keto acid in the binary enzyme−2-OG complex, suggesting a rearrangement of the chelated α-keto carboxylate upon substrate binding. In both the binary and ternary complexes, the interactions of the conserved (R/K)XS prototype with the C-5 carboxylate of the 2-oxoglutarate are maintained and dioxygen can bind to the position trans to either histidine of the facial triad, but not trans to the carboxylate. However, O_2 is suggested to bind trans to the glutamate residue of HPP dioxygenase, on the basis of a model of the enzyme−substrate complex generated by using the closely related structure of the extradiol enzyme BphC as a basis (Figure 13).[137] O_2 is also proposed to bind trans to the carboxylate residue in isopenicillin N synthase (IPNS, see next section). Perhaps the 2-His-1-carboxylate motif provides a platform upon which oxygen activation can occur trans to any of the three ligands; the implications of this variability in trans ligand for the subsequent O_2 chemistry remain to be investigated.

In the proposed mechanism, the binding of dioxygen leads to an adduct with significant iron(III) superoxide radical anion character (Figure 20D). Superoxide is a potent nucleophile that has been found capable of effecting the decarboxylation of α-keto acids,[222] particularly when the α-keto carbon is activated by a metal center. Furthermore, superoxide scavengers are competitive inhibitors of O_2 consumption in α-keto acid-dependent enzymes.[210,223] It is also clear that the oxidative decarboxylation of the α-keto acid can be uncoupled from substrate oxidation, particularly when no substrate or a poor substrate analogue is employed.[210,213,224−226] O_2 attack on the coordinated α-keto acid should lead to the formation of a high-valent intermediate that is responsible for the oxidation of substrate in α-keto carboxylate-dependent enzymes. Such a species has been postulated as an iron(IV)−peroxo species (Figure 20E) that can lose CO_2 to form an iron(II)−peracid adduct (not shown) and then undergo heterolytic cleavage of the O−O bond to yield an iron(IV)−oxo species (Figure 20F). Peracid substitution for the α-keto carboxylate/O_2 combination has been attempted but has not been successful in eliciting the desired oxidation in prolyl hydroxylase[227] and HPP dioxygenase.[228] This suggests that either a

peracid is not involved or such a species must be generated within the active site and cannot be introduced into the active site in a peroxide shunt-like manner.

Direct evidence for the involvement of an iron(IV) species in the enzyme mechanism has very recently been obtained from rapid freeze−quench Mössbauer studies of the reaction of the TauD−2-OG−taurine complex with O_2.[229] This intermediate with Mössbauer parameters $\Delta E_Q = 0.88$ mm/s and $\delta = 0.31$ mm/s is interpreted to have a high-spin iron(IV) center. Although the isomer shift approaches that of a high-spin iron(III) center,[230] one-electron cryoreduction of the intermediate affords a species with properties typical of a high-spin iron(III) center, thereby corroborating the iron(IV) oxidation state assignment. Bollinger, Krebs, and co-workers have also shown that this intermediate is mechanistically significant.[231] Its decay in the presence of taurine is retarded by the use of the C-1 dideuterated substrate isotopomer with a large primary kinetic isotope effect, estimated to be about 28−50. Thus, the high-valent species appears to carry out rate-determining hydrogen abstraction at the C-1 carbon of the substrate. This exciting result represents the first example of an iron(IV) intermediate observed for a mononuclear nonheme iron enzyme.

There is also indirect evidence for the involvement of an iron(IV)−oxo species for other enzymes in this class. HPP dioxygenase can catalyze sulfoxidations,[232] while thymine hydroxylase can catalyze olefin epoxidation, sulfoxidation, and N-demethylation besides the hydroxylation of the 5-methyl group of thymine,[233] a reactivity pattern reminiscent of cytochrome P450. Furthermore, ^{18}O from $H_2{}^{18}O$ can be incorporated into the oxygenated product for DAOCS,[234−236] CAS,[237] α-keto isocaproate oxygenase,[205] and HPP dioxygenase.[193] This label incorporation suggests an intermediate such as an iron−oxo or iron−hydroxyl species with a lifetime long enough to undergo solvent exchange. On the other hand, there is little oxygen incorporation from water into the hydroxylated products of prolyl hydroxylase, thymine hydroxylase, and aspargine hydroxylase.[233,238−242]

Substrate hydroxylation is postulated to occur via a mechanism analogous to that for cytochrome P450, that is, a two-step process involving hydrogen atom abstraction by the oxoiron(IV) species followed by oxygen rebound.[243] One difference is that cytochrome P450 uses a formally $Fe^{III}/Fe^{V}{=}O$ couple, while the α-keto acid-dependent enzymes must use a formally $Fe^{II}/Fe^{IV}{=}O$ couple. As observed in the crystal structure of the P450−camphor complex,[244] the substrate taurine is ideally positioned in the structure of the ternary TauD−2-OG−substrate complex for the hydroxylation of the target C−H bond (Figure 21B).[131] Kinetic isotope effects observed for thymine hydroxylase[233] and clavaminate synthase[245] support the two-step mechanism, as do experiments with radical probe substrate analogues for γ-butyrobetaine hydroxylase,[246] DAOCS,[247] and prolyl 4-hydroxylase.[248] For enzymes that catalyze ring cyclization or desaturation instead of hydroxylation, the rebound step is replaced by a step involving either oxidative ligand transfer to close a ring as in the second CAS-catalyzed reaction or a second hydrogen-atom abstraction to form a double bond as in the third CAS-catalyzed reaction (Figure 19H).

CO_2 is a product of reactions catalyzed by the α-keto acid-dependent enzymes. Steady-state kinetic studies suggest that carbon dioxide dissociation follows release of the hydroxylated product.[211,213,249] There is a crystal structure of an enzyme−succinate−CO_2 complex, obtained from a deletion mutant of DAOCS crystallized in the presence of succinate and $NaHCO_3$, that may serve as a model for an enzyme−product complex.[250] The carbon dioxide binds in a linear fashion at the site trans to the equatorial histidine, while the succinate carboxylate is bound across from the aspartate residue, sites originally occupied by the 2-OG carboxylate and keto functions, respectively. Yet succinate does not interact with the (R/K)XS motif that normally binds the C-5 anion of 2-oxoglutarate, raising some doubt as to whether this complex is catalytically relevant. Additional evidence for the binding of bicarbonate to the metal center comes from observations on self-hydroxylated TauD (see below) obtained upon decay of the binary enzyme−2-OG complex.[251,252] The initially formed iron(III)−DOPA chromophore has a band centered at 550 nm, which then red-shifts to 700 nm on standing, consistent with the loss of a charged ligand. The 700-nm chromophore can be converted back to the 550-nm species by addition of excess bicarbonate.[252]

α-Keto acid-dependent enzymes often have a requirement for ascorbate for maximal activity. Because ascorbate is consumed at sub-stoichiometric levels during the course of the catalytic cycle, the ascorbate requirement is believed to reverse enzymatic inactivation due to formation of the iron(III) enzyme that occurs when α-keto acid decarboxylation becomes uncoupled from substrate oxidation. Ascorbate is thus proposed to act as a reductant to return the metal center to its active iron(II) state.[211,213,224,226]

Synthetic complexes modeling α-keto carboxylate-dependent enzymes have played a key role in furthering our understanding of these enzymes. Several $[Fe^{II}(L)(\alpha\text{-keto acid})]$ complexes have been reported as functional models using tetradentate and tridentate ligands. The crystal structures of $[Fe^{II}(TPA)(BF)]^+$ (BF = benzoylformate), $[Fe^{II}(6\text{-}Me_3\text{-}TPA)(BF)]^+$ (Figure 22A), and $[Fe(Tp^{iPr,tBu})(BF)]$ (Figure 22B) show that an α-keto carboxylate can coordinate to the iron(II) center as either a monodentate or bidentate ligand.[116,253] However, only bidentate binding of the α-keto acid to the iron(II) center gives rise to the unique visible chromophore[111,112,116,253,254] (Figure 23A) that is also observed in the binary and ternary enzyme complexes (Figure 23B). These features are sensitive to the nature of the α-keto acid (benzoylformate vs pyruvate), the Lewis basicity of the supporting L (TPA vs 6-Me_3-TPA vs Tp^{R2}), and the coordination number of the metal center. For example, the addition of monodentate Lewis bases to five-coordinate $[Fe(Tp^{Ph2})(BF)]$ results in energy downshifts in both the charge-transfer bands and the vibrational features associated with the bidentate α-keto carboxylate.[111] Shifts in the opposite direction

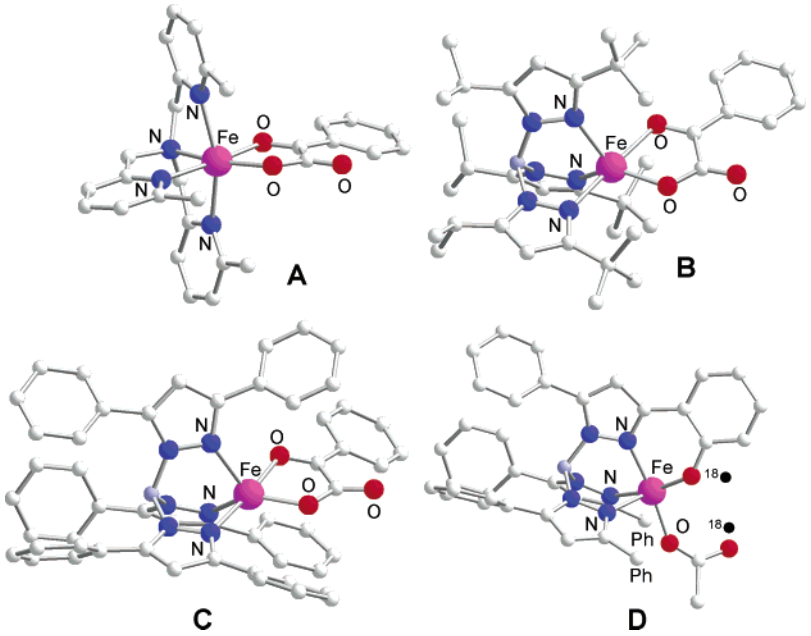

Figure 22. Models for α-keto acid dependent enzymes: (A) [Fe(6-Me$_3$-TPA)(BF)]$^+$, (B) [Fe(Tp^{iPr,tBu})(BF)], (C) [Fe(Tp^{Ph_2})(BF)], and (D) its oxygenation product [Fe(Tp^{Ph_2*})(O$_2$CR)].

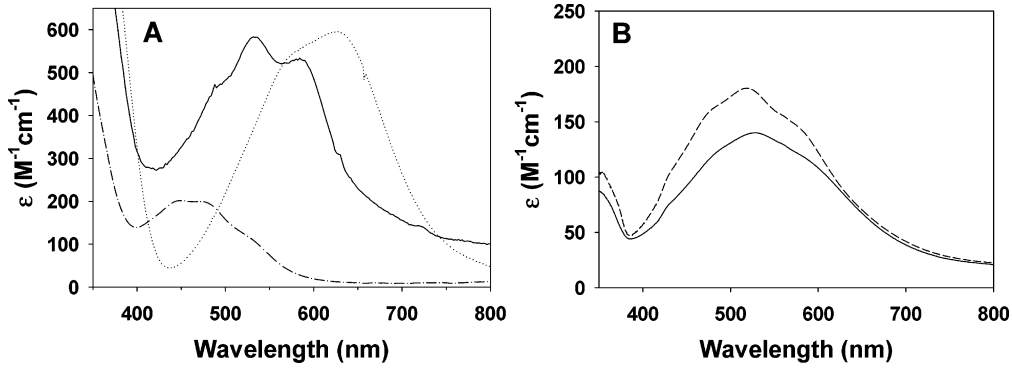

Figure 23. Visible spectra of [Fe(Tp^{Ph_2})(pyruvate)] (—•—), [Fe(Tp^{Ph2})(BF)] (—), and [Fe(Tp^{Ph_2})(BF)] + pyridine (···) in C_6D_6 (A), compared to those of the TauD/2-OG (—) and the TauD/2-OG/taurine (— —) complexes (B).

observed in the optical and vibrational features of the binary TauD−2-OG complex upon substrate binding[111] support the notion that the six-coordinate metal center in the binary complex becomes five-coordinate in the ternary complex prior to its interaction with O_2 (Figure 20, B → C).[220]

The iron(II)−α-keto carboxylate complexes exhibit a range of reactivity toward dioxygen. For example, [Fe(Tp^{iPr,tBu})(BF)] is inert to oxygen, despite having a coordinatively unsaturated metal center; its lack of reactivity is attributed to steric congestion about the iron(II) center.[253] On the other hand, the neutral tetradentate N4 ligands afford six-coordinate complexes that require days to undergo oxidative decarboxylation,[116] while the tridentate monoanionic Tp^{R_2} complexes (R = Me, Ph) react with O_2 within an hour.[112,254] The difference of nearly 2 orders of magnitude in reaction rate emphasizes the importance of a vacant site for O_2 coordination in promoting the oxidative decarboxylation of the bound α-keto carboxylate.

The rates of oxygenation have been investigated for two series of substituted benzoylformate complexes, [Fe(6-Me$_3$-TPA)(BF)]$^+$ and [Fe(Tp^{Ph_2})(BF)]. The rate of the oxidative decarboxylation increases as the substituent of the benzoylformate becomes more electron-withdrawing, affording Hammett ρ values of +1.07 and +1.3, respectively.[112,116] This trend suggests that oxidative decarboxylation involves a nucleophilic attack, most plausibly by attack of the iron(III)−superoxide at the keto carbon of benzoylformate initiating decarboxylation (Figure 20, D → E). Though the iron(III)−superoxide intermediate has not been directly observed, the proximity of the electrophilic α-keto functionality provides an efficient means for trapping the nascent nucleophilic superoxide to drive the reaction to completion. This effectively couples the oxidative decarboxylation of the α-keto carboxylate to the activation of dioxygen to generate the active oxidant.

All of the model complexes that react with O_2 afford quantitative yields of the decarboxylated α-keto acid, but in only two cases can the active oxidant be trapped by a substrate. Intermolecular olefin epoxidation has been observed in the case of [Fe^{II}(Tp^{Me_2})(BF)] complex.[254] This complex reacts with O_2 to form a species capable of stereospecific oxidation of *cis*-stilbene to its oxide as the product. However, *trans*-stilbene is not epoxidized, suggesting that the active oxidant is capable of steric discrimination.

The other example is an intramolecular hydroxylation of a ligand phenyl ring of [Fe(Tp^{Ph_2})(BF)] upon exposure to O_2 (Figure 22C,D).[110,112] The hydroxylated product is obtained within an hour in 70% yield. In contrast, the corresponding [Fe(Tp^{Ph_2})(benzoate)] complex also reacts with O_2 to give the same product in 55% yield, but this reaction requires 2−3 days, clearly demonstrating the key role the α-keto group plays in activating O_2. The use of $^{18}O_2$ results in the incorporation of one labeled oxygen into the benzoate product and the other into the hydroxylated phenyl ring of the Tp ligand, effectively capturing the dioxygenase nature of the enzymes. The absence of ^{18}O incorporation when the reaction is carried out in the presence of $H_2{}^{18}O$ suggests that the iron(IV)−oxo species, if involved in the mechanism, has too short a lifetime relative to $H_2{}^{18}O$ exchange in the biomimetic transformation. This may be due to the proximity of the phenyl group, which traps the electrophilic oxidizing species as it is formed in the course of the reaction.

The biomimetic arene hydroxylation reaction in fact anticipated the subsequent observation that some 2-OG-dependent enzymes can carry out hydroxylation of aromatic residues near the active site in the absence of the primary substrate. Thus, oxygen activation can still occur in the active sites of TfdA and TauD without the primary substrate, albeit much more slowly.[251,252,255] The oxidant generated under these conditions is utilized to hydroxylate a nearby aromatic amino acid residue such as Trp112 of TfdA or Tyr73 of TauD. These hydroxylated derivatives bind to the iron center in the enzyme and give rise to intense chromophores that have been identified by their characteristic resonance Raman vibrations. Interestingly, studies in $H_2{}^{18}O$ show that the oxygen incorporated into the hydroxylated residue derives solely from solvent water, and not from dioxygen.[252,255] Furthermore, a tyrosyl radical intermediate has been observed for TauD,[251] suggesting that the hydroxylation is a two-step process involving initial one-electron oxidation (or hydrogen-atom abstraction) of the aromatic residue followed by C−O bond formation (Figure 24). Thus, the putative Fe^{IV}═O oxidant in this reaction would be reduced to Fe^{III}—OH in the first step, so oxygen-atom exchange with solvent may occur at either the Fe^{IV} or the Fe^{III} stage prior to the rebound step. Such a self-hydroxylation may explain the isolation of a HPP dioxygenase that is blue in color due to a tyrosinate-to-iron(III) charge-transfer band.[256] Since there is no tyrosine residue in the vicinity of the iron active site in the crystal structure of an HPP dioxygenase,[137] the earlier reported blue HPP dioxygenase may arise from a similar post-translational modification of a nearby phenylalanine residue; this conjecture requires substantiation.

3.3. Isopenicillin N Synthase

Isopenicillin N synthase (IPNS) is a nonheme iron enzyme that activates O_2 and has the conserved HX-(D/E)X$_m$HX$_n$RXS sequence motif found in many 2-oxoglutarate-dependent enzymes but does not require 2-oxoglutarate for activity.[180,257] It is a microbial

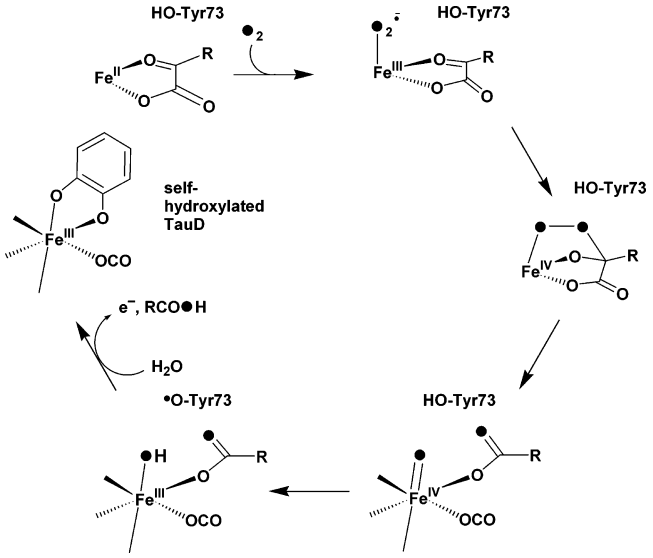

Figure 24. Proposed mechanism of TauD self-hydroxylation.

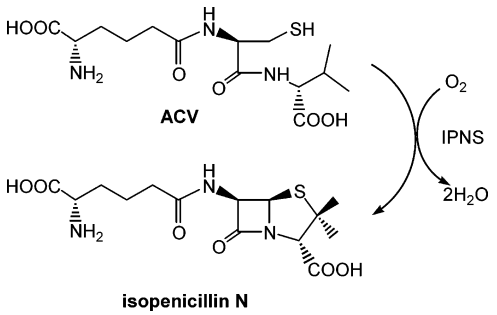

Figure 25. Reaction catalyzed by IPNS.

enzyme found in *Cephalosporium*, *Penicillium*, and *Streptomyces* strains that catalyzes the formation of isopenicillin N from δ-(L-α-aminoadipoyl)-L-cysteinyl-D-valine (ACV) (Figure 25). Crystallographic studies have established IPNS as another member of the superfamily of nonheme iron enzymes with active sites containing a 2-His-1-carboxylate facial triad. Indeed, the crystallographic information available for this enzyme is the most extensive of any member of this superfamily and provides a treasure trove of mechanistic insights. Only the Mn(II)-substituted IPNS from *Aspergillus nidulans* has been crystallized in the absence of substrate; its structure reveals a six-coordinate metal center with four endogenous protein ligands (His214, Asp216, His270, and Gln330) and two H_2O molecules occupying the remaining cis ligand sites (Figure 26A).[258] As shown by the crystal structure of the Fe^{II}IPNS−ACV complex, substrate binding results in the displacement of the Gln ligand by the ACV thiolate sulfur (Figure 26B),[259] confirming earlier EXAFS results that showed a sulfur scatterer at 2.3 Å.[260] The distal carboxylate of the adipoyl moiety of ACV interacts with the conserved RXS motif, corresponding to the 2-OG C-5 carboxylate interaction in 2-OG-dependent enzymes.

O_2 can interact with the metal center only at this stage. This suggests that the coordination of the ACV thiolate primes the iron(II) center for its reaction with O_2, presumably by shifting the Fe$^{III/II}$ redox potential to a more negative value, as proposed for the extra-

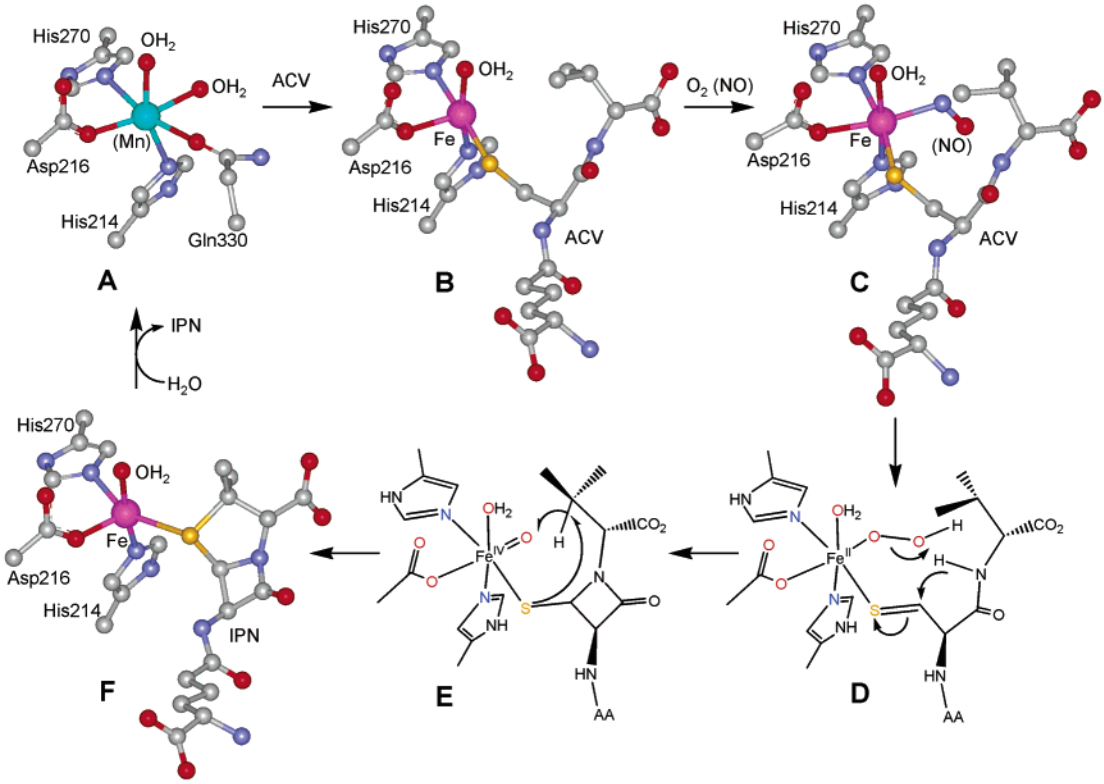

Figure 26. Proposed reaction sequence for IPNS using crystallographic information for (A) Mn·IPNS (1IPS.pdb), (B) Fe·IPNS·ACV (1BKO.pdb), (C) Fe·IPNS·ACV·NO (1BLZ.pdb), (D) proposed Fe^{II}—OOH, (E) proposed Fe^{IV}=O, and (F) Fe·IPNS·IPN (1QJE.pdb).

diol-cleaving dioxygenases and the 2-OG-dependent enzymes. To date, there is no spectroscopic evidence for an Fe^{II}·IPNS·ACV·O_2 adduct, as such an intermediate appears to be too reactive to be trapped. However, the corresponding Fe^{II}·IPNS·ACV·NO adduct has been studied. Exposure of NO to the substrate-bound iron(II) center engenders an $S = {}^3/_2$ EPR signal characteristic of high-spin iron(II)-nitrosyl adducts[261] and gives rise to a short (1.7 Å) Fe—NO bond observed by EXAFS.[260] The crystal structure of the ternary enzyme—substrate—NO complex (Figure 26C) confirms many aspects of the active site earlier deduced from spectroscopic experiments and shows that NO binds trans to Asp216 with its oxygen atom equidistant from both the valine nitrogen and the cysteinyl β-carbon.[262] Assuming that NO serves as an O_2 surrogate, these are the atoms from which a hydrogen atom must be abstracted to close the β-lactam ring in the first stage of isopenicillin formation.

The elegant and comprehensive work of Baldwin and co-workers[263] using a number of ACV analogues has shed light on the steps subsequent to O_2 binding and led to the mechanism for IPNS action shown in Figure 26. The reduction of O_2 occurs in two stages, with the sequential formation of the β-lactam and the thiazolidine rings corresponding to two distinct two-electron reduction steps. In the first stage, O_2 is reduced to the peroxide oxidation level concomitant with the oxidation of the Cys thiolate to a thioaldehyde (or some equivalent moiety) (Figure 26D). O—O bond heterolysis leads to the abstraction of the proton from the valinyl peptide nitrogen, generating an Fe^{IV}=O intermediate and the amidate anion. The latter then nucleophilically attacks the thiocarbonyl carbon to form the β-lactam ring and regenerate the thiolate (Figure 26E). The Fe^{IV}=O moiety then initiates the second stage of the reaction by abstraction of the valinyl C3—H, followed by C3—S bond formation to generate the thiazolidine ring (Figure 26F).

Much of the recent crystallographic work on IPNS has involved brief exposure of crystalline enzyme—substrate complexes to hyperbaric O_2, followed by cryo-crystallography.[264,265] With the natural substrate ACV, the enzyme—product complex is observed with the thiazolidine sulfur of isopenicillin coordinated to the metal center (Figure 26F). With AC*O*V, the substrate analogue wherein the valine peptide bond is converted to an ester linkage, β-lactam ring formation is not possible and the thiolate of the ACV substrate is instead oxidized to a thiocarboxylate, with one atom of O_2 incorporated into the thiocarboxylate (Figure 27A). On the other hand, ACmC, the substrate analogue where the valine residue is replaced by *S*-methylcysteine, affords a product wherein the reaction cycle is interrupted after the formation of the β-lactam ring; the Fe^{IV}=O moiety is instead trapped by the *S*-methylcysteine to form a sulfoxide that is coordinated to the iron center trans to the Asp residue (Figure 27B). This result corroborates the proposal that O_2 binds trans to the Asp residue, as indicated by the NO complex (Figure 26C), and is converted to an oxo group in the latter part of the reaction cycle. Besides oxo transfer to sulfide, the Fe^{IV}=O moiety can also epoxidize double bonds, as demonstrated by the substrate analogue with the valine replaced by allylglycine,[266] and can

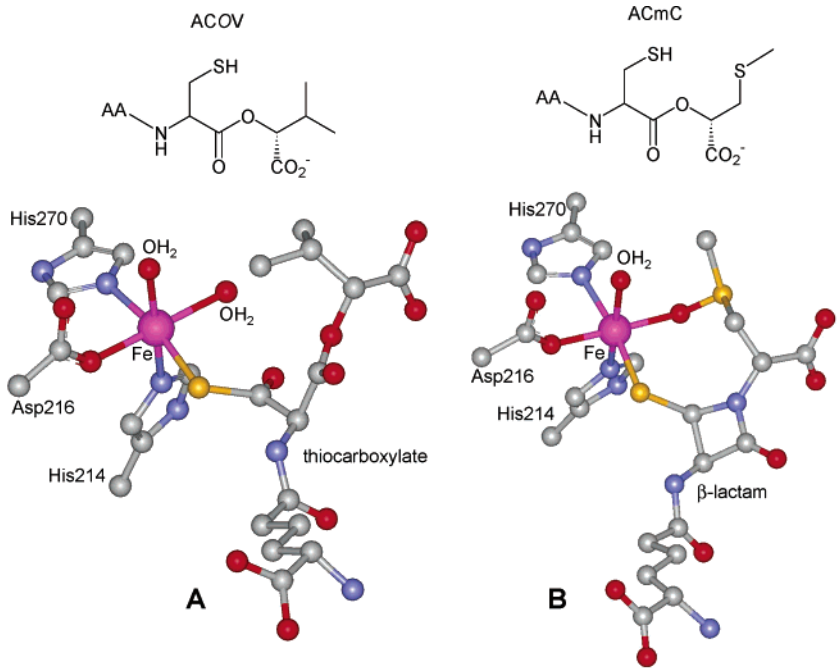

Figure 27. Active site structures of enzyme−product complexes from the oxidation of (A) ACOV (1HB4.pdb) and (B) ACmC (1QJF.pdb).

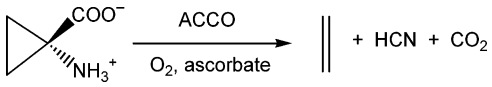

Figure 28. Reaction catalyzed by ACCO.

carry out hydrogen-atom abstraction, as shown by a ring-opening isomerization of the product derived from the cyclopropylalanine analogue.[267] Thus, there is strong experimental evidence for the various steps of the proposed IPNS mechanism (Figure 26). This scheme is strongly supported by DFT calculations,[268] but there are as yet no model studies that directly address the chemically intriguing steps of the mechanism.

3.4. ACCO, the Ethylene-Forming Enzyme

ACCO, or 1-aminocyclopropane-1-carboxylate oxidase, is an enzyme that produces the plant hormone ethylene to regulate many aspects of plant growth and development, including germination, fruit ripening, and senescence.[269,270] Ethylene is produced by the $2e^-$ oxidation of the unusual amino acid, 1-aminocyclopropane-1-carboxylate (ACC), along with HCN and CO_2 (Figure 28).[271−274] Like IPNS, ACCO is also a nonheme iron enzyme with the HX(D/E)X_mHX_nRXS sequence motif conserved in many 2-oxoglutarate-dependent enzymes but does not require 2-oxoglutarate for activity.[275,276] Instead it requires ascorbate and CO_2 (or bicarbonate) for activity.[277] Unlike the other enzymes discussed in this section, a crystal structure of ACCO is not yet available, so what is known about the iron center in ACCO is based on spectroscopic approaches and steady-state kinetics experiments.

An attractive mechanistic proposal that has been considered for ACCO involves initial coordination of the ascorbate to the iron(II) center.[278,279] Ascorbate has an enediol unit that would serve as an excellent bidentate ligand for iron and form a complex that would resemble the bidentate catecholate of the extradiol-cleaving dioxygenases or the 2-oxoglutarate of α-keto acid-dependent enzymes. Reaction with O_2 would then afford an iron-based oxidant or a diffusible reactive oxygen species[280] that would generate an ACC radical intermediate[270,281] to initiate cyclopropyl ring breakdown to form ethylene. The alternative is for the ACC to bind to the metal center since it too has the functionalities to form a five-membered chelate ring with the iron. Not surprisingly, with three substrates (plus CO_2 or bicarbonate) to assemble into the enzyme active site, it has been difficult to establish an order of binding for steady-state kinetic analysis, as illustrated by two recent independent studies. Brunhuber et al. find that either ascorbate or ACC can bind to the enzyme first but ascorbate is favored.[282] After one substrate is bound, then O_2 binds, followed by the other substrate. On the other hand, Thrower et al. conclude that ACC binding must precede O_2 binding.[283] Ascorbate binds third in the order, although its binding to the enzyme before ACC could not be rigorously ruled out.

Near-IR CD and magnetic circular dichroism studies that monitor the iron coordination environment[284] indicate that the active site iron is six-coordinate in resting Fe^{II}ACCO. In the presence of CO_2, the iron center becomes five-coordinate only when both ACC and ascorbate are present, consistent with the mechanistic paradigm for O_2 activation by this superfamily of enzymes (Figure 11). Thus, O_2 can bind only after all of the required components for a turnover are bound to the enzyme, thereby preventing adventitious generation of reactive oxygen species. However, in the absence of CO_2, ACC binding alone converts the iron center to five-coordinate;[284] this leads to uncoupling and inactivation of the enzyme.[285]

Direct spectroscopic evidence for substrate coordination to the iron has been obtained from ENDOR

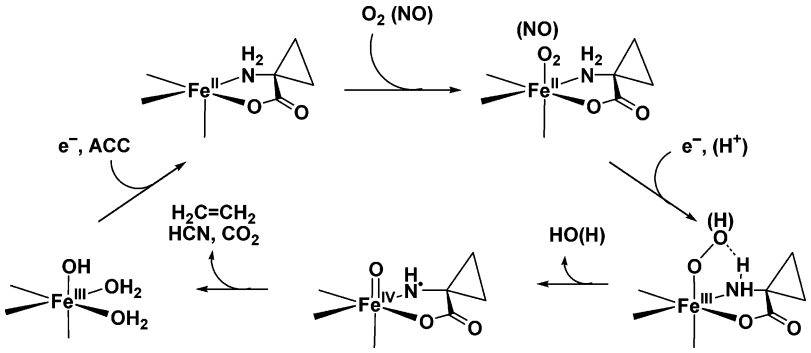

Figure 29. Hypothetical ACCO mechanism.

studies of the ternary Fe^{II}·ACCO·alanine·NO complex.[286] Alanine inhibits ACCO competitively with respect to ACC and is presumed to be a substrate analogue. This adduct exhibits an $S = {}^3/_2$ EPR signal typical of nonheme {Fe−NO}^{7} complexes. Studies with ^{15}N- and ^{17}O-labeled alanine demonstrate that it coordinates to the iron via both amino and carboxylate groups. The fact that an NO complex can be formed in the presence of alanine or ACC strongly suggests that ACC and O_2 can bind simultaneously to the iron. On the other hand, ascorbate binding is competitive with NO. These results, together with near-IR CD and MCD data,[284] concur with the steady-state kinetic analysis of Thrower et al.[283] and support a mechanism in which the iron serves to bind ACC and O_2 simultaneously (Figure 29). As with the enzymes discussed earlier in this section, this fixes the relative orientations of the two substrates within the active site to initiate catalysis. Ascorbate is proposed to play its reductant role subsequent to formation of the ternary E·S·O_2 complex, either simply by reducing the H_2O_2 that could be hypothetically produced in this 2e$^-$ oxidation of ACC or more engagedly by introducing its two electrons one at a time at key points of the cycle. The precise role of the requisite CO_2 or HCO_3^- is also not established and thus not illustrated.

Some insight into the roles of CO_2 and ascorbate in the ethylene formation mechanism has very recently been obtained from single-turnover experiments.[285] In these experiments, ethylene formation was observed in the absence of ascorbate, so ascorbate is not absolutely required for this reaction. In contrast, ethylene was formed only in the presence of added bicarbonate (under conditions where all dissolved CO_2 has been removed), so CO_2 or bicarbonate is essential for enzyme turnover. These observations support the minimal mechanism proposed in Figure 29.

There is, however, clearly an important role for ascorbate that can be deduced from these single-turnover experiments. In the absence of ascorbate, 0.35 mol of ethylene/mol of ACCO was formed, while all the iron(II) was converted to iron(III). It would thus appear that the iron(II) provides the necessary two electrons for the reaction in place of ascorbate and that the enzyme is only 70% efficient. However, ethylene formation occurred over a 30-min time scale, a rate of formation much slower than catalytic turnover. Interestingly, addition of 1 equiv of ascorbate resulted in the formation of an additional equivalent ethylene, but at a significantly more rapid rate. Since the concentration of ascorbate present was only 10% of the K_m value obtained from steady-state kinetic analysis, a new effector role for ascorbate has been postulated to rationalize these results. From these accumulated results, it is clear that the complexity of the ACCO chemistry presents a challenge for mechanistic enzymologists and will require further scrutiny.

3.5. Pterin-Dependent Hydroxylases

The pterin-dependent oxygenases, typified by the aryl amino acid hydroxylases, are a small family of closely related enzymes essential to mammalian physiology that use tetrahydrobiopterin (BH_4) as a two-electron-donating cofactor. Members of this class include phenylalanine (PheH), tyrosine (TryH), and tryptophan (TrpH) hydroxylases, which effect regiospecific aromatic hydroxylations of the namesake amino acids. The state of knowledge regarding these enzymes was exhaustively reviewed in the Bioinorganic Enzymology issue of *Chemical Reviews* in 1996,[287] and several more specific reviews have appeared since then.[3,288−290] The most significant recent advance in the knowledge of these enzymes is the availability of X-ray crystal structures for all three enzymes that constrain the mechanistic options for oxygen activation.[288]

Phenylalanine hydroxylase is located primarily in the liver and affords the major pathway for phenylalanine catabolism. In contrast, the other two enzymes function primarily within the central and peripheral nervous system, providing the rate-limiting initial steps in biosynthetic pathways for a range of neurotransmitters including dopamine, norepinephrine, and epinephrine for TyrH and serotonin and melatonin for TrpH. Dysfunctions of these essential enzymatic activities have been implicated in several severe neurological and psychological diseases, and this has stimulated the significant biochemical and biomedical research effort to date.

The mammalian (rat or human) enzymes are composed of identical 52-kDa subunits, which interact through a significantly conserved C-terminal domain of ca. 40 residues to form dimeric and tetrameric assemblies.[139,291] The middle ca. 270 residues are highly conserved in each enzyme (ca. 80% sequence homology) and contain the metal-binding site associated with catalysis, which is buried within the enzyme core.[288] The initial 100−170 N-terminal

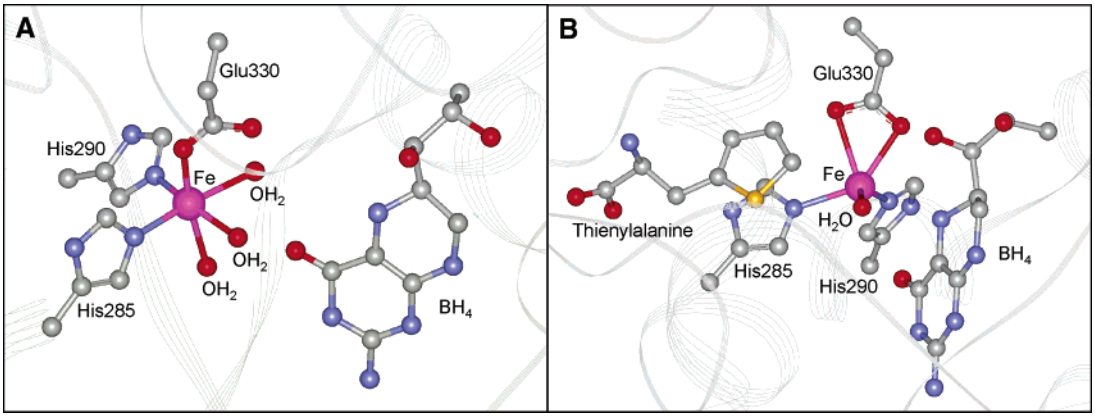

Figure 30. Crystal structures of phenylalanine hydroxylase: (A) the binary enzyme·BH_4 complex (1J8U.pdb) and (B) the ternary complex with L-thienylalanine (1KWO.pdb).

residues differ in each enzyme and afford regulatory domains that control enzymatic activities by distinct mechanisms. In hPheH for example, this domain appears to function as a gate that physically blocks the substrate channel leading to the active site.[140] Allosteric binding of substrate, which is stabilized by site-specific phosphorylation at Ser16,[292] apparently triggers a conformational change, which opens the gate and permits catalysis but is suppressed by BH_4 binding near the "hinge". Significantly, such complications can be avoided by expression of truncated deletion mutants lacking both the C- and N-terminal domains, which exhibit full, unregulated oxygenase activities. In fact, most recent biophysical and crystallographic studies have taken advantage of this observation.[293] Moreover, a monomeric, 30-kDa, iron-dependent PheH has been identified in a bacterium (*Chromobacterium violaceum*), which exhibits high sequence homology to the catalytic cores of the mammalian enzymes.[294] Steady-state kinetic studies indicate that bacterial PheH has a sequential binding order of substrate, cofactor, and then dioxygen.[295] However, mammalian PheH follows a random binding sequence,[296] while for mammalian TyrH the order is pterin, dioxygen, and finally substrate.[297] So a consensus reactant binding sequence for this family of pterin-dependent enzymes has not yet been established.

High-resolution crystal structures have now been solved for mammalian (human and/or rat) PheH,[139,140,298] TyrH,[142,299] and TrpH,[143] as well as for bacterial PheH.[141] Most of these structures have been obtained from enzymes with truncated catalytic domains in an inactive, oxidized form with bound iron(III) and BH_2. Very recently, structures have become available of the active human PheH catalytic domain as the iron(II) complex, the binary BH_4 complex, and ternary complexes with BH_4 and the substrate analogues L-thienylalanine (Figure 30) or L-norleucine.[300−302]

The iron active site can be found in a deep central cleft some 10 Å beneath the enzyme surface.[288] The iron center is six-coordinate, being ligated to a 2-His-1-carboxylate facial triad (consisting of His285, His290, and Glu330 for hPheH) and three water molecules (Figure 30A). His290 is disposed along a vector from iron toward the pterin and can be considered as the axial donor ligand; hence, His285 and Glu330 are designated equatorial. The pterin binds to a site located just beyond the iron center at the very base of the cleft and is π-stacked against a conserved phenylalanine (Phe254 in hPheH) located on the back wall of the cleft. The pterin also hydrogen bonds to a number of residues, particularly to a conserved glutamate (Glu286) via the hydroxypropyl side chain. The stereochemistry of the pterin cofactor oxidation product has been determined, and only the single diasteromer corresponding to hydroxylation of the structurally exposed face of the pterin is formed.[303] The distance from the metal to the reactive pterin C4a is on the order of 6 Å in both the iron(II) and iron(III) structures.

Unlike the cytochromes P450, which feature a large, hydrophobic distal pocket that will accommodate a range of aliphatic and aromatic substrates,[300] known substrates for the aryl amino acid hydroxylases are limited to a small range of natural and unnatural amino acids.[289] X-ray, NMR, and molecular mechanics studies indicate that the aromatic substrate binds in a hydrophobic pocket close to the iron and also via a hydrogen-bonding interaction between the amino acid carboxylate and a highly conserved arginine (Arg270), which is complemented by an alcohol side chain from residue 278 (Thr in PheH and TrpH, Ser in TyrH).[300,301,304,305] Removal of the salt bridge interaction by site-directed mutagenesis essentially abolishes substrate binding.[306] In the structure of the ternary complex, the reactive carbon is poised 4.2 Å from the active site iron, directly over the axial site trans to His290 (Figure 30B).[301]

Large changes are observed upon binding of substrate to form the ternary enzyme−pterin−substrate complex. As shown by the crystal structure of the ternary PheH·BH_4·L-thienylalanine complex, the iron center becomes five-coordinate and adopts a square pyramidal geometry (Figure 30B).[301] Two water ligands are lost, and monodentate Glu330 becomes bidentate. Moreover, the pterin is significantly displaced toward the iron center, as indicated by the decrease of Fe−C4a distance from 5.9 to 4.5 Å. These changes in principle facilitate dioxygen binding at the metal as well as attack of the nearby pterin. However, the single aqua ligand retained in the ternary

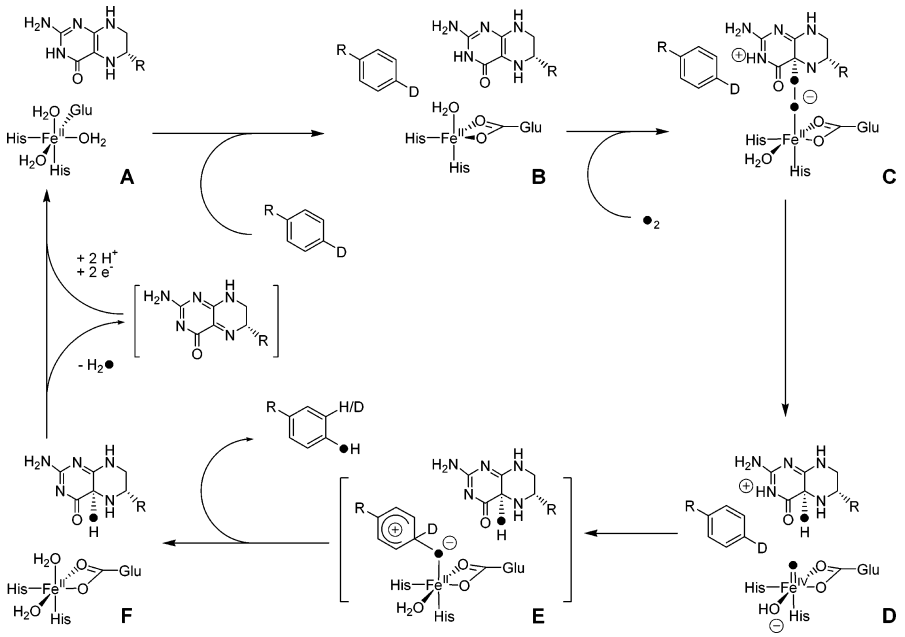

Figure 31. Proposed mechanism for pterin-dependent hydroxylases.

complex occupies the apical position of the square pyramid proximal to the BH_4 moiety, so formation of an Fe−O−O-pterin adduct would require the loss or shift of this water ligand. Near-IR, MCD, and XAS studies of the PheH−tetrahydropterin−phenylalanine complex in frozen solution are in accord with the crystallographic results, showing that the iron(II) center is six-coordinate in the resting iron(II) form and the binary complexes with either phenylalanine or a pterin cofactor analogue, but becomes five-coordinate square pyramidal upon formation of the ternary complex.[307,308]

The structural and spectroscopic studies serve as a firm foundation upon which to postulate a catalytic mechanism, but unfortunately they provide little insight into the activation of dioxygen within the reactive quaternary complex. In the consensus scheme presented in Figure 31, oxygen activation is obtained by formation of an adduct between the coordinatively unsaturated iron(II) center and the nearby C4a of the BH_4 cofactor, which is best described as an iron(II)−peroxypterin complex (Figure 31C).[3,287,289,309] Since no intermediate has been directly observed to date, formation of this adduct may be rate limiting. The putative Fe^{II}−O−O−pterin intermediate is then proposed to cleave heterolytically to form 4a-hydroxypterin (BH_3OH) and a reactive oxoiron(IV) species that carries out the electrophilic attack of the aromatic substrate (Figure 31D). This step is supported by the observation of the nearly quantitative incorporation of isotope from $^{18}O_2$ into the both the amino acid and BH_3OH products.[303,310,311] Pterin-dependent enzymes are thus proposed to utilize an Fe^{II}/Fe^{IV}═O couple, distinct from the formally Fe^{III}/Fe^{V}═O couple associated with cytochrome P450.[312] At the end of the catalytic cycle, release of the hydroxylated substrate and cofactor completes the turnover and returns the active site to its resting iron(II) state (Figure 31, F → A). Dehydration of BH_3OH eventually yields quinonoid dihydropterin (BH_2), which can be reductively recycled back to BH_4 by an external reductase.[309]

There is currently no consensus with respect to the mechanism of Fe−O−O−pterin adduct formation (Figure 32). Observation of an ^{18}O kinetic isotope effect for TyrH, $\Delta V/K = 1.017(2)$, coupled with the lack of solvent (H_2O, D_2O) isotope effects, indicates a significant O−O bond order change in the rate-determining step.[313] Stepwise O_2 binding may occur initially at Fe^{II} to form an $Fe^{III}-O_2^-$ species that subsequently couples to BH_4, as favored by recent DFT calculations.[314] In this case, the metal ion plays a role in stabilizing incipient charge on the O_2 unit and mitigating the spin barrier, and a metal-independent reaction trajectory could not be found. Alternatively, O_2 attacks initially at BH_4 to form a pterin hydroperoxide,[290,313] paralleling the chemistry of metal-free flavin-dependent oxygenases,[315] with the metal center subsequently required for activation of the peroxo species. Experiments on the E280K mutant of hPheH favor the latter option.[316] Despite the fact that the iron(II) center of this mutant enzyme remains six-coordinate in the ternary complex, pterin oxidation activity is nevertheless retained and in fact is enhanced 2-fold. A third option may be the concerted addition of O_2 to both the metal center and pterin.

The next step in the mechanism is O−O bond heterolysis of the Fe^{II}−O−O−pterin intermediate to form an Fe^{IV}═O species. Heterolysis is predicted by DFT calculations to be quite difficult for a tetrahedral iron(II) model,[317] but relatively facile for six-coordinate iron(II),[314] especially when assisted by protonation at the departing β-oxygen. Consistent with the weak ligand field, DFT calculations suggest a reactive oxoiron(IV) intermediate in a high-spin, $S = 2$ ground state.[318] This intermediate is postulated to attack a single carbon atom on aromatic substrates to form a 2,4-dienone intermediate, which subsequently tautomerizes to phenolic product. While this oxoiron(IV)

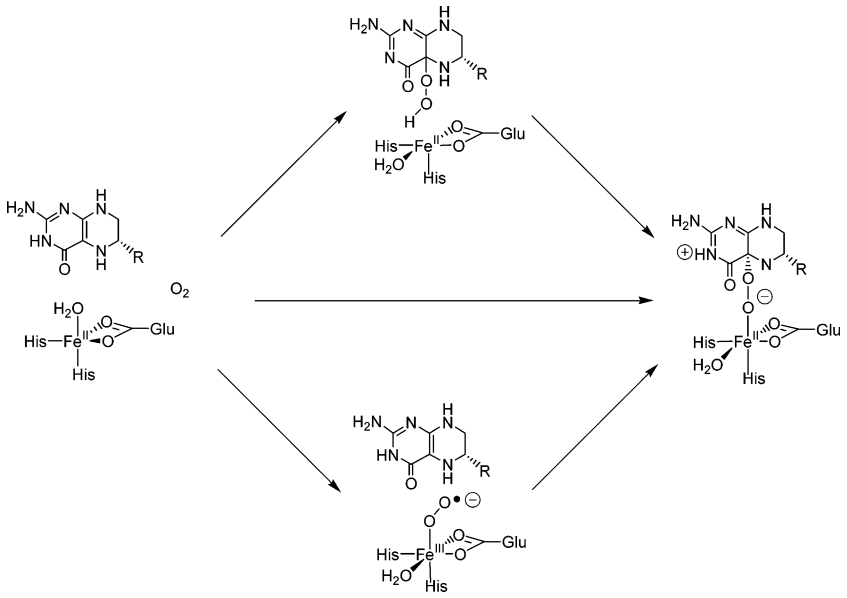

Figure 32. Mechanistic options for the O_2 adduct formation step in the iron- and pterin-dependent hydroxylases.

species has not been experimentally observed, there is indirect evidence implicating such an electrophilic hydroxylating agent. Besides arene hydroxylation, the pterin-dependent enzymes can accommodate a number of substrate analogues and carry out sulfoxidation, epoxidation, and benzylic hydroxylation,[289] a reactivity pattern closely related to that associated with the $Fe^{IV}(O)$(porphyrin radical) intermediate of cytochrome P450.[312] Second, TyrH can hydroxylate a series of para-substituted phenylalanines with consistent rates of pterin oxidation, but with increasing degrees of uncoupling as substrate analogues become electron-poor.[319,320] Correlation of arene hydroxylation against the consistent pterin oxidation rate was observed using the standard Hammett σ parameter, yielding $\rho = -4.3(7)$ for tetrahydrobiopterin and $-5.6(8)$ for the 6-methyltetrahydropterin cofactor analogue; these values are consistent with an electron-deficient transition state produced by an electrophilic oxidant.[319] Third, the hydroxylation of deuterated substrate by TrpH exhibits an inverse isotope effect that suggests a partially rate-limiting electrophilic substitution step in this specific instance.[321] Last, arene hydroxylation is often accompanied by a 1,2-hydrogen shift commonly referred to as an "NIH shift", by which substrates labeled with hydrogen isotopes at the site of attack are converted to metabolites with isotope retention on an adjacent carbon.[322] Such a shift is usually indicative of cationic intermediates associated with oxo atom transfer (Figure 31E), forming epoxides or 2,4-dieneones.[318,321−323]

Iron-catalyzed arene hydroxylation reactions may be considered as functional models of the pterin-dependent hydroxylases and have been investigated to gain mechanistic insight thus far unobtainable from enzymatic studies. Early examples include aqueous systems like Fenton's reagent (iron salts/H_2O_2),[324−327] and the Udenfriend system (Fe(EDTA)/ascorbate/O_2)[328] that appear to generate freely diffusing hydroxyl radicals that add to arenes. Phenol yields are generally poor, and isomeric mixtures are obtained from substituted arenes. Sawyer and co-

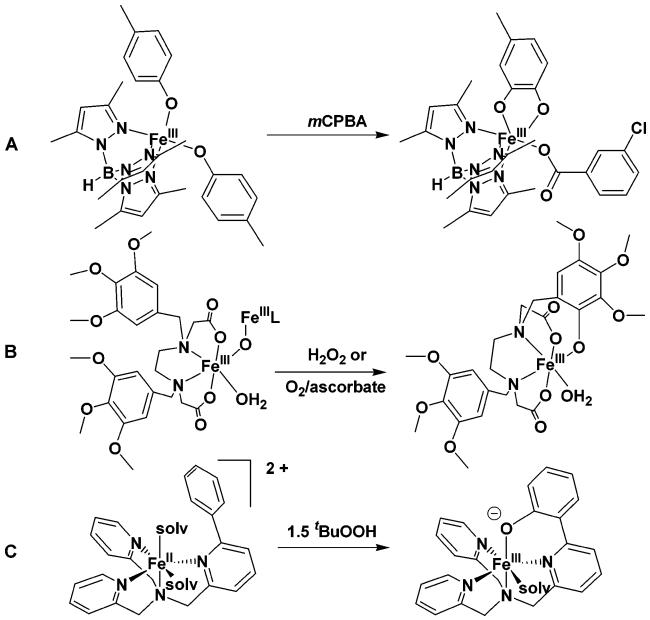

Figure 33. Model arene hydroxylation reactions.

workers have investigated a Fenton-like system in CH_3CN using $[Fe^{II}(bpy)_2]^{2+}$, $[Fe^{II}(picolinate)_2]$, or $[Fe^{II}$-(dipicolinate)] in combination with H_2O_2 and proposed that the change in solvent engenders a mechanistic shift from $HO^{\bullet}$ to a metal-centered oxidant because of the high nucleophilicity of peroxide combined with the strong anodic shift of the Fe^{II}/Fe^{III} couple.[329] But substrate conversions were modest, and no high-valent intermediates were characterized.[330]

More recent approaches to modeling arene hydroxylases have eschewed multiple-turnover reactions in favor of a more efficient "single-turnover" strategy to gain mechanistic insight. For these examples, the target arene is incorporated into the metal complex used to activate the added oxidant, so that the nascent metal-centered oxidant can be captured in an intramolecular reaction (Figure 33). The first example is a functional model for tyrosine

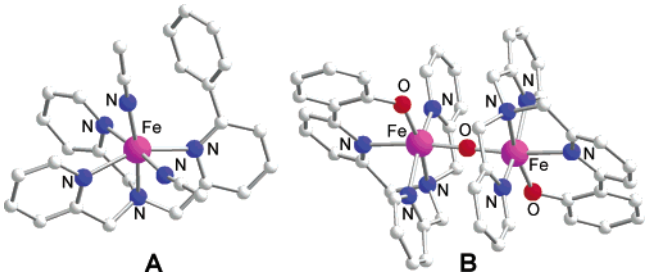

Figure 34. Crystal structures of $[Fe^{II}(6\text{-Ph-TPA})(NCCH_3)_2]^{2+}$ and the ortho hydroxylation product.

hydroxylase obtained by reaction of $[Fe^{III}(Tp^{iPr2})(OAr)_2]$ with 1 equiv of *m*CPBA in diethyl ether (Figure 33A) to form the corresponding catechol in quantitative yield.[331] Unfortunately, the reaction was too rapid even at −78 °C for the proposed $[Fe^{III}(Tp^{iPr2})(OAr)(O_3CR)]$ intermediate to be observed, and the mechanism of oxygen atom transfer was not elucidated.

A second example involves modification of the Udenfriend system by replacing two carboxymethyl side chains of EDTA to make the tetradentate *N*,*N*′-bis(3,4,5-trimethoxybenzyl)ethylenediamine-*N*,*N*′-diacetate ligand (Figure 33B).[332,333] The $[Fe^{III}_2(\mu\text{-O})(L)_2]$ complex reacts in aqueous solution with 3−5 equiv of H_2O_2 to form an intense blue chromophore (λ_{max} = 560 nm, $\epsilon = 1500\ M^{-1}\ cm^{-1}$), arising from a phenolate-to-iron(III) charge-transfer transition. NMR spectroscopy of the demetalated ligand shows *ortho*-hydroxylation of one of the two trimethyoxybenzyl substituents in 80% yield. The trimethoxybenzyl side chain can also be hydroxylated when the (μ-oxo)-diiron(III) complex is treated with excess ascorbate under aerobic conditions. Interestingly, isotope incorporation from $^{18}O_2$ into the product phenol is quantitative, with no exchange with $^{18}OH_2$ observed.

The related *N*,*N*′-bis(3,4,5-trimethoxybenzyl)-*N*,*N*′-bis(2-pyridylmethyl)-1,2-diaminoethane ligand affords a high-spin $[Fe^{II}(L)Cl_2]$ complex that reacts with H_2O_2 in acetonitrile to give *ortho*-hydroxylation of one *N*-3,4,5-trimethoxybenzyl substituent in 70% yield, as indicated by formation of a charge-transfer chromophore at 740 nm.[334] Incorporation of isotope from $H_2{}^{18}O_2$ is quantitative. In contrast, the $[Fe^{II}(L)(NCCH_3)_2]^{2+}$ complex cation does not react with H_2O_2 to produce a chromophore, but is instead an effective catalyst for epoxidation of cyclic olefins and stereoretentive hydroxylation of *cis*-1,2-dimethylcyclohexanol by added H_2O_2. It has been suggested that the chloride complex reacts with H_2O_2 by an outer-sphere mechanism to produce $^{\bullet}OH$, which mediates the "intramolecular" aromatic hydroxylation, while the solvento complex reacts by an inner-sphere mechanism to afford iron−peroxo and/or high-valent iron−oxo species that carry out intermolecular substrate oxidation. Hence, it seems that several distinct oxidizing species can be generated using the same supporting ligand under modestly differing conditions.

The third example involves the complex of the tetradentate tris(2-pyridylmethyl)amine (TPA) modified with a single α-phenyl substituent on one pyridyl arm (Figure 33C).[335,336] As shown in Figure 34A, the α-phenyl ring of $[Fe^{II}(6\text{-Ph-TPA})(NCCH_3)_2]^{2+}$ is ideally positioned for attack by an incipient Fe^{IV}=O moiety. Thus, treatment of the complex with 1.5 equiv of ^{t}BuOOH in acetonitrile solution results in *ortho*-hydroxylation of the phenyl substituent in 87% yield. The product is characterized by a phenolate-to-iron(III) LMCT band at 780 nm, which shifts to 486 nm upon treatment with base. From the latter solution, crystals of the oxo-bridged diiron(III) complex of the hydroxylated ligand are obtained (Figure 34B). Resonance Raman spectroscopy and electrospray mass spectrometry of the oxo-bridged dimer indicate quantitative incorporation of isotope into the phenolate using ^{t}Bu^{16}O^{18}OH as the oxidant. Thus, the phenolate oxygen is derived from the terminal peroxide oxygen. However, introduction of 20 vol % $H_2{}^{16}O$ into solution causes some loss of the ^{18}O label, as monitored by Raman spectroscopy, and the reverse is also observed in the reaction with ^{t}Bu^{16}O^{16}OH in the presence of $H_2{}^{18}O$. Thus, an intermediate capable of exchange with water, such as a metal−oxo species, must exist on a productive reaction pathway.

When the reaction of $[Fe^{II}(6\text{-Ph-TPA})(CH_3CN)_2]^{2+}$ with ^{t}BuOOH is carried out below −35 °C, an intermediate with an intense blue chromophore (λ_{max} = 650 nm) can be observed.[336] EPR and Raman studies of the intermediate are consistent with a spin isomeric mixture of Fe^{III}−OO^{t}Bu complexes, which decay to afford the hydroxylated ligand. The decomposition mechanism, whether by O−O bond homolysis or heterolysis, can be demonstrated by use of 2-methyl-1-phenyl-2-propyl hydroperoxide (MPPH), a probe that distinguishes between these possibilities.[337,338] No 2-methyl-1-phenyl-2-propyl alcohol was obtained, ruling out heterolytic O−O bond cleavage; instead, products consistent with benzyl radical formation were observed. The benzyl radical derives from rapid β-scission of the 2-methyl-1-phenyl-2-propoxyl radical that results from O−O bond homolysis. The formation of an alkoxyl radical from Fe^{III}−OOR requires concomitant formation of an Fe^{IV}=O species. The participation of this yet unobserved species in the reaction is already implicated by the ^{18}O-labeling experiments discussed above and by a significant NIH shift observed in the hydroxylation of *o*-6-Ph-TPA-d_1.[336] Taken together, the mechanistic evidence, albeit indirect, strongly supports the formation of oxoiron(IV) as the reactive hydroxylating intermediate. Thus, while the mechanism of oxoiron(IV) production in this model, from O−O bond homolysis of an Fe^{III}−OOR intermediate, is distinct from that of the O_2- and pterin-dependent enzymes, the essential arene hydroxylation step in the enzyme mechanism appears to be modeled accurately. Arene hydroxylation can also be obtained by reaction of $[Fe^{II}(6\text{-Ph-TPA})(CH_3CN)_2]^{2+}$ with iodosobenzene (PhI=O), and isolobal nitrene transfer is observed from reaction of phenyl-*N*-tosyliminoiodinane (PhI=NTs) to form an *o*-anilide complex.[339]

In contrast to the Fe(TPA) systems that promote O−O bond homolysis of Fe^{III}−OOR intermediates,[336,340] Foster and Caradonna have recently reported evidence for the O−O bond heterolysis of an Fe^{II}−OOR intermediate, mimicking the C → D step in Figure

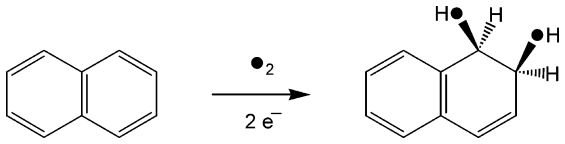

Figure 35. Naphthalene dioxygenase-catalyzed arene *cis*-dihydroxylation reaction.

31.[341] They observe that the diiron(II) complex $[Fe_2(H_2Hbamb)_2(N\text{-MeIm})_2]$ (H_4Hbamb = *N*,*N*′-bis(*o*-hydroxybenzoyl)-2,3-diamino-2,3-dimethylbutane; *N*-MeIm = *N*-methylimidazole) reacts with MPPH to afford nearly quantitative formation of the corresponding 2-methyl-1-phenyl-2-propyl alcohol with no indication of products derived from β-scission of the corresponding 2-methyl-1-phenyl-2-propoxyl radical. This reaction affords an oxidant capable of hydroxylating cyclohexane with excellent conversion and a high alcohol/ketone ratio. Although the precursor complex studied is not mononuclear and the oxidation is not of an arene, it is the first biomimetic example that bypasses the Fe^{III}−OOR intermediate stage found in a number of reactions of iron(II) precursors with ROOH[342] and promotes the facile heterolysis of an $Fe^{II}O$−OR bond, presumably forming a yet unobserved Fe^{IV}=O species.

3.6. Arene *cis*-Dihydroxylation by Rieske Dioxygenases

The *cis*-dihydroxylation of arenes catalyzed by Rieske dioxygenases constitutes the first step in the biodegradation of aromatic molecules by soil bacteria and leads in two subsequent steps to the formation of catechols,[5] which are in turn degraded by the intradiol- and extradiol-cleaving catechol dioxygenases discussed earlier in this review. The Rieske dioxygenases are thus important in bioremediation.[343−345] There is also strong interest in these enzymes as biotechnological tools since the enzyme-catalyzed reactions are both stereo- and enantiospecific and arene *cis*-dihydroxylation is a novel transformation not observed thus far in synthetic organic chemistry.[346−349] Rieske dioxygenases are multicomponent enzymes with an oxygenase component where O_2 activation and substrate dihydroxylation occur and a reductase component that mediates electron transfer between NAD(P)H and the oxygenase component. In the course of catalysis, both atoms of O_2 are incorporated into the *cis*-diol product (Figure 35).[5,347,350−352] Aside from *cis*-dihydroxylation, Rieske dioxygenases also catalyze a number of oxidations such as benzylic hydroxylation, desaturation, sulfoxidation, and O- and N-dealkylation.[350,353] This large range of oxidative transformations indicates that Rieske dioxygenases may be even more versatile than the cytochromes P450.

There is thus far only one Rieske dioxygenase that is crystallographically characterized (Figure 36).[144,354,355] The structure of the oxygenase component of naphthalene 1,2-dioxygenase (NDO) from *Pseudomonas putida*, the enzyme that catalyzes the formation of *cis*-(1*R*,2*S*)-1,2-dihydroxy-1,2-dihydronaphthalene from naphthalene, solved in 1998 at 2.25 Å resolution,[144] shows two metal centers, a mononuclear iron center where O_2 binding and activation presumably take place and a nearby

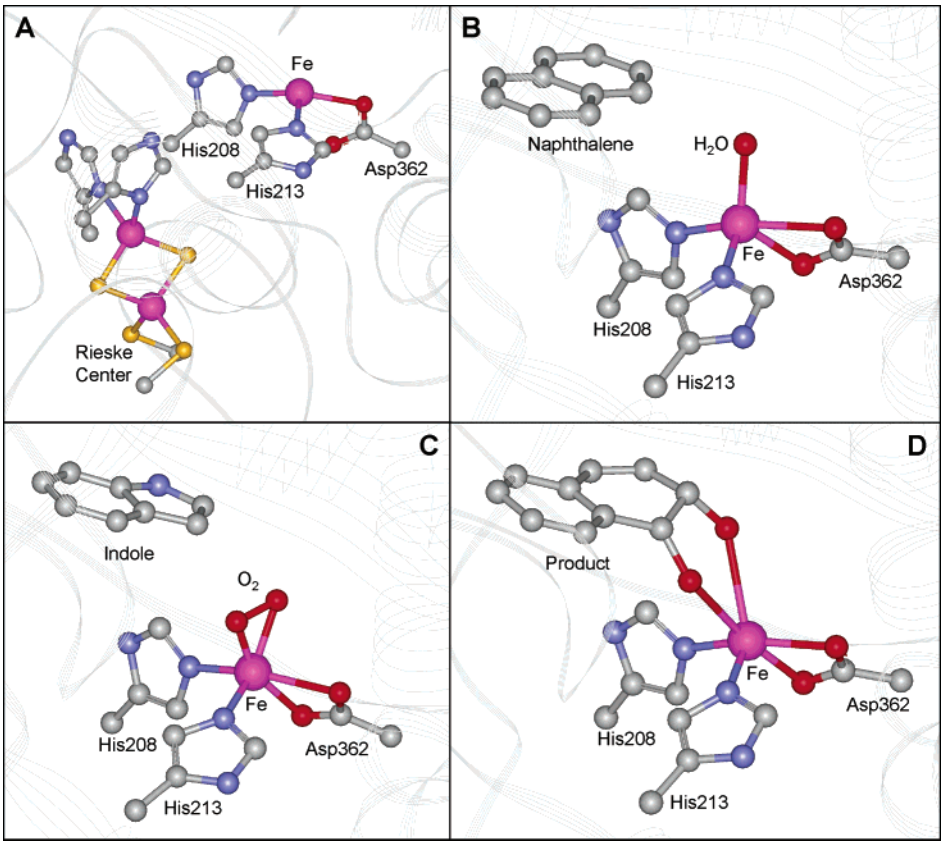

Figure 36. Crystallographic information on the active sites of naphthalene dioxygenase: (A) Fe·NDO (1NDO.pdb), (B) Fe·NDO·naphthalene (1O7G.pdb), (C) Fe·NDO·indole·O_2 (1O7N.pdb), and (D) Fe·NDO·product (1O7P.pdb).

Rieske-type Fe_2S_2 cluster, which deliver electrons to the mononuclear center in a controlled fashion during catalysis. These results confirm earlier notions derived from spectroscopic studies mainly on phthalate dioxygenase (PDO).[356−360] The mononuclear iron center of NDO is coordinated to two histidine residues (His208 and His213) and a bidentate aspartate (Asp362) (Figure 36A),[144,354,355] occupying four sites of the metal center in a variation of the 2-His-1-carboxylate facial triad widely distributed among nonheme oxygenases involved in O_2 activation.[105,106] A water molecule occupies a fifth coordination site, and there is an asparagine residue 3.7 Å from the iron in the vicinity of the sixth coordination site. The Rieske cluster with its characteristic $Fe_2S_2(Cys)_2$-$(His)_2$ core is 12 Å away with His104 on the cluster connected to His208 on the monoiron center by hydrogen bonding to Asp205. Structures of the oxygenase component with bound naphthalene (Figure 36B) or the substrate analogue indole are also available and show a substrate binding pocket nearby that orients the double bond to be attacked in position for substrate oxidation 4 Å away from the monoiron center.

Spectroscopic studies also provide insight into the coupling of substrate binding and the redox state of the Rieske cluster to changes at the mononuclear iron center in preparation for oxygen activation. MCD studies on PDO show that the iron(II) center is six-coordinate and becomes five-coordinate upon substrate binding.[360] This substrate-triggered change follows the general mechanistic paradigm for oxygen activation by iron(II) enzymes with 2-His-1-carboxylate active sites (Figure 11).[4] NO, an O_2 analogue, binds to the mononuclear iron(II) site of NDO and converts the EPR-silent high-spin iron(II) center into an EPR-active $S = {}^3/_2$ $\{Fe-NO\}^7$ center.[361] ENDOR studies of the NO adduct show that protons on the naphthalene substrate are dipolarly coupled to the paramagnetic center, indicating that the substrate remains in the crystallographically characterized binding pocket even after NO binding.[362,363] Furthermore, the substrate is sensitive to the redox state of the Rieske cluster and undergoes an allosteric shift toward the mononuclear nonheme iron center upon reduction of the Rieske cluster.

An exciting recent development is the crystallographic characterization of O_2 adducts of NDO in the absence and in the presence of substrate, the first example for a nonheme iron enzyme.[354,355] The crystal structure of the reduced enzyme exposed to O_2 in the absence of substrate shows a side-on-bound dioxygen moiety with Fe−O distances of 2.2 and 2.3 Å. The observed O−O distance of 1.4 Å suggests the reduction of O_2 to the peroxide level. The same experiment performed with crystals previously soaked in solutions of the substrate analogue indole and then exposed to O_2 shows an even more tightly bound side-on-bound peroxo species with Fe−O distances of 1.8 and 2.0 Å and an O−O bond distance of 1.4 Å (Figure 36C). The Fe−O bond distances of the latter are in good agreement with $Fe-O_{peroxo}$ bond lengths obtained from the EXAFS analysis for the model compound $[Fe(N4Py)(\eta^2\text{-}O_2)]^+$ (1.93 Å; N4Py = *N*-(bis(2-pyridyl)-methyl)-*N*,*N*-bis(2-pyridylmethyl)-amine),[364] and from the crystal structure of a heme/copper complex with a $\mu\text{-}\eta^1{:}\eta^2$-peroxo bridge (1.89 and 2.03 Å)[365] (see next section for a more detailed discussion). The asymmetry of the bound dioxygen moiety in the enzyme structures suggests the strong possibility that it may be a side-on-bound hydroperoxide. The observation of these side-on-bound dioxygen intermediates in two crystal forms differs from an earlier observation by the same group of a dioxygen adduct in which one oxygen atom is bound to the metal center and the other to the C3 carbon atom of the substrate analogue indole.[354] This structure may be construed to be an intermediate subsequent to the initially formed side-on-bound dioxygen complex, demonstrating dioxygen attack on substrate. Last, the crystal structure of an enzyme−product complex demonstrates that the *cis*-dihydroxylated product coordinates the iron center as a bidentate ligand to the metal center (Figure 36D).[355] Product release occurs only after the two redox sites are reduced to initiate another round of catalysis.

Although early studies on PDO have shown that the oxygenase and the reductase components form an essential complex for catalytic turnover,[366,367] recent studies on NDO[361] and benzoate 1,2-dioxygenase (BzDO) [368] demonstrate that the fully reduced oxygenase component alone is competent to activate O_2. In the absence of substrate, the fully reduced oxygenase reacts slowly with O_2, resulting in the autoxidation of the enzyme. The addition of substrate accelerates this reaction, producing nearly a single turnover of product *cis*-dihydrodiol. The rate of this reaction is in fact more than 1 order of magnitude faster than the overall catalytic turnover rate, suggesting that other steps control the overall kinetics. At this stage, both the monoiron center and the Rieske cluster are oxidized and the product can be recovered from the enzyme only via a procedure involving thermal denaturation and chemical extraction.[361,368] The tighter binding of the product diol at this stage is not surprising, given the expectation that the Lewis acidic iron(III) center should have a strong affinity for the diol oxygens. Product release could then be triggered by reduction of the oxygenase by the reductase and probably constitutes the rate-determining step during catalysis.

The above observations can be considered together to assemble the following mechanistic sequence. The fully reduced enzyme binds the arene substrate to initiate the reaction. O_2 binding followed by electron transfer from the reduced Rieske cluster generates the O_2 adduct shown. Its side-on binding mode is demonstrated by the crystal structures, and its description as a peroxide is supported by the 1.4 Å O−O bond length. Further corroboration comes from biochemical studies on NDO with benzene as a substrate analogue;[369] in this case, the reduction of O_2 is uncoupled from substrate dihydroxylation, and H_2O_2 is released with no benzene oxidation, presumably the result of protonation of the putative Fe^{III}−OOH intermediate. The fully oxidized NDO has also been shown to undergo a peroxide shunt, catalyzing the single-turnover oxidation of naphthalene with

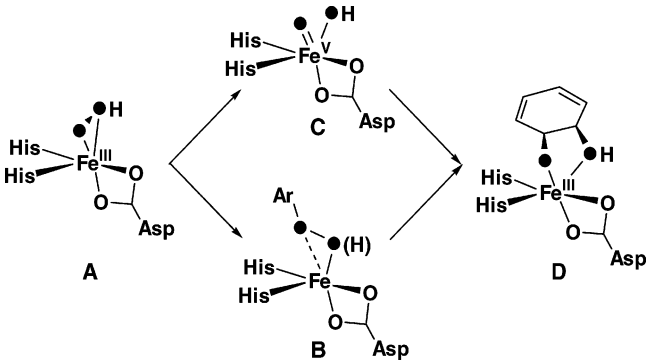

Figure 37. Possible fate of the key O_2 intermediate in the Rieske dioxygenase cycle.

H_2O_2 to afford the corresponding *cis*-(1*R*,2*S*)-1,2-dihydroxy-1,2-dihydronaphthalene product.[370] Isotope labeling studies show almost full incorporation of the two O atoms of the peroxide into the *cis*-diol product. Thus, substrate oxidation can be effected by an iron(III)−peroxo moiety. Due to the greater reactivity of biomimetic Fe^{III}−OOH species compared to their conjugate base counterparts,[371−373] the former is favored as the more likely oxidizing species in the Rieske dioxygenases.

The Fe^{III}−η^2-OOH intermediate may then attack the substrate directly to form the (η^1-alkylperoxo)-iron species (Figure 37B) found in an NDO crystal structure,[354] but the chemistry underlying this transformation is difficult to envision. The fact that the O−O bond remains intact suggests a nucleophilic attack of the substrate by the bound peroxide, but how this should come about is not clear. Alternatively, the Fe^{III}−η^2-OOH intermediate may undergo O−O bond cleavage and convert to an electrophilic HO−Fe^{V}=O species (Figure 37C) prior to substrate attack. Such a species would be akin to the high-valent *cis*-dioxometal species such as OsO_4, RuO_4, or MnO_4^- well known to effect *cis*-dihydroxylation of olefins.[374−376] The involvement of an iron−oxo species in the catalytic mechanism may be implicated by the incorporation of $H_2{}^{18}O$ into the product. Indeed, a small amount of oxygen from water (3−10%) is incorporated into the naphthalene *cis*-diol product in the peroxide shunt studies of Wolfe et al.[370] Furthermore, Wackett et al. have found significant label incorporation from $H_2{}^{18}O$ (70%) in the oxidation of the substrate analogue indane by toluene dioxygenase to 1-indanol.[377] These results argue for the involvement of an intermediate that allows solvent to be incorporated into the product.

The novel chemistry carried out by the Rieske dioxygenases has inspired efforts to obtain functional models of these enzymes. Although biomimetic arene *cis*-dihydroxylation has not been attained, the first examples of synthetic nonheme iron complexes capable of catalyzing the *cis*-dihydroxylation of olefins have been discovered by Que and coworkers.[117−119,378−380] While the biomimetic complexes are not capable of O_2 activation, they efficiently utilize H_2O_2 as oxidant to achieve olefin *cis*-dihydroxylation, mimicking the peroxide shunt pathway demonstrated for NDO.[370] In some cases, as much as 95% of the H_2O_2 added is converted to *cis*-diol. Furthermore, a chiral analogue of one of these complexes in fact catalyzes the *cis*-dihydroxylation of *cis*-2-heptene with high enantioselectivity (80−88% ee).[381]

The *cis*-dihydroxylation catalysts are exemplified by three complexes, $[Fe^{II}(BPMEN)(CH_3CN)_2]^{2+}$, $[Fe^{II}(TPA)(CH_3CN)_2]^{2+}$, and $[Fe^{II}(6\text{-}Me_3\text{-}TPA)(CH_3CN)_2]^{2+}$ (Figure 38), all of which oxidize a range of olefins. It is notable that both epoxide and *cis*-diol products are obtained in many cases and that the epoxide/*cis*-diol ratio depends on the nature of the tetradentate N4 ligand. For example, BPMEN strongly favors epoxide formation (8:1) with cyclooctene as substrate, while 6-Me_3-TPA strongly favors *cis*-dihydroxylation (1:4). These results emphasize an emerging idea that epoxidation and *cis*-dihydroxylation reflect different reactivities of a common iron−peroxo intermediate, the balance between the two pathways being exquisitely tuned by the ligand topology and the spin state of the metal center.[118]

Three sets of experiments emphasize the contrasting behaviors of the TPA and 6-Me_3-TPA complexes. First, $[Fe^{II}(TPA)(CH_3CN)_2]^{2+}$ and $[Fe^{II}(6\text{-}Me_3\text{-}TPA)(CH_3CN)_2]^{2+}$ react with ^{t}BuOOH to afford respectively low-spin and high-spin Fe^{III}−OO^{t}Bu intermediates.[342] The change in spin state is due to the 6-methyl substituents on the TPA ligand, which introduce steric constraints on the iron center. It is assumed

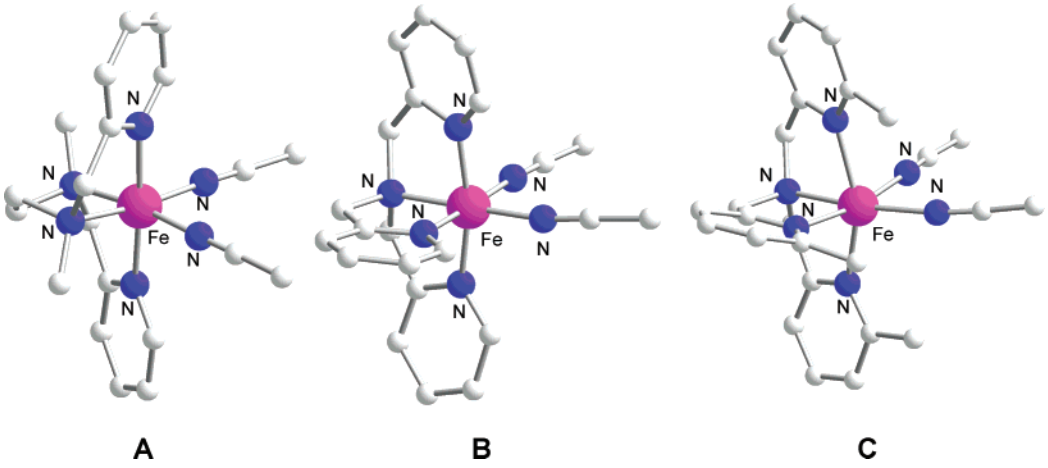

Figure 38. Crystal structures of $[Fe^{II}(BPMEN)(CH_3CN)_2]^{2+}$, $[Fe^{II}(TPA)(CH_3CN)_2]^{2+}$, and $[Fe^{II}(6\text{-}Me_3\text{-}TPA)(CH_3CN)_2]^{2+}$.

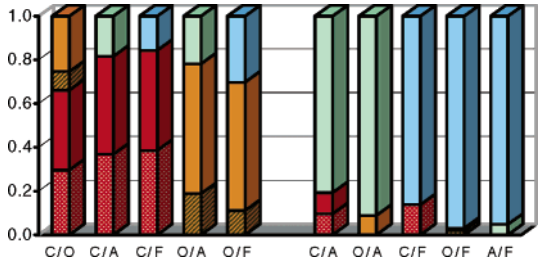

Figure 39. Competition experiments for the oxidation of olefin pairs by $[Fe^{II}(TPA)(CH_3CN)_2]^{2+}$ (left) and $[Fe^{II}(6\text{-}Me_3\text{-}TPA)(CH_3CN)_2]^{2+}$ (right): C = cyclooctene (red), O = 1-octene (orange), A = *tert*-butyl acrylate (green), F = dimethyl fumarate (blue). Solid blocks represent the fraction of *cis*-diol formed, while patterned blocks represent the fraction of epoxide formed. Reprinted with permission from ref 380. Copyright 2003 American Chemical Society.

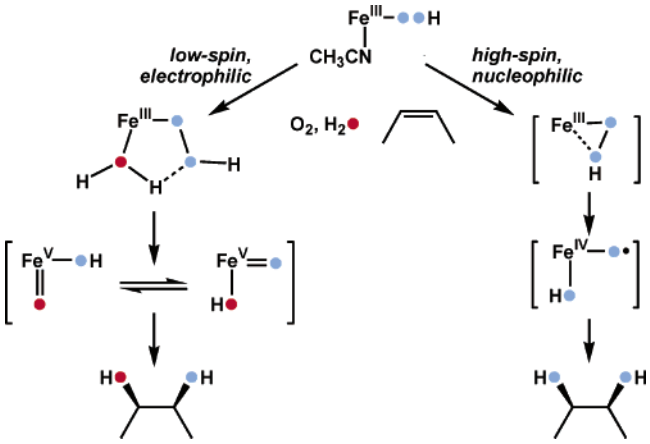

Figure 40. Mechanistic pathways for biomimetic *cis*-dihydroxylation.

that this spin-state difference extends to the corresponding Fe^{III}—OOH intermediates, but only the low-spin $[Fe^{III}(TPA)(OOH)]^{2+}$ complex has been trapped and characterized.[382,383] Second, competition experiments between electron-rich and electron-deficient olefins show that the TPA catalyst prefers to oxidize electron-rich olefins, while the 6-Me_3-TPA catalyst prefers to oxidize electron-deficient olefins (Figure 39).[380] These results have been interpreted as indicating the generation of an electrophilic oxidant for the former and a nucleophilic oxidant for the latter. Third, ^{18}O-isotope labeling experiments reveal a dramatic difference in the source of the diol oxygens. For the former, one diol oxygen derives from $H_2{}^{18}O_2$, while the other derives from $H_2{}^{18}O$; for the latter, both diol oxygens come from $H_2{}^{18}O_2$, thereby mimicking the dioxygenase nature of the enzyme-catalyzed dihydroxylation chemistry (Figure 40).

An overall mechanistic scheme for this family of catalysts is proposed in Figure 40. Taking into account the fact that the corresponding pentadentate N4Py complex is not a catalyst for olefin oxidation,[117] even though a low-spin Fe^{III}(N4Py)—OOH intermediate can be observed,[383,384] the mechanism requires a complex to have two cis-labile sites with which to activate the hydroperoxo ligand. In the low-spin pathway, the hydroperoxide occupies one site and water the other site. Hydrogen bonding of a water proton with the terminal oxygen of the bound hydroperoxide forms a five-membered ring that facilitates O—O bond heterolysis and expulsion of water to form the electrophilic HO—Fe^{V}=O oxidant responsible for diol formation. The novel isotope labeling result provides the strongest argument in favor of such an oxidant. The viability of this pathway has also been tested by DFT calculations, and no insurmountable activation barriers were found.[385] Epoxides formed in the low-spin pathway also show ^{18}O incorporation from $H_2{}^{18}O$, implying that the epoxidizing agent is closely related to the *cis*-dihydroxylating species.[117]

Less evidence is available to support the high-spin pathway. The observation that both diol oxygens derive from H_2O_2 and the requirement for two cis-labile sites suggest that peroxide activation may occur via a side-on-bound species.[117,378] This postulate in fact anticipated the observation of such a side-on-bound dioxygen moiety in the crystal structure of NDO.[355] The possible nucleophilicity of this side-on peroxo species is precedented by the nucleophilicity established for η^2-peroxoiron(III) porphyrin complexes[386] and attributed to a high-spin Fe^{III}—OOH intermediate.[387] However, the possibility that the Fe^{III}—η^2-OOH moiety further cleaves to form a high-valent iron—oxo species that then carries out the dihydroxylation, as in the low-spin pathway, cannot be excluded at this time. Clearly more work needs to be done to clarify the mechanistic issues in this intriguing catalytic system. Insights derived from this effort will surely also have an impact on our understanding of enzymatic *cis*-dihydroxylation.

4. Bio-Inspired Oxidation Catalysis

The olefin oxidation catalysts discussed in the previous section on Rieske dioxygenases are quite versatile, being capable of utilizing H_2O_2 also for stereospecific alkane hydroxylation.[382,388] These efforts were preceded by in-depth investigations of a number of systems capable of alkane oxidation, particularly the "Gif systems" developed by Barton,[389—392] the Fenton-like systems explored by Sawyer,[329,393] and nonheme iron complex/^{t}BuOOH combinations pioneered by Fish[394—397] and followed up by Que, Ménage, and Mascharak with other ligand systems.[398—403] However, in none of the above studies was the oxidant established to be a metal-based species capable of stereospecific hydroxylation, analogous to the high-valent oxoiron(IV) porphyrin radical intermediate generally accepted to be the principal oxidizing species in heme-catalyzed alkane hydroxylation and olefin epoxidation.[243] Indeed, evidence for the formation of Fe^{III}—OO^{t}Bu intermediates was obtained in two instances,[404,405] but decomposition of such intermediates was subsequently demonstrated by Ingold and co-workers to involve O—O bond homolysis to generate an alkoxyl radical as the primary oxidant for the hydroxylation reaction.[337,340,406]

These studies have stimulated further investigation into iron catalysts capable of utilizing H_2O_2 as oxidant to afford products indicative of metal-based alkane oxidations,[407] by analogy to the peroxide shunt reactions observed for several iron enzymes. These include (μ-oxo)diiron(III) complexes of bipy and phen[401,408,409] and the aforementioned monoiron(II) complexes of tetradentate N4 ligands with the TPA

and BPMEN ligand frameworks.[119,334,382,388,410] Key indicators of a metal-based oxidation are large cyclohexanol/cyclohexanone ratios and KIE values for cyclohexane hydroxylation higher than those associated with HO•. More importantly, these catalysts carry out the stereoselective hydroxylation of the tertiary C−H bonds of *cis*-1,2-dimethylcyclohexane, the majority affording %RC values above 95%. Further support for a metal-based oxidant is the observation that the (μ-oxo)diiron(III) complex with a chiral bpy ligand catalyzes enantioselective sulfoxidation (40% ee) and hydroxylation of benzylic C−H bonds (7−15%).[411,412]

In the course of these studies, evidence for Fe^{III}−OOH intermediates as the oxidizing species has been obtained in several instances,[382,383,388,411,413,414] some of which will be discussed in detail in the following section. However, the fact that some ^{18}O from $H_2{}^{18}O$ becomes incorporated into the alcohol products in the reactions with Fe(BPMEN) and Fe(TPA) catalysts also supports the notion that some of these Fe^{III}−OOH intermediates can also serve as precursors to the actual (though yet unobserved) HO−Fe^{V}=O oxidant,[118,385,388,410] as discussed in the preceding section for the *cis*-dihydroxylation catalysts.[117]

Along a similar vein, Kodera et al. have spectroscopically characterized a thermally stable (μ-oxo)-(μ-1,2-peroxo)diiron(III) of a dinucleating hexapyridine ligand.[415] This species is unreactive toward alkanes but can be activated upon treatment with acyl chlorides in DMF to carry out the hydroxylation of cyclohexane with only a trace amount of cyclohexanone. It is proposed that the peroxo bridge is acylated to form an acylperoxo species that undergoes O−O bond heterolysis to generate an oxidant powerful enough to cleave the cyclohexane C−H bond. Indeed, the precursor (μ-oxo)diiron(III) complex catalyzes over 1000 turnovers of cyclohexane hydroxylation with *m*-chloroperbenzoic acid as oxidant.[416]

A very recent addition to this relatively exclusive group of alkane hydroxylation catalysts is a complex reported by Foster and Caradonna, [Fe_2(H_2Hbamb)$_2$-(*N*-MeIm)$_2$] (H_4Hbamb = *N*,*N*′-bis(*o*-hydroxybenzoyl)-2,3-diamino-2,3-dimethylbutane; *N*-MeIm = *N*-methylimidazole), and mentioned earlier in the pterin-dependent enzyme section.[341] This complex uses MPPH (2-methyl-1-phenylpropyl 2-hydroperoxide) to oxidize cyclohexane efficiently to cyclohexanol. The fact that MPPH activation yields only the corresponding 2-methyl-1-phenyl-2-propanol and the lack of any evidence for the formation of the corresponding alkoxyl radical argue for a heterolytic O−O bond cleavage mechanism to form an Fe^{IV}=O species that is presumed to carry out the alkane hydroxylation. This is the first biomimetic example with evidence implicating an Fe^{IV}=O species in cleaving the 99.3 kcal/mol bond of cyclohexane and is thus clearly a result worth further detailed investigation.

Several examples of synthetically efficient nonheme iron olefin oxidation catalysts have been reported. Stack and co-workers showed that [Fe^{III}_2(μ-O)(phen)$_4$(H_2O)$_2$]$^{4+}$ catalyzes the epoxidation of a range of olefins (including terminal olefins) with peracetic acid as oxidant with low catalyst loading

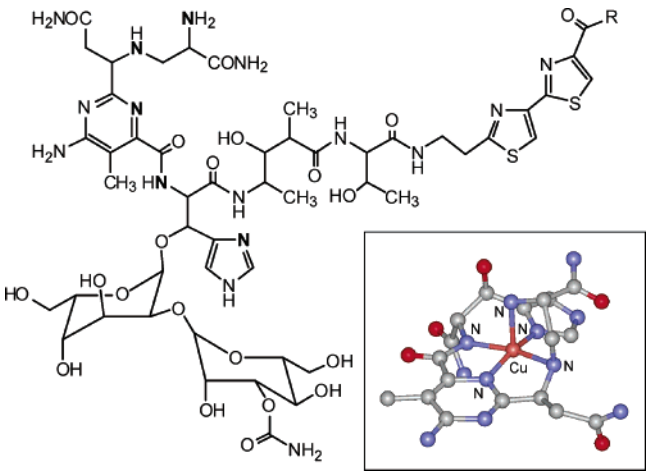

Figure 41. Structure of the anti-tumor drug bleomycin, with the bolded atoms indicating sites for metal coordination. (Inset) The metal coordination sphere as observed in the crystal structure of Cu^{II}BLM bound to the bleomycin binding protein (1JIF.pdb).

(0.25 mol %) and fast reaction times (<5 min) at 0 °C.[417] With the more biomimetic oxidant H_2O_2, Jacobsen and co-workers found that [Fe^{II}(BPMEN)-(CH_3CN)$_2$]$^{2+}$ can be a synthetically useful olefin epoxidation catalyst at 5 mol % catalyst loading, with isolated epoxide yields as high as 90%.[418] Nam, Que, and co-workers reported that the corresponding [Fe^{II}(TPA)(CH_3CN)$_2$]$^{2+}$ complex is also a good olefin oxidation catalyst under analogous reaction conditions but favors *cis*-dihydroxylation over epoxidation by at least a 3:1 ratio.[379] The examples listed in this section augur a promising future for the discovery and development of bio-inspired oxidation catalysts.

5. Trapped Reaction Intermediates

The mechanistic pathways of the various nonheme iron enzymes and biomimetic catalysts discussed above often invoke the participation of iron−peroxo and iron−oxo intermediates. In the following two sections, we present the available data for such species that have actually been trapped under appropriate experimental conditions. These results justify their proposed involvement in the various mechanistic schemes and serve as the foundation upon which to base an understanding of their reactivities.

5.1. Iron−Peroxo Intermediates

Among iron−peroxo intermediates, the most extensively studied is activated bleomycin (BLM, Figure 41), implicated in the reactivity of a family of glycopeptide-derived antibiotics that have anti-tumor activity. Bleomycins depend on iron(II) and O_2 to effect the double-stranded oxidative cleavage of target DNA. Activated BLM or ABLM, the last intermediate observed prior to DNA cleavage, has been identified by electrospray mass spectrometry to be an Fe^{III}−OOH complex.[419] Much work has been carried out to understand the properties of ABLM and its mode of action, and these have been the subject of comprehensive reviews.[420−422] The most salient points will be summarized here for the purposes of this review.

Bleomycin has been found to act as a pentadentate ligand to the metal center in the crystal structure of the copper(II) complex bound to the bleomycin binding protein and provides a square pyramidal N5 coordination environment with the ligating atoms indicated in boldface in Figure 41.[423] Solution NMR and MCD studies have suggested that the sugar carbamoyl goup may act as a sixth ligand in iron(II) and cobalt(II) complexes,[424−426] but one coordination site must become available for the binding of exogenous ligands such as O_2 and CO. It should be noted that the amide NH becomes deprotonated upon metal complexation, so the N5 ligand is monoanionic, thus lowering the potential of the iron(II) center sufficiently to allow an O_2 adduct to form. Strong backbonding from the pyrimidine ligand is suggested to reduce the tendency of the oxy complex to dissociate into Fe^{III}BLM and superoxide.[427,428] ABLM is formed by the addition of one electron to the O_2 adduct of Fe^{II}BLM or by the addition of H_2O_2 to Fe^{III}BLM, by analogy to the peroxide shunt in cytochrome P450. Furthermore, ABLM hydroxylates naphthalene and 4-deuterioanisole (to 4-methoxy-2-deuteriophenol with concomitant NIH shift), epoxidizes olefins, and demethylates *N*,*N*-dimethylaniline.[420] The parallel with some of the oxidation chemistry associated with cytochrome P450 has led investigators to consider whether activated BLM may serve as the precursor to a formally Fe^{V}═O species that is responsible for substrate oxidation.

ABLM exhibits $S = {}^1/_2$ EPR signals with $g = 2.26$, 2.17, and 1.94, indicative of a low-spin iron(III) center, a designation corroborated by Mössbauer spectroscopy.[429] EXAFS studies show the presence of a shell of 2.5 O/N scatterers at 1.89 Å and another shell of 3 O/N scatterers at 2.03 Å, with no evidence for a short Fe−O distance that may be associated with an Fe═O unit.[430] These spectroscopic results, together with the earlier mentioned electrospray mass spectrometric data,[419] unequivocally establish ABLM as a low-spin Fe^{III}−OOH complex.

The Fe^{III}−OOH description implies that the two oxidizing equivalents needed for the aforementioned oxidation chemistry would be localized on the peroxo ligand, instead of on the metal center. Thus, attempts have been made to gain more insight into the properties of the low-spin Fe^{III}−OOH moiety by resonance Raman spectroscopy. However, the amidate ligand gives rise to intense absorption features in all iron complexes of BLM, and these features obscure the hydroperoxo-to-iron(III) charge-transfer transition expected for ABLM.[422,427,428,431] Solomon and co-workers have attributed this outcome to the greater strength of the iron(III)−amidate interaction, which fixes within the molecular frame the orientation of the half-filled t_{2g} orbital that would serve as the acceptor orbital involved in the LMCT transitions. Thus, the donor p orbital of the amidate ligand lies in the plane of this half-filled t_{2g} orbital and has good π overlap that results in an intense LMCT band. Consequently, the corresponding orbital for the hydroperoxo ligand lies on the axis perpendicular to this orbital, so its much smaller overlap with the half-filled metal t_{2g} orbital would give rise to an LMCT band of much lower intensity.

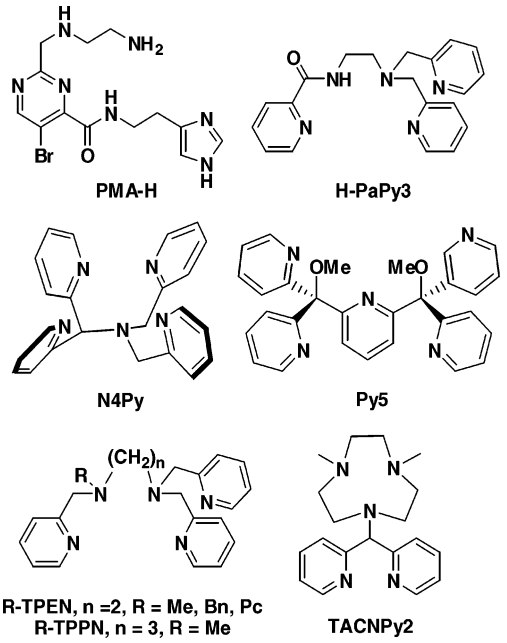

Figure 42. Pentadentate N5 ligands used for modeling activated bleomycin.

Model complexes have played an important role in enhancing our understanding of the iron−peroxo interaction in ABLM and validate the picture proposed by Solomon. Early on, Mascharak and co-workers designed the PMA-H ligand (Figure 42), which most closely matches the BLM ligand environment around the iron center.[427,432,433] Like Fe−BLM, Fe^{II}PMA reacts with O_2 to generate a low-spin iron(III) intermediate with EPR parameters nearly identical to those of activated BLM. However, no direct spectroscopic evidence for the Fe^{III}−OOH formulation of the intermediate has been reported. Complexes of other pentadentate N5 ligands incorporating an amidate moiety have also been synthesized with similar outcomes.[434]

More recently, metastable purple Fe^{III}−OOH complexes of neutral pentadentate N5 ligands such as N4Py, Py5, and R-TPEN (Figure 42, Table 4) have been trapped at low temperature and characterized by a variety of spectroscopic methods.[364,372,383,384,435−442] Unlike the FeBLM and Fe(PMA) complexes, the latter complexes can be obtained only by treatment of iron(II) or iron(III) precursors with excess H_2O_2 at low temperature. Their formulation as $[Fe^{III}(L)(OOH)]^{2+}$ species has been established in several instances by the use of electrospray mass spectrometry. They also exhibit $S = {}^1/_2$ EPR spectra similar to those of activated BLM, as expected for low-spin iron(III) centers. Analysis of the EPR data carried out by Girerd and co-workers[435] within the framework of the Griffith model classifies the Fe^{III}−OOH complexes into three subsets: those with four to five pyridine ligands, those with three pyridines, and those having either an amidate or a thiolate ligand. So the introduction of an anionic ligand into the pentadentate ligand set does significantly, but not surprisingly, affect the electronic properties of the low-spin Fe^{III}−OOH unit.

Table 4. Properties of Low-Spin Iron(III)−Hydroperoxo Complexes

complex	λ_{max}, nm (ϵ, M^{-1} cm^{-1})	ν(Fe−O), cm^{-1} ($\Delta^{18}O$)	ν(O−O), cm^{-1} ($\Delta^{18}O$)	EPR	δ, mm/s	ΔE_Q, mm/s	ref
[Fe(BLM)(OOH)]				2.26, 2.17, 1.94	0.10	−3.0	429
[Fe(PMA)(OOH)]$^+$				2.22, 2.17, 1.94			432
[Fe(PaPy3)(OOH)]$^+$	480 (1800)			2.25, 2.17, 1.95			434
[Fe(N4Py)(OOH)]$^{2+}$	547 (1300)	632 (−16) (−5 ^{2}H)	790 (−44)	2.16, 2.12, 1.98	0.17	−1.6	364, 383
[Fe(Py5)(OOH)]$^{2+}$	592	627	806	2.15, 2.13, 1.98			364
[Fe(H-TPEN)(OOH)]$^{2+}$	531 (950)	625 (−23)	801 (−51)	2.19, 2.14, 1.96			440
[Fe(Me-TPEN)(OOH)]$^{2+}$	537 (1000)	617 (−17)	796 (−45)	2.19, 2.12, 1.95	0.19	−2.01	440, 443
[Fe(Bn-TPEN)(OOH)]$^{2+}$				2.20, 2.16, 1.96	0.17	−2.07	437, 444
[Fe(Pc-TPEN)(OOH)]$^{2+}$	541 (900)	617	796	2.22, 2.15, 1.97			440
[Fe(phen)$_2$(py)(OOH)]$^{2+}$				2.13, 2.12, 1.97			438
[Fe(bipy)$_2$(py)(OOH)]$^{2+}$				2.14, 2.11, 1.97			438
[Fe(pb)$_2$(OOH)]$^{2+}$		623	811	2.18, 2.18, 197	0.23	1.71	414
[(pb)$_2$Fe-O-Fe(pb)$_2$(OOH)]$^{3+}$		618 (−26)	806 (−44)	EPR-silent, $S = 2$ ($S_1 = {}^5/_2$, $S_2 = {}^1/_2$)	0.23	1.64	411, 413
[Fe(TPA)(OOH)]$^{2+}$	538 (1050)	624 (−19)	803 (−44)	2.19, 2.15, 1.97			383
[Fe(S^{Me_2}N$_4$(tren))(OOH)]$^+$	452 (2800)		784 (−31)	2.14, 1.97			445
[Fe(6-Me2-Pc-TPEN)(OOH)]$^{2+}$	530			(2.20, 2.18) 2.12, (1.97, 1.96)			446
[Fe(Me-TPPN)(OOH)]$^{2+}$	550 (>600)	609	799	2.155, 2.1, 1.92			447

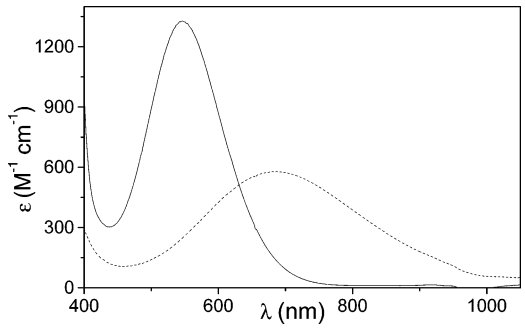

Figure 43. Visible spectra of [Fe^{III}(N4Py)(η^1-OOH)]$^{2+}$ (−) and its conjugate base [Fe^{III}(N4Py)(η^2-O$_2$)]$^+$ (- - -). Reprinted with permission from ref 364. Copyright 2003 American Chemical Society.

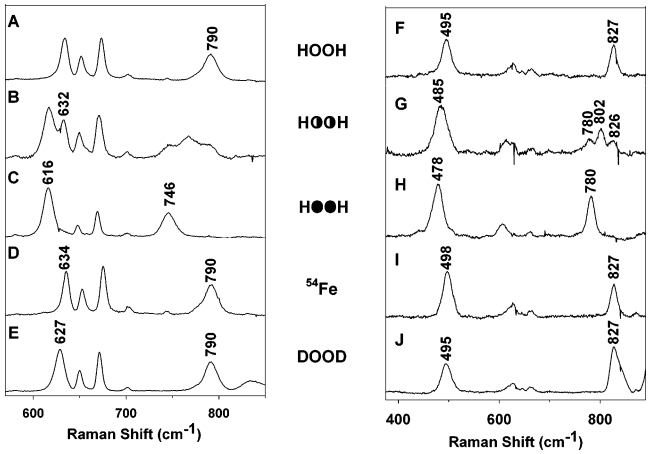

Figure 44. Resonance Raman spectra for [Fe^{III}(N4Py)(η^1-OOH)]$^{2+}$ and [Fe^{III}(N4Py)(η^2-O$_2$)]$^+$ in CH_3OH. Reprinted with permission from ref 364. Copyright 2003 American Chemical Society.

The Fe^{III}−OOH complexes of neutral pentadentate N5 ligands have visible spectra with absorption maxima near 550 nm and extinction coefficients of about 1000 M^{-1} cm^{-1} (Table 4, Figure 43). Due to the absence of other chromophores, this band can readily be assigned to the hydroperoxo-to-iron(III) charge-transfer transition. Low-temperature MCD experiments on [Fe^{III}(N4Py)(OOH)]$^{2+}$ have identified an additional weak band near 1600 nm that can be assigned to the highest energy d−d transition within the t_{2g}^5 subshell.[431] This observed energy (6200 cm^{-1}) in fact matches the value calculated (6455 cm^{-1}) for this transition from the EPR g values.

Excitation into the ∼550-nm band of these Fe^{III}−OOH complexes elicits resonance-enhanced ^{18}O-isotope-sensitive Raman vibrations at ∼600 and ∼800 cm^{-1} (Figure 44, Table 4), corroborating its assignment as the hydroperoxo-to-iron(III) charge-transfer band.[364,383,440,443] The feature at ∼800 cm^{-1} downshifts with ^{18}O labeling by about 45 cm^{-1}, as expected for a diatomic O−O stretch from a simple Hooke's law calculation. The feature at ∼600 cm^{-1}, on the other hand, decreases in energy by 16−23 cm^{-1}, slightly smaller than the 28 cm^{-1} downshift calculated for an Fe−O stretch. A small downshift is also observed for the N4Py intermediate when the experiment is carried out in the presence of D_2O, suggesting the involvement of the entire hydroperoxide ligand in the deformation, so the vibration is assigned to ν_{Fe-OOH}.

Among the Fe^{III}−OOH complexes, the N4Py complex has been studied the most extensively, including the mixed isotope labeling experiment[364] and a normal coordinate analysis[431] that unequivocally establish the η^1-OOH binding mode. The resonance Raman spectrum of [Fe^{III}(N4Py)(η^1-OOH)]$^{2+}$ derived from 50% ^{18}O-labeled H_2O_2 (Figure 44B) shows the ν_{Fe-OOH} feature split only into two bands with energies and intensities corresponding to those observed for the pure isotopomers (Figure 44A,C). The ν_{O-O} feature, on the other hand, splits into three bands at 746, 768, and 790 cm^{-1}, with an area ratio of approximately 1:2:1, corresponding to the respective O−O stretching vibrations of the $^{18}O^{18}O$, $^{16}O^{18}O$, and $^{16}O^{16}O$ isotopomers. But the line width at half-height for the mixed isotopomer is ∼50% larger than those associated with the two pure isotopomers, suggesting the presence of unresolved contributions from distinct Fe−$^{16}O^{18}$OH and Fe−$^{18}O^{16}$OH isotopomers. This qualitative picture is confirmed by a normal coordinate analysis that shows the ∼800 cm^{-1} feature to be an

Table 5. Raman Vibrations of Iron−Peroxo Complexes and Corresponding Force Constants Derived from Normal Coordinate Analysis

	ν_{Fe-O}, cm^{-1}	k_{Fe-O}, mdyn/Å	ν_{O-O}, cm^{-1}	k_{O-O}, mdyn/Å	ref
ls-[Fe^{III}(N4Py)(η^1-OOH)]$^{2+}$	632	3.62	790	3.05	431
ls-[Fe^{III}(TPA)(η^1-OO^{t}Bu)]$^{2+}$	696	3.53	796	2.92	448
hs-[Fe^{III}(6-Me_3-TPA)(η^1-OO^{t}Bu)]$^{2+}$	637	2.87	860	3.55	89
hs-[Fe^{III}($Tp^{tBu,iPr}$)(η^1-OO^{t}Bu)]$^{+}$	625 (618)[a]	(2.19)[a]	860 (876)[a]	(3.93)[a]	317
hs-[Fe(EDTA)(η^2-O_2)]$^{3-}$	459	1.56	816	3.02	371
hs-[Fe_2(Tp^{iPr2})$_2$(O_2CR)$_2$(μ−1,2-O_2)]	421	1.99	876	3.07	449

[a] Values from DFT calculations on [Fe^{III}(Tp)(η^1-OO^{t}Bu)]$^{+}$.

almost pure ν_{O-O} vibration (75% ΔO−O and 15% ΔFe−O) and the ∼600 cm^{-1} feature to consist of 62% ΔFe−O, 8% ΔO−O, and 22% ΔFe−O−O.

Similar Raman spectra are observed for low-spin iron(III)−peroxo complexes of the tetradentate ligand TPA, which is closely related to the N4Py ligand. For example, [Fe^{III}(TPA)(OOH)]$^{2+}$ exhibits vibrations at 624 and 803 cm^{-1} with respective downshifts of 19 and 44 cm^{-1} upon ^{18}O substitution.[383] These features match those of [Fe^{III}(N4Py)(OOH)]$^{2+}$ quite well (Table 4), although the greater instability of the former has thus far made in-depth studies difficult. On the other hand, [Fe^{III}(TPA)(OO^{t}Bu)]$^{2+}$ is much more stable and exhibits peaks at 490, 696, and 796 cm^{-1}.[342] Only the latter two are sensitive to the introduction of ^{18}O at the terminal oxygen of ^{t}BuOOH, but all three are affected by deuteration of the ^{t}Bu hydrogens. Thus, the 490 cm^{-1} peak can be assigned to a ^{t}Bu deformation mode. The 796 cm^{-1} peak is comparable in energy to the ν_{O-O} observed for [Fe^{III}(N4Py)(OOH)]$^{2+}$. Because it downshifts 18 cm^{-1} with the use of ^{t}BuO^{18}OH but upshifts by 7 cm^{-1} upon deuteration of the ^{t}Bu group, it is assigned to the ν_{O-O} with 72% ΔO−O and 11% ΔC−O character.[448] The 696 cm^{-1} peak has complex isotope substitution behavior but can be assigned to a vibration with 61% ΔFe−O, 16% ΔC−O, and 6% ΔC−C character. Despite the large difference in the observed ν_{Fe-O} values for [Fe^{III}(N4Py)(OOH)]$^{2+}$ and [Fe^{III}(TPA)(OO^{t}Bu)]$^{2+}$, the NCA analysis reveals very similar Fe−O and O−O force constants (Table 5).[431,448] The common thread among these three peroxo complexes is the low-spin iron(III) center, which must exert a similar effect on the bound peroxides.

Introduction of methyl substituents α to the pyridine nitrogens of TPA generates steric interactions with the metal center to favor the high-spin state.[342] This applies to the Fe^{II} oxidation state, as exemplified by low-spin [Fe^{II}(TPA)(CH_3CN)$_2$]$^{2+}$ and high-spin [Fe^{II}(6-Me_3-TPA)(CH_3CN)$_2$]$^{2+}$, and to the corresponding Fe^{III}−OO^{t}Bu complexes. Thus, [Fe^{II}(6-Me_3-TPA)(OO^{t}Bu)]$^{2+}$ exhibits a g = 4.3 EPR signal typical of high-spin iron(III) and a Raman spectrum consisting of peaks at 469, 637, 842, and 876 cm^{-1}, which are distinct from those of its low-spin TPA counterpart (Table 5). All features are affected by the introduction of ^{18}O at the terminal oxygen of ^{t}BuOOH and by deuteration of the ^{t}Bu hydrogens, indicating substantial mixing between iron−peroxo and *tert*-butyl modes. The 842 and 876 cm^{-1} peaks collapse into one peak at 860 cm^{-1} upon d^9-substitution, thereby identifying it as the ν_{O-O}, an assignment supported by NCA analysis (75% ΔO−O and 10% ΔC−C character).[89] Note that the O−O vibrational frequency is about 60 cm^{-1} higher than in the low-spin TPA complex, with a corresponding increase in the O−O force constant (Table 5). On the other hand, the 637 cm^{-1} peak, assigned primarily to the ν_{Fe-O}, has 47% ΔFe−O and 26% ΔC−O character, corresponding to an Fe−O force constant that is 20% smaller than that of its TPA analogue. Thus, relative to its high-spin counterpart, [Fe^{III}(TPA)(OO^{t}Bu)]$^{2+}$ has a stronger Fe−O bond and a weaker O−O bond.[89]

Other high-spin iron−peroxo complexes follow this pattern. Masuda and co-workers observed Raman features at 621 and 830 cm^{-1} for [Fe^{III}(H_2BPPA)(OOH)]$^{2+}$ (Figure 45A, Table 6).[387] Along the lines of the 6-Me_3-TPA complex discussed in the previous paragraph, the two α-HNCO^{t}Bu substituents on the TPA framework of H_2BPPA apparently introduce enough steric hindrance to make the iron(III) center high-spin. On the other hand, Suzuki and co-workers have cleverly used the bidentate quinaldate ligand to introduce a more oxygen-rich ligand environment for the iron(III) center and obtained high-spin peroxo complexes of [Fe^{III}(quinaldate)$_2$]$^{+}$.[450] The reaction of [Fe^{III}_2(μ-OH)$_2$(quinaldate)$_4$] with 2 equiv of base and excess H_2O_2 in DMF at −60 °C affords deep blue [Fe^{III}(quinaldate)$_2$(OOH)], which exhibits an EPR signal at g = 4.3 and a ν_{O-O} of 877 cm^{-1} in its resonance Raman spectrum. More interestingly, the same reaction carried out in the presence of CO_2 affords the first example of an isolated and crystallographically characterized metal−peroxycarbonate complex, [Fe^{III}(quinaldate)$_2$(κ^2-OOCO_2)]$^{-}$ (Figure 45B). This complex exhibits a number of ^{18}O- and ^{13}C-isotope-sensitive Raman features (Table 6); those at 547 and 884 cm^{-1} have the right frequencies and ^{18}O-isotope shifts to be assigned to ν_{Fe-O} and ν_{O-O}, respectively, but a normal coordinate analysis of these data should be carried out. High-spin diiron(III) complexes with either terminal or bridging peroxo groups also exhibit Raman features at similar ferquencies, including the Fe^{III}−η^1-OOH units of the invertebrate dioxygen carrier oxyhemerythrin[451] and its model complex [Fe^{III}_2(μ-O)(μ-Ph_4DBA)(TMEDA)$_2$(η^1-OOH)] (Figure 45C)[453] and the Fe^{III}−O−O−Fe^{III} units of O_2 adducts of diiron(II) complexes[435] (Table 6).

A perusal of Tables 4−6 emphasizes the generalization that low-spin iron(III)−peroxo complexes have higher ν_{Fe-O} and lower ν_{O-O} frequencies than their high-spin counterparts. This comparison suggests that coordination to the low-spin iron(III) center strengthens the Fe−O bond and weakens the peroxo O−O bond. This effect was first noted by Harris and

Table 6. Properties of High-Spin Iron(III)−Peroxo Complexes

complex	λ_{max}, nm (ϵ, M^{-1} cm^{-1})	ν(Fe−O), cm^{-1} ($\Delta^{18}O$)	ν(O−O), cm^{-1} ($\Delta^{18}O$)	EPR E/D	δ, mm/s	ΔE_Q, mm/s	ref
		η^1-Peroxo					
$[Fe(H_2BPPA)(OOH)]^{2+}$	568 (1200)	621 (−22)	830 (−17) (−4 ^2H)	0.07			387
$[Fe(quinaldate)_2(OOH)]$	deep blue		877 (−46)				450
oxyhemerythrin	500 (2300)	503 (−23)	844 (−47)		0.52	0.95	451, 452
$[Fe_2(\mu\text{-}O)(\mu\text{-}Ph_4DBA)(TMEDA)_2\text{-}(\eta^1\text{-}OOH)]$	470 (2600)		843 (−46)		0.53	0.99	453
					0.53	1.57	
$[Fe_2(Tp^{iPr_2})_2(O_2CR)_2(\mu\text{-}1,2\text{-}O_2)]$		418 (−9)	876 (−49)		0.66	1.40	108, 454
$[Fe_2(\mu\text{-}O)(\mu\text{-}1,2\text{-}O_2)\text{-}(6\text{-}Me_3\text{-}TPA)_2]^{2+}$	490, 640 (1100)	462 (−19) 531 (−21)	848 (−46)		0.54	1.68	455−457
$[Fe_2(N\text{-}Et\text{-}HPTB)(\mu\text{-}1,2\text{-}O_2)\text{-}(\mu\text{-}O_2CPh)]^{2+}$	588 (1500)	476 (−16)	900 (−50)		0.52	0.72	458
$[Fe_2(Ph\text{-}bimp)(\mu\text{-}1,2\text{-}O_2)(\mu\text{-}O_2CPh)]^{2+}$					0.58	0.74	459
					0.65	1.70	
$[Fe(quinaldate)_2(OOCO_2)]^-$	440 (1450)	547(−23) 577 (−14) 728 (−18)	884 (−43) 966 (−20) (−6 ^{13}C)	0.33			450
		η^2-Peroxo					
$[Fe(OEP)(O_2)]^-$		n.o.	805 (−46)	0.29	0.67	0.62	460
$[(5\text{-}Me_3\text{-}TPA)Cu(\mu\text{-}\eta^1\text{:}\eta^2\text{-}O_2)Fe(TMP)]$			790 (−44)				365
$[Fe^{III}(EDTA)(O_2)]^{3-}$	520 (520)	459 (−13)	816 (−40)	0.21	0.65	0.72	371, 461
$[Fe(N4Py)(O_2)]^+$	685 (520)	495 (−17)	827 (−46)	0.11	0.61	1.11	364, 372
$[Fe(Me\text{-}TPEN)(O_2)]^+$	740 (500)	470 (−16)	819 (−45)	0.08	0.64	1.37	440, 441, 462
$[(Bn\text{-}TPEN)Fe(O_2)]^+$				0.08	0.63	1.12	444, 462
$[Fe(Pc\text{-}TPEN)(O_2)]^+$	755 (450)	470	817	0.10			439, 440

Loew[463] in their DFT calculations of the putative low-spin Fe^{III}−OOH intermediate in the cytochrome P450 mechanism and spectroscopically verified for the first time in these nonheme iron(III)−peroxo complexes. Further experimental support comes from the nice correlation found by Roelfes et al.,[364] showing a decrease in the ν_{O-O}'s of a series of $[Fe^{III}(N5)(OOH)]$ complexes in parallel with the $Fe^{III/II}$ redox potentials of their precursor iron(II) complexes; so the more electron-donating the N5 ligand, the lower the potential and the weaker the O−O bond. The high-spin iron(III) peroxo complexes, however, exhibit ν_{Fe-O} values that range from 421 to 630 cm^{-1}, a large variation in energy that deserves further scrutiny.

One other class of iron(III)−peroxo complexes can be generated by treatment of the purple low-spin $[Fe^{III}(N5)(\eta^1\text{-}OOH)]$ complexes with base (Figures 43 and 44, Table 6).[364,372,439−441,462] Formation of the conjugate bases is confirmed by electrospray mass spectrometry and results in a red shift in their absorption maxima to about 700 nm with a halving of their intensities. These blue species have high-spin iron(III) centers that exhibit Mössbauer isomer shift values (0.61−0.65 mm/s, Table 6) that are at the higher end of the range for such centers.[230] This high isomer shift may be considered indicative of the presence of a side-on-bound peroxo ligand, although such values have also been observed for some, but not all, (μ-1,2-peroxo)diiron(III) complexes (Table 6).[454,459]

The resonance Raman spectra of the blue high-spin peroxo complexes show ν_{O-O}'s about 20 cm^{-1} higher than those of their conjugate acids, which downshift by the requisite 45 cm^{-1} for a diatomic vibration upon ^{18}O-labeling. The ν_{Fe-O}'s are found just below 500 cm^{-1} and downshift by 16−17 cm^{-1}. Unlike for their $[Fe^{III}(N5)(\eta^1\text{-}OOH)]^{2+}$ counterparts, neither vibration is affected by the presence of D_2O. Mixed isotope experiments on $[Fe^{III}(N4Py)(\eta^2\text{-}O_2)]^+$ strongly implicate a side-on-bound peroxo ligand (Figure 44G).[364,372] The ν_{O-O} splits into three peaks at 780, 802, and 826 cm^{-1}, straightforwardly assignable to the $^{18}O^{18}O$, $^{16}O^{18}O$, and $^{16}O^{16}O$ isotopomers, respectively. The three features have comparable line widths and a 1:2:1 peak area ratio, exactly the pattern expected for a symmetrically bound peroxide. Interestingly, the ν_{Fe-O} feature does not split into two peaks corresponding to the Fe−^{16}O and the Fe−^{18}O extremes but instead shifts to a frequency that is intermediate between them. This result suggests that the 495 cm^{-1} mode of $[Fe^{III}(N4Py)(\eta^2\text{-}O_2)]^+$ is a triatomic, rather than a diatomic, vibration involving the Fe and the two peroxide oxygens, most plausibly the symmetric combination for stretching the two Fe−O bonds, corroborating an assignment based on a detailed analysis of $[Fe(EDTA)(\eta^2\text{-}O_2)]^{3-}$.[371]

The (η^2-peroxo)iron binding mode is precedented in the corresponding Fe^{III}(porphyrin) and Fe^{III}(EDTA) complexes.[371,460] The porphyrin complexes, typically prepared by the reaction of the iron(II) precursors with superoxide, are high-spin iron(III) species, as the peroxo ligand pulls the metal center out of the porphyrin plane to accommodate the η^2-binding mode, thereby weakening the ligand field interaction. This out-of-plane geometry is illustrated by the crystal structure of the corresponding manganese(III) complex, and the peroxo oxygens lie on an axis coplanar with an axis that connects two trans nitrogens of the porphyrin.[464] Detailed spectroscopic studies on the classic Fe(EDTA) complex formed at pH 10 with excess H_2O_2, carried out by Neese and Solomon,[371] have led to the description of the molecule as a six-coordinate high-spin iron(III) center with side-on peroxo binding, resulting in the displacement of two of the carboxylates. Application of this model to the structure of $[Fe^{III}(N4Py)(\eta^2\text{-}O_2)]^+$ requires the dissociation of one of the pyridine ligands. However, Roelfes et al. favor an alternative

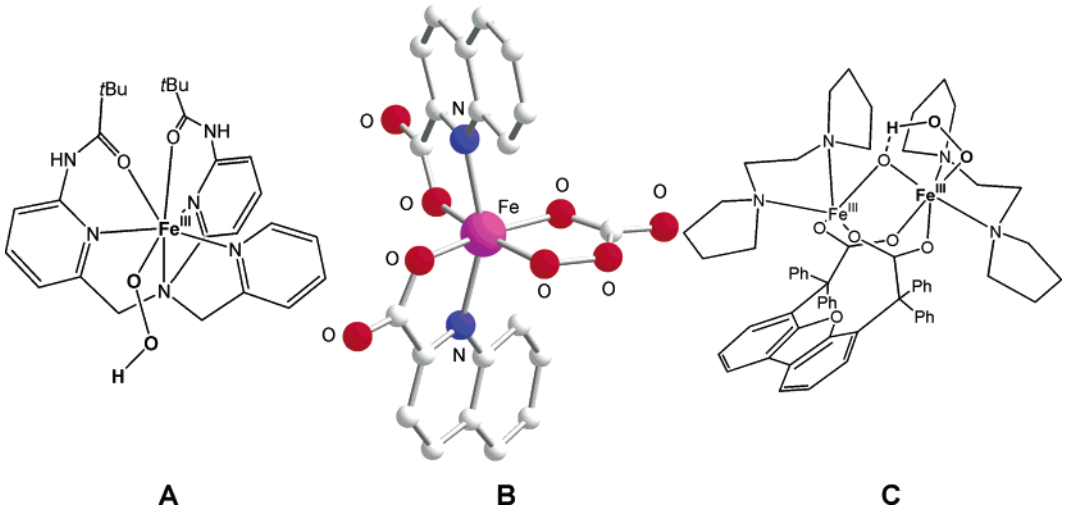

Figure 45. Structures of (A) $[Fe^{III}(H_2BPPA)(\eta^1\text{-}OOH)]^{2+}$ (proposed), (B) $[Fe^{III}(quinaldate)_2(\kappa^2\text{-}CO_4)]^-$ (solved), and (C) $[Fe^{III}_2(\mu\text{-}O)(\mu\text{-}Ph_4DBA)(TMEDA)_2(\eta^1\text{-}OOH)]$ (proposed).

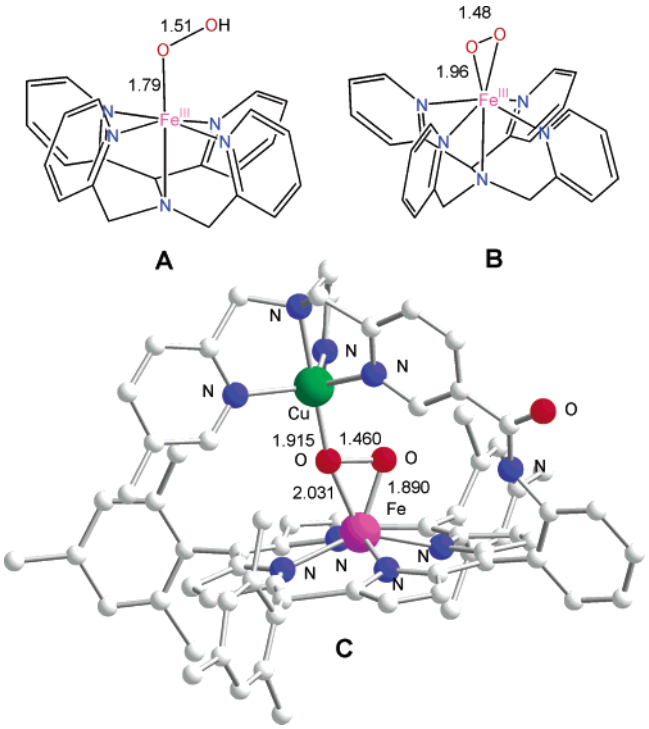

Figure 46. Structures of (A) $[Fe^{III}(N4Py)(\eta^1\text{-}OOH)]^+$ and (B) $[Fe^{III}(N4Py)(\eta^2\text{-}O_2)]^+$ from DFT geometry optimization and of (C) $[(5\text{-}Me_3\text{-}TPA)Cu^{II}(\mu\text{-}\eta^1\text{:}\eta^2\text{-}O_2)Fe^{III}(TMP)]^+$ from X-ray crystallography.

seven-coordinate structure based on DFT geometry optimization (Figure 46B).[364] In this structure that is akin to that of the porphyrin complexes, the side-on peroxo ligand pulls the iron center out of the plane defined by the four pyridine nitrogens and lies above two of the four pyridine nitrogens. This stretches the $Fe-N_{amine}$ distance to 2.39 Å. The bond distances derived from the DFT calculations are consistent with those obtained from an EXAFS analysis of $[Fe^{III}(N4Py)(\eta^2\text{-}O_2)]^+$ (Table 7).

Due to their instability, there is a paucity of crystallographic information on iron(III)−peroxo complexes. To date, there are crystal structures for only one monoiron−peroxo complex, $[Fe(quinaldate)_2(\kappa^2\text{-}OOCO_2)]^-$,[450] three diiron−peroxo complexes,[454,459,465] and a heme−copper heterodimer (Table 7).[365] The four nonheme complexes all have high-spin iron(III) centers with $Fe-O_{peroxo}$ bond lengths in the narrow range of 1.88−1.94 Å, despite having metal centers of differing Lewis acidity. EXAFS analysis of $[Fe^{III}(N4Py)(\eta^2\text{-}O_2)]^+$ and DFT calculations on high-spin $[Fe^{III}(6\text{-}Me_3\text{-}TPA)(OO^tBu)]^{2+}$ also afford $Fe-O_{peroxo}$ bonds in this range.[89,364] In contrast, $Fe-O_{peroxo}$ distances for low-spin iron(III)−peroxo complexes obtained from EXAFS analyses and DFT calculations exhibit a much larger range of values (Table 7). Within this small subset, the $Fe-O_{peroxo}$ distances are as short as 1.76−1.78 Å for $[Fe^{III}(N4Py)(OOH)]^{2+}$ and $[Fe^{III}(TPA)(OO^tBu)]^{2+}$ to as long as 1.97−1.98 Å for ABLM and $[Fe^{III}(PaPy3)(OOH)]^+$, with an intermediate 1.86 Å for $[Fe^{III}(S^{Me_2}N_4(tren))(OOH)]^+$.[364,422,431,445,448,466] These $Fe-O_{peroxo}$ distance variations correlate with the intensity of the hydroperoxo-to-iron(III) LMCT band and reflect the presence of another ligand (e.g., amidate and thiolate) that can compete for the interaction with the key half-filled t_{2g} orbital.

The very recently reported structure of a remarkably stable $\mu\text{-}\eta^1\text{:}\eta^2$-peroxo heterodimer with side-on binding to a heme center and end-on binding to a Cu(TPA) unit provides some badly needed new structural insight. Like the (η^2-peroxo)manganese structure,[464] the side-on-bound peroxo unit lies above the porphyrin plane and eclipses two of the pyrrole nitrogens. One Fe−O bond length is 1.890(6) Å, well within the narrow range found for other high-spin iron(III) peroxo complexes, while the other oxygen that bridges to the Cu(TPA) unit has a longer 2.031(4) Å Fe−O bond length. The copper half of the structure resembles that found by Karlin for $[Cu^{II}_2(O_2)(TPA)_2]^{2+}$.[467] Thus, this heme/copper structure may be construed as a model for a side-on-bound Fe−OOH unit with the copper center substituting for the proton.

A key issue for these iron-peroxo complexes is their reactivity, i.e., whether the O−O bonds cleave by homolytic or heterolytic mechanisms and what types of oxidations can be effected. For side-on peroxo complexes, it is clear from the small amount of data

Table 7. Available Structural Information for Activated Bleomycin (ABLM) and Synthetic Nonheme Iron−Peroxo Complexes from EXAFS Analysis, X-ray Crystallography, and DFT Calculations

complex	EXAFS fit [XRD data] (DFT results)	ref
ABLM	2.5 N @ 1.89 Å; 3 N @ 2.03 Å (Fe−O_{peroxo}, 1.972 Å by DFT)	422
$[Fe^{III}(PaPy3)(\eta^1\text{-OOH})]^+$	1 N/O @ 1.84 Å (amidate); 4 N/O @ 1.98 Å	466
$[Fe^{III}(S^{Me_2}N_4(tren))(\eta^1\text{-OOH})]^+$	1 N/O @ 1.86 Å (η^1-OOH) 1 S @ 2.33 Å; 4 N/O @ 2.01 Å	445
$[Fe^{III}(N4Py)(\eta^1\text{-OOH})]^{2+}$	1 N/O @ 1.76 Å (η^1-OOH); 4 N/O @ 1.96 Å (Fe−O_{peroxo}, 1.804 Å by DFT)	364, 431
$[Fe^{III}(TPA)(\eta^1\text{-OO}^t\text{Bu})]^{2+}$	1 N/O @ 1.78 Å (η^1-OOR); 4 N/O @ 1.96 Å (Fe−O_{peroxo}, 1.825 Å by DFT)	*a*, 448
$[Fe^{III}(6\text{-Me}_3\text{-TPA})(\eta^1\text{-OO}^t\text{Bu})]^{2+}$	Fe−O_{peroxo}, 1.943 Å by DFT	89
$[Fe^{III}(Tp^{tBu,iPr})(\eta^1\text{-OO}^t\text{Bu})]^+$	Fe−O_{peroxo} 1.843 Å by DFT	317
$[Fe(quinaldate)_2(\kappa^2\text{-OOC(O)O})]^-$	[Fe−O_{peroxo}, 1.936(3) Å by XRD]	450
$[Fe^{III}(N4Py)(\eta^2\text{-O}_2)]^+$	2 N/O @ 1.93 Å (η^2-O_2); 3 N/O @ 2.20 Å (Fe−O_{peroxo}, 1,956, 1.958 Å by DFT)	364
$[Fe^{III}_2(Ph\text{-bimp})(O_2CR)(\mu\text{-1,2-O}_2)]^{2+}$	[Fe−O_{peroxo}, 1.944(4) and 1.864(4) Å by XRD]	459
$[Fe^{III}_2(N\text{-Et-HPTB})(\mu\text{-1,2-O}_2)(OPPh_3)_2]^{3+}$	[Fe−O_{peroxo}, 1.880(4) by XRD]	465
$[Fe^{III}_2(Tp^{iPr_2})_2(O_2CR)_2(\mu\text{-1,2-O}_2)]$	[Fe−O_{peroxo}, 1.881(6) and 1.877(6) Å by XRD]	454
$[Fe^{III}_2(O)(Ph_4DBA)(\eta^1\text{-OOH})(TMEDA)_2]^+$	1 N/O @ 1.79 Å (μ-O); 2 N/O @ 2.01 Å (η^1-OOH?); 3 N/O @ 2.18 Å	453
$[(5\text{-Me}_3\text{-TPA})Cu^{II}(\mu\text{-}\eta^1\text{:}\eta^2\text{-O}_2)Fe^{III}(TMP)]^+$	[Fe−O_{peroxo}, 1.890(6) and 2.031(4), and Cu−O_{peroxo}, 1.915(5) Å by XRD]	365

[a] Chen, K.; Que, L., unpublished results.

available that these complexes are unreactive and thus require activation to be mechanistically significant in oxidative transformations.[371,372] Low-spin Fe^{III}−(η^1-OOR) complexes, on the other hand, readily undergo O−O bond homolysis to form RO• radicals and Fe^{IV}=O species. DFT calculations estimate a barrier of 60−80 kJ/mol for the O−O bond homolysis along an O−O bond-stretching trajectory that follows the initial interaction between the low-spin iron(III) center and the peroxide.[448] Such Fe−OOR intermediates have been implicated in catalytic alkane hydroxylation systems employing Fe(TPA) complex/ROOH combinations.[398,399,402,405,468] Particularly persuasive evidence for the homolysis of the O−O bond in Fe−OOR species has been obtained by the use of MPPH (2-methyl-1-phenylpropane-2-hydroperoxide) in place of the more common ^{t}BuOOH.[337,338,340,406] The alkoxyl radical derived from the former readily undergoes β-scission to form benzyl radical and so gives rise to products that are diagnostic of O−O bond homolysis. The putative Fe^{IV}=O moiety thus formed in such a homolysis has been trapped in both intramolecular and intermolecular reactions.[335,336,340,469] These results lay the foundation for the generation and characterization of mononuclear oxoiron(IV) complexes to be discussed in the next section. There is less insight into the reactivity of high-spin Fe^{III}−OOR species, and the current consensus from one experimental and one computational study is that such species decay by homolysis of the Fe−O bond to form the iron(II) complex and ROO• radical.[88,89]

The reactivity of the Fe^{III}−OOH intermediates has stimulated the most discussions in the literature, due to the important role of activated bleomycin in DNA cleavage. Early on, it was postulated that a formally Fe^{V}(O) oxidant derived from O−O heterolysis may be involved in oxidations by activated bleomycin, paralleling the cytochrome P450 paradigm.[470] However, recent DFT calculations show that the amidate radical is much higher in energy than the corresponding oxidized porphyrin radical and therefore inaccessible.[422,431] An alternative pathway is a homolytic mechanism to form hydroxyl radical that serves as the oxidant, but the kinetic isotope effects observed for cleavage of the DNA ribose C4′−H bonds are too large to be compatible with this mechanism.[420,471] It is thus proposed that the Fe^{III}−OOH moiety itself serves as the oxidant, and O−O bond homolysis occurs concomitant with C−H bond cleavage.[422] As has been discussed in the sections on Reiske dioxygenases and bio-inspired oxidation catalysis, there are other pathways for activating the Fe^{III}−OOH moiety in the absence of the amidate functionality in which an Fe^{V}(O)(OH) oxidant is implicated, and a novel family of iron catalysts has been found that carry out a range of stereospecific hydrocarbon oxidations.[118,407]

5.2. High-Valent Iron–Oxo Intermediates

High-valent iron−oxo species have commonly been invoked as intermediates in the reactions of nonheme iron enzymes with O_2. But only for three enzymes have iron(IV) intermediates been trapped and characterized. These are intermediate Q of the diiron methane monooxygenase and intermediate X of the diiron ribonucleotide reductase,[472] both discovered in the 1990s and discussed in a different review in this volume, and that very recently discovered for the 2-OG-dependent monoiron TauD.[229] In all three cases, the iron(IV) centers are high-spin. Within this same time frame have also emerged the first synthetic nonheme iron(IV) complexes with N/O ligands.

One common ligand theme has been the use of the amido functionality that takes advantage of its strong σ donor ability to access and stabilize the iron(IV) oxidation state. In pioneering efforts, Collins and coworkers have prepared thermally stable high-valent complexes with tetraamido macrocyclic ligands.[473−475] One complex, $[Fe^{IV}(\eta^4\text{-L}_{mac*})Cl]$, has Mössbauer parameters $\Delta E_Q = 0.89$ mm^{-1} and $\delta = -0.04$ mm s^{-1} and behavior in high field that identify it as having

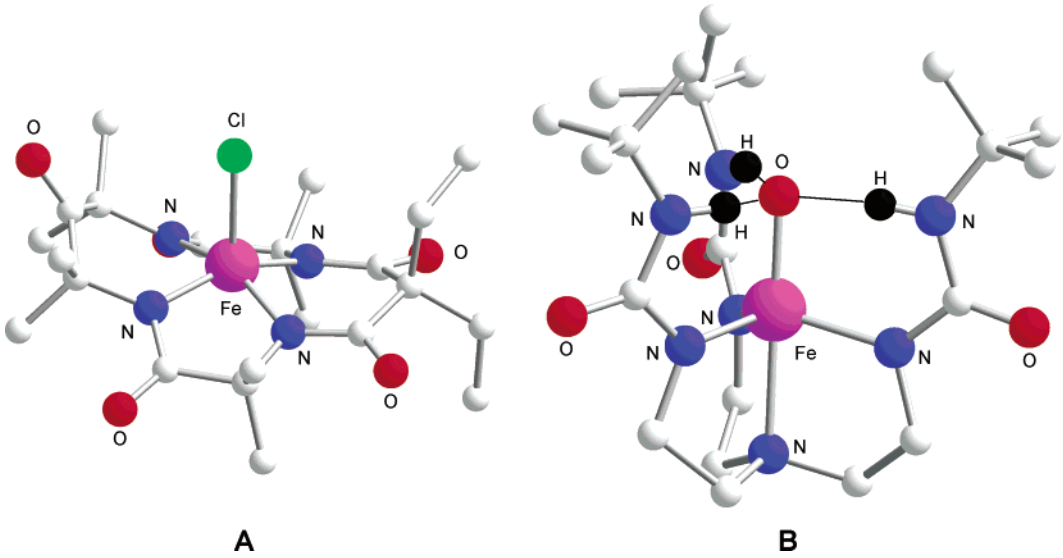

Figure 47. Crystal structures of $[Fe^{IV}(\eta^4\text{-}L_{mac*})Cl]$ (A) and $[Fe^{III}(L_{N3})(O)]^{2-}$ (B).

an $S = 2$ center; it is thus far the only crystallographically characterized example of a square pyramidal high-spin iron(IV) complex (Figure 47A). On the other hand, Schrock and Cummins have used a tripodal triamido ligand to prepare a thermally sensitive diamagnetic trigonal bipyramidal iron(IV) complex formulated as $[Fe^{IV}(L)(CN)]$, $L = [(^tBuMe_2Si\text{-}NCH_2CH_2N)_3N]^{3-}$.[476] More recently, Borovik and coworkers have used another triamido ligand, the tris-[(*N′-tert*-butylureaylato)-*N*-ethyl]amine trianion (L_{N3}), to synthesize the first crystallographically characterized example of a mononuclear oxoiron(III) species (Figure 47B).[477] Interestingly, this complex is obtained by the reaction of its iron(II) precursor with O_2. It is postulated that a (μ-1,2-peroxo)diiron(III) intermediate is initially formed that then undergoes O−O bond homolysis to generate an unobserved oxoiron(IV) species that is in turn reduced to the iron(III) oxidation state by solvent or added dihydroanthracene. This oxoiron(III) complex, like its (μ-oxo)-diiron(III) counterparts,[84] has an Fe−O bond length of 1.813(3) Å. It exhibits a ν_{Fe-O} at 671 cm^{-1} in its FTIR spectrum, with a downshift of 26 cm^{-1} when $^{18}O_2$ is used in the sample preparation. Notably, the rather basic oxo atom in this complex is stabilized by three hydrogen bonds from the N−H groups of the ligand. It is also readily protonated, and the structure of the Fe^{III}−OH derivative has been solved.[478] The O−H bond dissociation enthalpies of the iron(II) and iron(III) complexes were determined to be 66(4) and 115(4) kcal/mol, respectively, by a thermodynamic cycle.[479] This study provides a thermodynamic basis to predict that the corresponding oxoiron(IV) species should be a powerful hydrogen abstraction agent. Unfortunately, this high-valent species has not been observed, probably owing to its high potential reactivity.

Parallel to these efforts, Wieghardt and co-workers have successfully prepared high-valent nitridoiron complexes by photolysis of iron(III) azide precursors.[480−483] Thus, irradiation of $Fe^{III}(N_3)$ complexes of macrocylic N3 or N4 ligands like TACN or cyclam affords dinuclear species containing $Fe^{III}(\mu\text{-}N)Fe^{IV}$ ($S = {}^1/_2$ and ${}^3/_2$) cores or mononuclear $Fe^V{=}N$ complexes ($S = {}^3/_2$), as deduced from analysis of their EPR and Mössbauer properties. These results demonstrate that even neutral polydentate amine ligands can support high iron oxidation states under the appropriate conditions. With the use of tetradentate diamido ligands in this chemistry, diamagnetic Fe^{IV}-(μ-N)Fe^{IV} complexes can also be obtained and characterized by X-ray crystallography.[484]

Synthetic efforts in the past 10 years have demonstrated that the oxoiron(IV) state is in fact synthetically accessible in a nonheme ligand environment. Bis(oxo)diiron(III,IV) complexes of neutral tetradentate tripodal N4 ligands that serve as models for high-valent intermediates in nonheme diiron enzymes have been obtained and characterized spectroscopically.[456,457,485−488] Indeed, one of these, $[Fe_2O_2(5\text{-}Et_3\text{-}TPA)_2](ClO_4)_3$, has been crystallographically characterized and shown to have a valence-delocalized ($S = {}^3/_2$) $Fe_2(\mu\text{-}O)_2$ diamond core.[489] Another diiron(III,IV) complex with a valence-delocalized core ($S = {}^1/_2$, $S_1' = {}^5/_2$, $S_2' = 2$) can be generated by the reaction of O_2 and a diiron(II) complex with four bulky diarylbenzoate ligands, but its structure is not established.[490] Very recently added to this select group are $[(L)Fe^{III}(\mu\text{-}O)(\mu\text{-}O_2CR)_2Fe^{IV}(L')]^{3+}$ (L, L′ = TACN, Me_3TACN, Tp) and $[(Me_3TACN)Cr^{III}(\mu\text{-}O)(\mu\text{-}O_2CR)_2Fe^{IV}(Me_3TACN)]^{3+}$, which can be generated by one-electron oxidation of their dimetal(III) precursors.[491] The iron(IV) centers in these $M^{III}Fe^{IV}$ complexes have an $S = 1$ spin state that is antiferromagnetically coupled to either a high-spin iron(III) ($S = {}^5/_2$) or a chromium(III) ($S = {}^3/_2$) center.

The first hint that a mononuclear iron(IV)−oxo species can be obtained, reported by Wieghardt and co-workers in 2000,[483] involves the generation of such a species by the reaction of $[Fe^{III}$(cyclam acetate)-(OTf)$]^+$ (cyclam acetate = 1-carboxymethyl-1,4,8,11-tetraazacyclotetradecane) with O_3 at −80 °C. However, its instability and low yield precluded detailed characterization beyond its Mössbauer spectrum, which is best interpreted as arising from an $S = 1$ iron(IV) center. More recently, Rohde et al. have investigated the reaction of the iron(II) complex of a

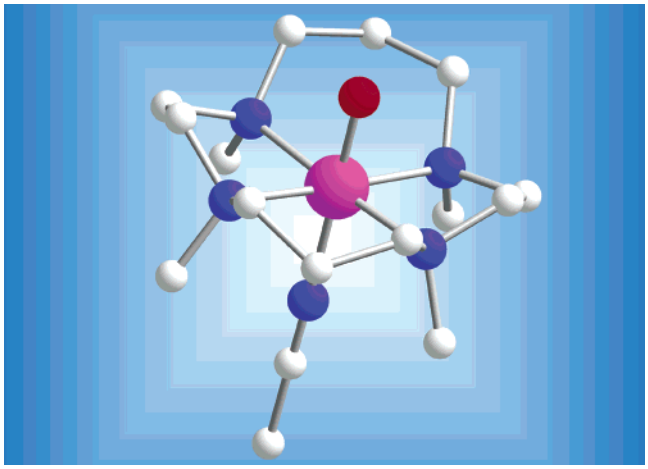

Figure 48. Crystal structure of $[Fe^{IV}(O)(TMC)(CH_3CN)]^{2+}$.

closely related macrocycle TMC (TMC = 1,4,8,11-tetramethyl-1,4,8,11-tetraazacyclotetradecane) with PhIO and obtained in high yield $[Fe^{IV}(O)(TMC)(NCCH_3)](OTf)_2$, which persists for weeks at −40 °C.[492] Its remarkable thermal stability has led to its crystallization and the solution of the first high-resolution structure of a complex with a terminal Fe^{IV}═O unit (Figure 48). These pivotal results have opened the door to a rich oxoiron(IV) chemistry that has just begun to be explored.

$[Fe^{IV}(O)(TMC)(NCCH_3)]^{2+}$ is a pale green complex with an absorption maximum in the near-IR region (λ_{max} = 820 nm, ϵ = 400 M^{-1} cm^{-1}), the only electronic transition observed above 400 nm.[492] It exhibits in zero applied field a Mössbauer doublet with an isomer shift δ = 0.17(1) mm s^{-1} and a quadrupole splitting ΔE_Q = 1.24(1) mm s^{-1}. Mössbauer analysis at different fields provides parameters that led to the conclusion that it is an S = 1 Fe(IV) paramagnet. Its crystal structure reveals a 1.646(3) Å Fe−O distance, a value that closely matches r_{Fe-O} values deduced from EXAFS analysis of oxoiron(IV) units in synthetic and biological porphyrin complexes.[493−495] The 1.646(3) Å distance observed is much shorter than the 1.813(3) Å terminal Fe−O distance for the oxoiron(III) complex of Borovik,[477] reflecting the stronger Fe−O bonding interactions between the tetravalent iron and the terminal oxo ligand. Correspondingly, the Fe−O stretch observed in FTIR experiments is found at 834 cm^1 ($\Delta^{18}O$ = −34 cm^{-1}, as expected for an Fe−O diatomic vibration), typical of values found for corresponding Fe^{IV}═O units with heme ligands,[496] but significantly higher than the 671 cm^{-1} value associated with the oxoiron(III) complex of Borovik. [477]

With the existence of an oxoiron(IV) complex firmly established by crystallography, its spectroscopic properties can now be used as the basis for recognizing the formation of like species with other ligands. Indeed, oxoiron(IV) complexes have been prepared with three other types of neutral ligands: the tripodal tetradentate TPA,[497,498] the linear tetradentate BPMCN with a β topology,[499] and the pentadentate N4Py and R-TPEN family.[500,501] Different oxidants are required for the various transformations, as summarized in the reactions listed below:

$$Fe^{II}(L)(OTf)_2 + PhIO \rightarrow [Fe^{IV}(O)(L)]^{2+}$$
(L = TMC, N4Py, Bn-TPEN)

$$[Fe^{II}(L)(Cl)](PF_6) + ClO^- \rightarrow [Fe^{IV}(O)(L)]^{2+}$$
(L = Me-TPEN, Me-TPPN)

$$Fe^{II}(L)(OTf)_2 + RCO_3H \rightarrow [Fe^{IV}(O)(L)]^{2+}$$
(L = TMC, TPA, β-BPMCN, N4Py, Bn-TPEN)

$$Fe^{II}(L)(OTf)_2 + {}^tBuOOH \rightarrow [Fe^{III}(L)(OO{}^tBu)]^{2+} \rightarrow [Fe^{IV}(O)(L)]^{2+}$$
(L = TPA, β-BPMCN)

The properties of the mononuclear oxoiron(IV) complexes characterized so far are compared in Tables 8 and 9. They all exhibit near-IR transitions with relatively low extinction coefficients (Figure 49). Their low intensities suggest that these are not charge-transfer transitions but more likely ligand field in origin. In support, efforts to obtain resonance Raman spectra by excitation into the near-IR band have thus far been unsuccessful. Furthermore, with the exception of the cyclam acetate complex, there appears to be a trend of increasing energy with the number of pyridines in the ligand, which would be consistent with a ligand field assignment. In-depth CD and MCD spectroscopic analysis in progress should clarify this point shortly.[502]

XAS analysis of these oxoiron(IV) complexes provides useful structural insight in lieu of an X-ray structure. Fits to the EXAFS region show the presence of a short (1.65−1.67 Å) Fe−O bond for all complexes studied thus far. These complexes also exhibit an intense 1s → 3d pre-edge transition, with an area of 25−30 units, which is much higher than is commonly seen for six-coordinate iron complexes (4−10 units)[510−512] but comparable to those observed for high-valent iron−oxo porphyrin complexes (27−38 units).[495,513] Like d−d transitions, the 1s → 3d pre-

Table 8. Comparison of $[Fe^{IV}(O)L]_n$ Complexes with S = 1 Sites

	L =					
	cyclam acetate	N4Py	TMC	TPA	BPMCN	BPMCN
n	1	1	1	1	1	2
λ_{max} (nm)	676	693	820	724	753	656, 845
ϵ_{max} (M^{-1} cm^{-1})		400	400	300	280	4000, 3000
XAS pre-edge peak area			30(4)	30(4)	28(2)	10(2)
r(Fe−O) (Å)			1.646(3) (XRD)	1.67(2) (XAS)	1.65(2)	1.79(2) (XAS)
$t_{1/2}$ at −40 °C	∼1 min		>24 d	>24 h		∼minutes
$t_{1/2}$ at 25 °C		60 h	10 h			
ref	483	500	492	497	499	503

Table 9. Mössbauer Parameters for Oxoiron(IV) (and Related) Compounds

complexes	δ, mm/s	ΔE_Q, mm/s	$[A_{x,y,z}/g\beta]$, T	ref
High-Spin Oxoiron(III) Centers				
$[Fe^{III}(O)(L_{N3})]^{2-}$ (77 K)	0.30	0.71		477
(μ-oxo)diiron(III) complexes	0.45−0.55	1.3−2.4		84
Low-Spin Iron(IV) Centers				
$[Fe^{IV}(O)$(cyclam acetate)$]^+$	0.01	1.37	[−23,−23,−10]	483
$[Fe^{IV}(O)(TMC)(CH_3CN)]^{2+}$	0.17	1.23	[−25,−20,−3]	492
$[Fe^{IV}(O)(TPA)(CH_3CN)]^{2+}$	0.01	0.93	[−22.5,−21.9,−6]	497
$[Fe^{IV}(O)(BPMCN)]^{2+}$	0.07	1.04	[−22.5,−19,−5]	499
$[Fe^{IV}(O)(N4Py)]^{2+}$	−0.04	0.93		500
$[Fe^{IV}(O)(Bn\text{-}TPEN)]^{2+}$	0.01	0.87		500
$[Fe^{IV}(O)(Me\text{-}TPPN)]^{2+}$ [a]	0.03	1.21	[−18,−20.6,−0.4]	501
$[Fe^{IV}_2(\mu\text{-}O)_2(BPMCN)_2]^{4+}$	0.10	1.75	[−22,−17.1,−1.1]	503
$[Fe^{III,IV}_2(\mu\text{-}O)(\mu\text{-}OAc)_2(TACN)_2]^{3+}$ (major species)	0.05	1.14	[−11.3,−21,−2.5]	491
$[Fe^{III,IV}_2(\mu\text{-}O)(\mu\text{-}OAc)_2(Me_3\text{-}TACN)_2]^{3+}$	0.026	1.74	[−15.5,−15.5,−15.5]	491
$[Fe^{III,IV}_2(\mu\text{-}O)(\mu\text{-}OAc)_2(Tp)_2]^{+}$	0.00	1.07	[−18.5,−18.5,0]	491
$[(Tp)Fe^{III}(\mu\text{-}O)(\mu\text{-}OAc)_2Fe^{IV}(Me_3\text{-}TACN)]^{2+}$	0.04	1.68	[−21.8,−14.8,−13.3]	491
$[(Me_3\text{-}TACN)Cr^{III}(\mu\text{-}O)\text{-}(\mu\text{-}OAc)_2Fe^{IV}(TACN)]^{3+}$	−0.002	1.215	[−15.0,−15.0,−21]	491
$[Fe^{III,IV}_2(\mu\text{-}O)_2(5\text{-}Me_3\text{-}TPA)_2]^{3+}$ (valence delocalized)	0.14	0.49		485
Fe^{IV}(O)(porphyrin) complexes	0.04−0.12	1.3−2.3		504
HRP compound II	0.03	1.51	[−19.3,−19.3,−6.5]	505
High-Spin Iron(IV) Centers				
$[Fe^{IV}(\eta^4\text{-}L_{mac*})(Cl)]$	−0.04	0.89	[−18,−15,−10.8]	474
$[Fe^{III,IV}_2(O)_2(6\text{-}Me\text{-}TPA)_2]^{3+}$	0.08	0.5	[14.5,26.5,26.5]	486
$[Fe^{III,IV}_2(O)_2(6\text{-}Me_3\text{-}TPA)_2(H_2O)]^{3+}$	0.10	1.14	[17,25,20]	488
"$[Fe^{III}Fe^{IV}(O_2CAr^{Tol})_4]^{3+}$"	0.12	0.6	[22.9,19.9,22.9]	490
TauD intermediate	0.31	−0.88	[−20,−20,−15]	229
E. coli RNR R2-X	0.26	−0.6	[20.0,26.7,26.7]	506
Mc MMOH-Q	0.21, 0.14	0.68, 0.55		507
Mc MMOH-Q_X	0.14	−0.6	[19,22,23]	508
Mt MMOH-Q	0.17	0.53		509

[a] Its alternative formulation as $[Fe^{IV}(OMe)(Me\text{-}TPPN)]^{3+}$ cannot be excluded with the available data.

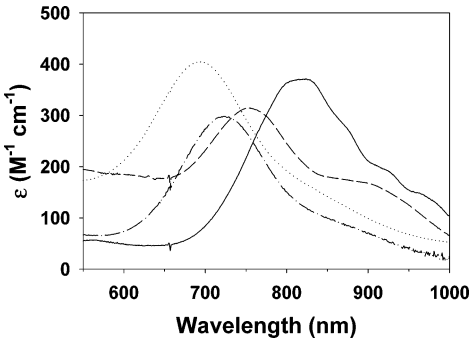

Figure 49. Near-IR spectra of $[Fe^{IV}(O)(L)]$ complexes: L = TMC (−), N4Py (···) TPA (−·−), and β-BPMCN (− −).

edge transition is sensitive to the symmetry of the metal coordination environment and becomes more intense as the metal environment becomes less centrosymmetric. So the presence of a terminal oxo ligand would be expected to impose a significant distortion on the iron coordination environment and give rise to an intense pre-edge peak.

A perusal of Table 9 shows that all nonheme $S = 1$ oxoiron(IV) complexes studied thus far exhibit remarkably similar spin Hamiltonian parameters, obtained from Mössbauer analysis, despite differences in the nature of the supporting ligands. They also closely resemble the parameters found for iron(IV) centers found for compounds I and II of heme peroxidases and their biomimetic counterparts.[504] The observed isomer shift (δ) values span a range of −0.04 to +0.17 mm/s, with the TMC complex alone at the high end and with porphyrin and pyridine-rich complexes congregating at the low end. This trend may reflect the extent of electron donation from the ligand to the iron(IV) center. The isomer shifts of the few available synthetic $S = 2$ iron(IV) complexes also appear to fit into this range, so the isomer shift may not be a useful tool to discriminate between spin states of iron(IV) centers. The three iron(IV) centers associated with high-valent enzyme intermediates are all deduced to be high spin, but only intermediate Q of methane monooxygenase has an isomer shift that falls within this range.[507−509] Those of TauD[229] and intermediate X of ribonucleotide reductase[506] are at least 0.09 mm/s higher, approaching the lower limit of the range for $S = {}^5/_2$ iron(III) centers. Notably, the iron(IV) center of TauD and the Fe(III) center of $[Fe^{III}(O)(L_{N3})]^{2-}$ have essentially the same isomer shift. These observations have led to the suggestion that the putative oxoiron(IV) units in these latter two enzyme intermediates may have enhanced $Fe^{III}-O^{\bullet}$ character. This intriguing notion and the factors that modulate the electronic structure description of these oxoiron(IV) centers clearly deserve further study.

The different oxidants required to generate the oxoiron(IV) complexes raise intriguing mechanistic questions. The PhIO and ClO^- reactions presumably involve simple oxygen-atom transfer, while the peracid oxidations, requiring only a stoichiometric amount of reagent to effect nearly quantitative conversion, must entail a heterolytic O−O bond cleavage mechanism. The observation that ^{t}BuOOH can also serve as an oxidant to form oxoiron(IV) complexes deserves special comment. It has been established for some time that transient low-spin $Fe^{III}OO^tBu$ intermedi-

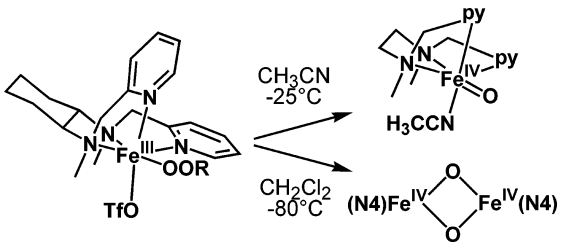

Figure 50. Solvent dependence of the decomposition of $[Fe^{III}(\beta\text{-BPMCN})(OO^tBu)]^{2+}$ to oxoiron(IV) complexes.

ates can be formed in the reactions of iron(II) or iron(III) complexes with ^{t}BuOOH[342,404,405] and that they decompose by O−O bond homolysis pathways.[89,335,336,340,448,469] Until recently, the weak oxoiron(IV) near-IR chromophore that must form in the course of O−O bond homolysis has not been reported, being obscured by the intense alkylperoxo-to-iron(III) charge-transfer band ($\lambda_{max} \approx 600$ nm, $\epsilon_M \approx 2000$) of the precursor Fe^{III}−OOR intermediate. In the earlier experiments, a large excess (typically 10-fold or greater) of ROOH was used to maximize the Fe^{III}−OOR chromophore, and this condition, not surprisingly, accelerated the decay of the oxoiron(IV) species. More recently, the use of only a 2-fold excess of ^{t}BuOOH in its reaction with the Fe^{II}(TPA) complex led to the observation of the oxoiron(IV) complex.[498] Furthermore, the addition of Lewis bases like pyridine or pyridine *N*-oxide accelerated the conversion of Fe^{III}−OOR to Fe^{IV}=O and enhanced the yield of $[Fe^{IV}(O)(TPA)]^{2+}$, demonstrating a dramatic "push" effect on the decomposition of the iron−peroxo complex. These examples illustrate a rather complex reaction landscape for the formation of oxoiron(IV) complexes.

The reaction of the related $Fe^{II}(\beta\text{-BPMCN})(OTf)_2$ with ^{t}BuOOH exhibits additional complexity, revealing an even richer chemistry. While the decay of $[Fe^{III}(\beta\text{-BPMCN})(OO^tBu)]^{2+}$ in acetonitrile at −25 °C affords the already described $S = 1$ $[Fe^{IV}(O)(BPMCN)]^{2+}$ species,[499] a different iron(IV) complex is generated in CH_2Cl_2 at −80 °C that also exhibits low-energy ($\lambda_{max} = 656$, 845 nm) transitions, but which are an order of magnitude more intense.[503] Resonance Raman and XAS experiments establish that this complex has an $Fe^{IV}_2(\mu\text{-O})_2$ diamond core that presumably results from dimerization of the Fe^{IV}(O) unit. The features that distinguish it from its mononuclear analogue are a much less intense 1s → 3d pre-edge absorption and an Fe−O bond length of 1.79 Å. Its observed higher intensity absorption bands likely arise from primarily metal-to-metal transitions of the $Fe^{IV}_2(\mu\text{-O})_2$ diamond core, as recently established for the related valence-delocalized $[Fe_2(\mu\text{-O})_2(5\text{-Et}_3\text{-TPA})_2](ClO_4)_3$ complex.[485,489,514,515] To date, despite having low-spin metal centers, this diiron(IV) complex is the only synthetic complex that has the $Fe^{IV}_2(\mu\text{-O})_2$ diamond core proposed for intermediate Q of methane monooxygenase.[516] The two different product outcomes can be rationalized by the ligating ability of the solvent (Figure 50). The nascent Fe^{IV}(O) species derived from O−O bond homolysis of the Fe^{III}−OOR intermediate is readily intercepted by CH_3CN and stabilized by the solvent, but dimerizes instead in the non-coordinating CH_2Cl_2.

The handful of oxoiron(IV) complexes available exhibit varying thermal stabilities (Table 8) and reactivities toward substrates. The TMC complex, for example, is stable for at least a month at −40 °C but only converts PPh_3 to $OPPh_3$; neither thioanisole nor 2,4-di-*tert*-butylphenol is oxidized under these conditions.[492] On the other hand, the TPA complex is stable for less than a day at −40 °C but carries out oxo transfer to PPh_3, thioanisole, and even cyclooctene.[497] $[Fe^{IV}_2(\mu\text{-O})_2(BPMCN)_2]^{4+}$, with a lifetime of only minutes at −40 °C, can oxidize adamantane to 1-adamantanol and 2-adamantanone in 56% and 20% respective yields.[503] So not surprisingly, the reactivities of these oxoiron(IV) complexes of tetradentate ligands correlate inversely with their thermal stabilities. The oxoiron(IV) complex of the pentadentate N4Py appears to be an exception; it exhibits a remarkable thermal stability ($t_{1/2} \approx 60$ h at 25 °C) yet can attack even the C−H bonds of cyclohexane.[500] Clearly the chemistry of these synthetic oxoiron(IV) complexes affords an interesting reaction landscape that is worth further in-depth exploration.

6. Outlook

In the eight years since the publication of our review on mononuclear nonheme iron dioxygen activating enzymes in the special Bioinorganic Enzymology issue of *Chemical Reviews*,[1] there has been a veritable explosion of information that has accumulated for this class of enzymes. Dozens of crystal structures are now available not only of enzymes in their resting states but also of binary and ternary complexes that provide insight into how the active sites change upon substrate and/or cofactor binding. The progress in the structural biology aspects has been complemented by the development of powerful spectroscopic methods that can be used to probe the relatively inaccessible high-spin iron(II) center,[3,4] and computational tools that shed light on electronic structure.[517] The spectroscopic results generally corroborate the various mechanistic ideas that have evolved from the crystallographic studies and have led to a general paradigm for oxygen activation at a mononuclear nonheme iron(II) center. While much has been learned about the steps leading to dioxygen binding, much less is known of the steps subsequent to oxygen activation. With the sole exception of the 2-OG-dependent enzyme TauD, no intermediates subsequent to O−O bond cleavage but prior to product formation have been observed. For TauD, a catalytically relevant iron(IV) center[229] and tyrosyl radical[251] have recently been discovered. Thus, much work needs to be done to uncover details of enzyme mechanisms after dioxygen activation.

In 1996, there were few functional models for mononuclear nonheme iron enzymes. The most systematically studied was a class of iron(III) catecholate complexes that reacted with O_2 to afford intradiol cleavage of the catecholate in high yield, and initial efforts to model the 2-OG-dependent enzymes had just been reported. Eight years later, there are functional models for extradiol-cleaving dioxygenases, 2-OG-dependent enzymes, pterin-dependent enzymes, and Rieske dioxygenases, all providing op-

portunities to obtain more detailed information about the steps that occur subsequent to O−O bond cleavage. A number of iron−peroxo intermediates have been trapped and spectroscopically characterized; two even have crystal structures. Last, the elusive oxoiron(IV) unit has also been stabilized sufficiently to be observed in several ligand environments, and one of these has even been crystallized. It is clear that much has been learned since 1996, but this dramatic progress simply sets the stage for the next eight years, during which time we hope to gain detailed molecular insight into how Nature activates dioxygen at a mononuclear nonheme iron center.

7. Acknowledgment

This work was supported by a research grant (L.Q., MERIT award GM-33162) and a predoctoral traineeship (M.P.M., GM-08700) from the National Institutes of Health, and a grant from the Ramon y Cajal Program (M.C., MCYT, Spain). L.Q. thanks his many collaborators, past and present, who contributed to the results from the Que laboratory cited in this review. He particularly acknowledges Professors John Lipscomb and Eckard Münck, with whom he has had fruitful interactions in the nonheme iron area that span 30 years.

8. References

(1) Que, L., Jr.; Ho, R. Y. N. *Chem. Rev.* **1996**, *96*, 2607.
(2) Nordlund, P. In *Handbook on Metalloproteins*; Bertini, I., Sigel, A., Sigel, H., Eds.; Marcel Dekker: New York, 2001; pp 461−570.
(3) Solomon, E. I.; Brunold, T. C.; Davis, M. I.; Kemsley, J. N.; Lee, S.-K.; Lehnert, N.; Neese, F.; Skulan, A. J.; Yang, Y.-S.; Zhou, J. *Chem. Rev.* **2000**, *100*, 235.
(4) Solomon, E. I.; Decker, A.; Lehnert, N. *Proc. Natl. Acad. Sci. U.S.A.* **2003**, *100*, 3589.
(5) *Microbial Degradation of Organic Compounds*; Gibson, D. T., Ed.; Marcel Dekker: New York, 1984.
(6) Lipscomb, J. D.; Orville, A. M. In *Metal Ions in Biological Systems*; Sigel, H., Sigel, A., Eds.; Marcel Dekker: New York, 1992; Vol. 28, pp 243−298.
(7) Bugg, T. D. H.; Sanvoisin, J.; Spence, E. L. *Biochem. Soc. Trans.* **1997**, *25*, 81.
(8) Que, L., Jr.; Reynolds, M. F. In *Metal Ions in Biological Systems*; Sigel, H., Sigel, A., Eds.; Marcel Dekker: New York, 2000; Vol. 37, pp 505−525.
(9) Bugg, T. D. H.; Winfield, C. J. *Nat. Prod. Rep.* **1998**, *5*, 513.
(10) Bugg, T. D. H.; Lin, G. *Chem. Commun.* **2001**, *11*, 941.
(11) Que, L., Jr.; Widom, J.; Crawford, R. L. *J. Biol. Chem.* **1981**, *256*, 10941.
(12) Boldt, Y. R.; Sadowsky, M. J.; Ellis, L. B. M.; Que, L., Jr.; Wackett, L. P. *J. Bacteriol.* **1995**, *177*, 1225.
(13) Whiting, A. K.; Boldt, Y. R.; Hendrich, M. P.; Wackett, L. P.; Que, L., Jr. *Biochemistry* **1996**, *35*, 160.
(14) Hatta, T.; Mukerjee-Dhar, G.; Damborsky, J.; Kiyohara, H.; Kimbara, K. *J. Biol. Chem.* **2003**, *278*, 21483.
(15) Ohlendorf, D. H.; Lipscomb, J. D.; Weber, P. C. *Nature* **1988**, *336*, 403.
(16) Ohlendorf, D. H.; Orville, A. M.; Lipscomb, J. D. *J. Mol. Biol.* **1994**, *244*, 586.
(17) Orville, A. M.; Lipscomb, J. D.; Ohlendorf, D. H. *Biochemistry* **1997**, *36*, 10052.
(18) Elgren, T. E.; Orville, A. M.; Kelly, K. A.; Lipscomb, J. D.; Ohlendorf, D. H.; Que, L., Jr. *Biochemistry* **1997**, *36*, 11504.
(19) Orville, A. M.; Elango, N.; Lipscomb, J. D.; Ohlendorf, D. H. *Biochemistry* **1997**, *36*, 10039.
(20) Vetting, M. W.; Ohlendorf, D. H. *Structure* **2000**, *8*, 429.
(21) True, A. E.; Orville, A. M.; Pearce, L. L.; Lipscomb, J. D.; Que, L., Jr. *Biochemistry* **1990**, *29*, 10847.
(22) Que, L., Jr.; Lipscomb, J. D.; Münck, E.; Wood, J. M. *Biochim. Biophys. Acta* **1977**, *485*, 60.
(23) Que, L., Jr.; Lipscomb, J. D.; Zimmermann, R.; Münck, E.; Orme-Johnson, N. R.; Orme-Johnson, W. H. *Biochim. Biophys. Acta* **1976**, *452*, 320.
(24) Bull, C.; Ballou, D. P.; Otsuka, S. *J. Biol. Chem.* **1981**, *256*, 12681.
(25) Walsh, T. A.; Ballou, D. P.; Mayer, R.; Que, L., Jr. *J. Biol. Chem.* **1983**, *258*, 14422.
(26) Orville, A. M.; Lipscomb, J. D. *J. Biol. Chem.* **1993**, *268*, 8596.
(27) Wasinger, E. C.; Davis, M. I.; Pau, M. Y. M.; Orville, A. M.; Zaleski, J. M.; Hedman, B.; Lipscomb, J. D.; Hodgson, K. O.; Solomon, E. I. *Inorg. Chem.* **2002**, *42*, 365.
(28) Cox, D. D.; Que, L., Jr. *J. Am. Chem. Soc.* **1988**, *110*, 8085.
(29) Jang, H. G.; Cox, D. D.; Que, L., Jr. *J. Am. Chem. Soc.* **1991**, *113*, 9200.
(30) Krüger, H.-J. In *Biomimetic Oxidations Catalyzed by Metal Complexes*; Meunier, B., Ed.; Imperial College Press: London, 2000.
(31) Heistand, R. H., II; Roe, A. L.; Que, L., Jr. *Inorg. Chem.* **1982**, *21*, 676.
(32) Heistand, R. H., II; Lauffer, R. B.; Fikrig, E.; Que, L., Jr. *J. Am. Chem. Soc.* **1982**, *104*, 2789.
(33) Viswanathan, R.; Palaniandavar, M.; Balasubramanian, T.; Muthiah, T. P. *Inorg. Chem.* **1998**, *37*, 2943.
(34) Spartalian, K.; Carrano, C. J. *Inorg. Chem.* **1989**, *28*, 19.
(35) Mialane, P.; Anxolabéhère-Mallart, E.; Blondin, G.; Nivorojkine, A.; Guilhem, J.; Tchertanova, L.; Cesario, M.; Ravi, N.; Bominaar, E.; J.-J., G.; Münck, E. *Inorg. Chim. Acta* **1997**, *263*, 367.
(36) Fujii, H.; Funahashi, Y. *Angew. Chem., Int. Ed.* **2002**, *41*, 3638.
(37) Que, L., Jr.; Epstein, R. M. *Biochemistry* **1981**, *20*, 2545.
(38) Que, L., Jr.; Kolanczyk, R. C.; White, L. S. *J. Am. Chem. Soc.* **1987**, *109*, 5373.
(39) Funabiki, T.; Sakamoto, H.; Yoshida, S.; Tamara, L. *J. Chem. Soc., Chem. Commun.* **1979**, 754.
(40) Funabiki, T.; Mizoguchi, A.; Sugimoto, T.; Tada, S.; Tsuji, M.; Sakamoto, H.; Yoshida, S. *J. Am. Chem. Soc.* **1986**, *108*, 2921.
(41) Weller, M. G.; Weser, U. *J. Am. Chem. Soc.* **1982**, *104*, 3752.
(42) White, L. S.; Nilsson, P. V.; Pignolet, L. H.; Que, L., Jr. *J. Am. Chem. Soc.* **1984**, *106*, 8312.
(43) Que, L., Jr.; Kolanczyk, R. C.; White, L. S. *J. Am. Chem. Soc.* **1987**, *109*, 5373.
(44) Cox, D. D.; Benkovic, S. J.; Bloom, L. M.; Bradley, F. C.; Nelson, M. J.; Que, L., Jr.; Wallick, D. E. *J. Am. Chem. Soc.* **1988**, *110*, 2026.
(45) Sawyer, D. T. *Oxygen Chemistry*; Oxford University Press: New York, 1991.
(46) Bianchini, C.; Frediani, P.; Laschi, F.; Meli, A.; Vizza, F.; Zanello, P. *Inorg. Chem.* **1990**, *29*, 3402.
(47) Barbaro, P.; Bianchini, C.; Mealli, C.; Meli, A. *J. Am. Chem. Soc.* **1991**, *113*, 3181.
(48) Barbaro, P.; Bianchini, C.; Linn, K.; Mealli, C.; Meli, A.; Vizza, F.; Zanello, P. *Inorg. Chim. Acta* **1992**, *198−200*, 31.
(49) Dutta, S.; Peng, S.-M.; Bhattacharya, S. *Inorg. Chem.* **2000**, *39*, 2231.
(50) Pascaly, M.; Duda, M.; Schweppe, F.; Zurlinden, K.; Muller, F. K.; Krebs, B. *J. Chem. Soc., Dalton Trans.* **2001**, 828.
(51) Duda, M.; Pascaly, M.; Krebs, B. *J. Chem. Soc., Chem. Commun.* **1997**, 835.
(52) Mialane, P.; Tchertanova, L.; Banse, F.; Sainton, J.; Girerd, J.-J. *Inorg. Chem.* **2000**, *39*, 2440.
(53) Pascaly, M.; Nazikkol, C.; Schweppe, F.; Wiedemann, A.; Zurlinden, K.; Krebs, B. *Z. Anorg. Allg. Chem.* **2000**, *626*, 50.
(54) Koch, W. O.; Krüger, H.-J. *Angew. Chem., Int. Ed. Engl.* **1995**, *34*, 2671.
(55) Jo, D.-H.; Chiou, Y.-M.; Que, L., Jr. *Inorg. Chem.* **2001**, *40*, 3181.
(56) Raffard, N.; Carina, R.; Simaan, A. J.; Sainton, J.; Rivière, E.; Tchertanov, L.; Bourcier, S.; Bouchoux, G.; Delroisse, M.; Banse, F.; Girerd, J.-J. *Eur. J. Inorg. Chem.* **2001**, 2249.
(57) Funabiki, T.; Yamazaki, T.; Fukui, A.; Tanaka, T.; Yoshida, S. *Angew. Chem., Int. Ed.* **1998**, *37*, 513.
(58) Broderick, J. B.; O'Halloran, T. V. *Biochemistry* **1991**, *30*, 7349.
(59) Hinteregger, C.; Loidi, M.; Streichsbier, F. *FEMS Microbiol. Lett.* **1992**, *97*, 261.
(60) Funabiki, T.; Sugio, D.; Inui, N.; M., M.; Hitomi, Y. *Chem. Commun.* **2002**, 412.
(61) Lim, J. H.; Lee, H. J.; Lee, K.-B.; Jang, H. G. *Bull. Korean Chem. Soc.* **1997**, *18*, 1166.
(62) Dei, A.; Gatteschi, D.; Pardi, L. *Inorg. Chem.* **1993**, *32*, 1389.
(63) Siedow, J. N. *Annu. Rev. Plant Physiol. Plant Mol. Biol.* **1991**, *42*, 145.
(64) Yamamoto, S. *Biochim. Biophys. Acta* **1992**, *1128*, 117.
(65) Nelson, M. J.; Seitz, S. P. In *Active Oxygen in Biochemistry*; Valentine, J. S., Foote, C. S., Greenberg, A., Liebman, J. F., Eds.; Chapman & Hall: London, 1995.
(66) Samuelsson, B.; Dahlen, S.-E.; Lindgren, J. A.; Rouzer, C. A.; Serhan, C. N. *Science* **1987**, *237*, 1171.
(67) Sigal, E. *Am. J. Physiol.* **1991**, *260*, L13.
(68) Rioux, N.; Castonguay, A. *Carcinogenesis* **1998**, *19*, 1393.
(69) Boyington, J. C.; Gaffney, B. J.; Amzel, L. M. *Science* **1993**, *260*, 1482.
(70) Minor, W.; Steczko, J.; Bolin, J. T.; Otwinowski, Z.; Axelrod, B. *Biochemistry* **1993**, *32*, 6320.
(71) Minor, W.; Steczko, J.; Stec, R.; Otwinowski, Z.; Bolin, J. T.; Walter, R.; Axelrod, B. *Biochemistry* **1996**, *35*, 10687.

(72) Skrzypczak-Jankun, E.; Amzel, L. M.; Kroa, B. A.; Funk, M. O., Jr. *Proteins: Struct., Funct. Genet.* **1997**, *29*, 15.
(73) Tomchick, D. R.; Phan, P.; Cymborowski, M.; Minor, W.; Holman, T. R. *Biochemistry* **2001**, *40*, 7509.
(74) Gillmor, S. A.; Villaseñor, A.; Fletterick, R.; Sigal, E.; Browner, M. F. *Nat. Struct. Biol.* **1997**, 1003.
(75) Nelson, M. J. *Biochemistry* **1988**, *27*, 4273.
(76) Nelson, M. J.; Seitz, S. P.; Cowling, R. A. *Biochemistry* **1990**, *29*, 6897.
(77) Jonsson, T.; Glickman, M. H.; Sun, S.; Klinman, J. P. *J. Am. Chem. Soc.* **1996**, *118*, 10319.
(78) Zhang, Y.; Gebhard, M. S.; Solomon, E. I. *J. Am. Chem. Soc.* **1991**, *113*, 5162.
(79) Slappendel, S.; Velkink, G. A.; Vleigenthart, J. F. G.; Aasa, R.; Malmstrom, B. G. *Biochim. Biophys. Acta* **1981**, *667*, 77.
(80) Holman, T. R.; Zhou, J.; Solomon, E. I. *J. Am. Chem. Soc.* **1998**, *120*, 12564.
(81) Scarrow, R. C.; Trimitsis, M. G.; Buck, C. P.; Grove, G. N.; Cowling, R. A.; Nelson, M. J. *Biochemistry* **1994**, *33*, 15023.
(82) Skrzypczak-Jankun, E.; Bross, R. A.; Carroll, R. T.; Dunham, W. R.; Funk, M. O., Jr. *J. Am. Chem. Soc.* **2001**, *123*, 10814.
(83) Mandal, S. K.; Que, L., Jr. *Inorg. Chem.* **1997**, *36*, 5424.
(84) Kurtz, D. M., Jr. *Chem. Rev.* **1990**, *90*, 585.
(85) Ogo, S.; Wada, S.; Watanabe, Y.; Iwase, M.; Wada, A.; Harata, M.; Jitsukawa, K.; Masuda, H.; Einaga, H. *Angew. Chem., Int. Ed.* **1998**, *37*, 2102.
(86) Ogo, S.; Yamahara, R.; Roach, M.; Suenobu, T.; Aki, M.; Ogura, T.; Kitagawa, T.; Masuda, H.; Fukuzumi, S.; Watanabe, Y. *Inorg. Chem.* **2002**, *41*, 5513.
(87) Zang, Y.; Elgren, T. E.; Dong, Y.; Que, L., Jr. *J. Am. Chem. Soc.* **1993**, *115*, 811.
(88) Kim, J.; Zang, Y.; Costas, M.; Harrison, R. G.; Wilkinson, E. C.; Que, L., Jr *J. Biol. Inorg. Chem.* **2001**, *6*, 275.
(89) Lehnert, N.; Ho, R. Y. N.; Que, L., Jr.; Solomon, E. I. *J. Am. Chem. Soc.* **2001**, *123*, 12802.
(90) Glickman, M. H.; Wiseman, J. S.; Klinman, J. P. *J. Am. Chem. Soc.* **1994**, *116*, 793.
(91) Hwang, C.-C.; Grissom, C. B. *J. Am. Chem. Soc.* **1994**, *116*, 795.
(92) Glickman, M. H.; Klinman, J. P. *Biochemistry* **1995**, *34*, 14077.
(93) Lewis, E. R.; Johansen, E.; Holman, T. R. *J. Am. Chem. Soc.* **1999**, *121*, 1395.
(94) Lehnert, N.; Solomon, E. I. *J. Biol. Inorg. Chem.* **2003**, *8*, 294.
(95) Jonas, R. T.; Stack, T. D. P. *J. Am. Chem. Soc.* **1997**, *119*, 8566.
(96) Roth, J. P.; Mayer, J. M. *Inorg. Chem.* **1999**, *38*, 2760.
(97) Goldsmith, C. R.; Jonas, R. T.; Stack, T. D. P. *J. Am. Chem. Soc.* **2002**, *124*, 83.
(98) Gardner, K. A.; Mayer, J. M. *Science* **1995**, *269*, 1849.
(99) Roth, J. P.; Lovell, S.; Mayer, J. M. *J. Am. Chem. Soc.* **2000**, *122*, 5486.
(100) Roth, J. P.; Yoder, J. C.; Won, T.-J.; Mayer, J. M. *Science* **2001**, *294*, 2524.
(101) Lockwood, M. A.; Blubaugh, T. J.; Collier, A. M.; S. Lovell; Mayer, J. M. *Angew. Chem., Int. Ed.* **1999**, *38*, 225.
(102) Mayer, J. M. *Acc. Chem. Res.* **1998**, *31*, 441.
(103) Bakac, A. *J. Am. Chem. Soc.* **2000**, *122*, 1092.
(104) Yoder, J. C.; Roth, J. P.; Gussenhoven, E. M.; Larsen, A. S.; Mayer, J. M. *J. Am. Chem. Soc.* **2003**, *125*, 2629.
(105) Hegg, E. L.; Que, L., Jr. *Eur. J. Biochem.* **1997**, *250*, 625.
(106) Que, L., Jr. *Nat. Struct. Biol.* **2000**, *7*, 182.
(107) Kitajima, N.; Tolman, W. B. *Prog. Inorg. Chem.* **1995**, *43*, 419.
(108) Kitajima, N.; Tamura, N.; Amagai, H.; Fukui, H.; Moro-oka, Y.; Mizutani, Y.; Kitagawa, T.; Mathur, R.; Heerwegh, K.; Reed, C. A.; Randall, C. R.; Que, L., Jr.; Tatsumi, K. *J. Am. Chem. Soc.* **1994**, *116*, 9071.
(109) Ogihara, T.; Hikichi, S.; Akita, M.; Moro-oka, Y. *Inorg. Chem.* **1998**, *37*, 2614.
(110) Hegg, E. L.; Ho, R. Y. N.; Que, L., Jr. *J. Am. Chem. Soc.* **1999**, *121*, 1972.
(111) Ho, R. Y. N.; Mehn, M. P.; Hegg, E. L.; Liu, A.; Ryle, M. J.; Hausinger, R. P.; Que, L., Jr. *J. Am. Chem. Soc.* **2001**, *123*, 5022.
(112) Mehn, M. P.; Fujisawa, K.; Hegg, E. L.; Que, L., Jr. *J. Am. Chem. Soc.* **2003**, *125*, 7828.
(113) Ito, M.; Que, L., Jr. *Angew. Chem., Int. Ed. Engl.* **1997**, *36*, 1342.
(114) Lin, G.; Reid, G.; Bugg, T. D. H. *J. Am. Chem. Soc.* **2001**, *123*, 5030.
(115) Chiou, Y.-M.; Que, L., Jr. *Inorg. Chem.* **1995**, *34*, 3577.
(116) Chiou, Y.-M.; Que, L., Jr. *J. Am. Chem. Soc.* **1995**, *117*, 3999.
(117) Chen, K.; Costas, M.; Kim, J.; Tipton, A. K.; Que, L., Jr. *J. Am. Chem. Soc.* **2002**, *124*, 3026.
(118) Chen, K.; Costas, M.; Que, L., Jr. *J. Chem. Soc., Dalton Trans.* **2002**, 672.
(119) Costas, M.; Que, L., Jr. *Angew. Chem., Int. Ed.* **2002**, *41*, 2179.
(120) Beck, A.; Weibert, B.; Burzlaff, N. I. *Eur. J. Inorg. Chem.* **2001**, 521.
(121) Beck, A.; Barth, A.; Huebner, E.; Burzlaff, N. *Inorg. Chem.* **2003**, *42*, 7182.
(122) Sugiyama, K.; Senda, T.; Narita, H.; Yamamoto, T.; Kimbara, K.; Fukuda, M.; Yano, K.; Mitsui, Y. *Proc. Jpn. Acad., Ser. B* **1995**, *71*, 32.
(123) Han, S.; Eltis, L. D.; Timmis, K. N.; Muchmore, S. W.; Bolin, J. T. *Science* **1995**, *270*, 976.
(124) Kita, A.; Kita, S.; Fujisawa, I.; Inaka, K.; Ishida, T.; Horiike, K.; Nozaki, M.; Miki, K. *Structure* **1999**, *7*, 25.
(125) (a) Vetting, M. W. Ph.D. Thesis, University of Minnesota, 2002. (b) Vetting, M. W.; Wackett, L. P.; Que, L., Jr.; Lipscomb, J. D.; Ohlendorf, D. H. *J. Bacteriol.* **2004**, in press.
(126) Sugimoto, K.; Senda, T.; Aoshima, H.; Masai, E.; Fukuda, M.; Mitsui, Y. *Structure* **1999**, *7*, 953.
(127) Titus, G. P.; Mueller, H. A.; Burgner, J.; Córdoba, S. R. d.; Penalva, M. A.; Timm, D. E. *Nat. Struct. Biol.* **2000**, *7*, 542.
(128) Valegård, K.; vanScheltinga, A. C. T.; Lloyd, M. D.; Hara, T.; Ramaswamy, S.; Perrakis, A.; Thompson, A.; Lee, H.-J.; Baldwin, J. E.; Schofield, C. J.; Hajdu, J.; Andersson, I. *Nature* **1998**, *394*, 805.
(129) Zhang, Z.; Ren, J.; Stammers, D. K.; Baldwin, J. E.; Harlos, K.; Schofield, C. J. *Nat. Struct. Biol.* **2000**, *7*, 127.
(130) Clifton, I. J.; Hsueh, L.-C.; Baldwin, J. E.; Harlos, K.; Schofield, C. J. *Eur. J. Biochem.* **2001**, *268*, 6625.
(131) Elkins, J. M.; Ryle, M. J.; Clifton, I. J.; Hotopp, J. C. D.; Lloyd, J. S.; Burzlaff, N. I.; Baldwin, J. E.; Hausinger, R. P.; Roach, P. L. *Biochemistry* **2002**, *41*, 5185.
(132) O'Brien, J. R.; Schuller, D. J.; Yang, V. S.; Dillard, B. D.; Lanzillotta, W. N. *Biochemistry* **2003**, 5547.
(133) Wilmouth, R. C.; Turnbull, J. J.; Welford, R. W. D.; Clifton, I. J.; Prescott, A. G.; Schofield, C. J. *Structure* **2002**, *10*, 93.
(134) Dann, C. E., III; Bruick, R. K.; Deisenhofer, J. *Proc. Natl. Acad. Sci. U.S.A.* **2002**, *99*, 15351.
(135) Elkins, J. M.; Hewitson, K. S.; McNeill, L. A.; Seibel, J. F.; Schlemminger, I.; Pugh, C. W.; Ratcliffe, P. J.; Schofield, C. J. *J. Biol. Chem.* **2003**, *278*, 1802.
(136) Clifton, I. J.; Doan, L. X.; Sleeman, M. C.; Topf, M.; Suzuki, H.; Wilmouth, R. C.; Schofield, C. J. *J. Biol. Chem.* **2003**, *278*, 20843.
(137) Serre, L.; Sailland, A.; Sy, D.; Boudec, P.; Rolland, A.; Pebay-Peyroula, E.; Cohen-Addad, C. *Structure* **1999**, *7*, 977.
(138) Roach, P. L.; Clifton, I. J.; Fulop, V.; Harlos, K.; Barton, G. J.; Hajdu, J.; Andersson, I.; Schofield, C. J.; Baldwin, J. E. *Nature* **1995**, *375*, 700.
(139) Fusetti, F.; Erlandsen, H.; Flatmark, T.; Stevens, R. C. *J. Biol. Chem.* **1998**, *273*, 16962.
(140) Kobe, B.; Jennings, I. G.; House, C. M.; Michell, B. J.; Goodwill, K. E.; Santarsiero, B. D.; Stevens, R. C.; Cotton, R. G. H.; Kemp, B. E. *Nat. Struct. Biol.* **1999**, *6*, 442.
(141) Erlandsen, H.; Kim, J. Y.; Patch, M. G.; Han, A.; Volner, A.; Abu-Omar, M. M.; Stevens, R. C. *J. Mol. Biol.* **2002**, *320*, 645.
(142) Goodwill, K. E.; Sabatier, C.; Marks, C.; Raag, R.; Fitzpatrick, P. F.; Stevens, R. C. *Nat. Struct. Biol.* **1997**, *4*, 578.
(143) Wang, L.; Erlandsen, H.; Haavik, J.; Knappskog, P. M.; Stevens, R. C. *Biochemistry* **2002**, *41*, 12569.
(144) Kauppi, B.; Lee, K.; Carredano, E.; Parales, R. E.; Gibson, D. T.; Eklund, H.; Ramaswamy, S. *Structure* **1998**, *6*, 571.
(145) Eltis, L. D.; Bolin, J. T. *J. Bacteriol.* **1996**, *178*, 5930.
(146) Arciero, D. M.; Orville, A. M.; Lipscomb, J. D. *J. Biol. Chem.* **1985**, *260*, 14035.
(147) Vaillancourt, F. H.; Barbosa, C. J.; Spiro, T. G.; Bolin, J. T.; Blades, M. W.; Turner, R. F. B.; Eltis, L. D. *J. Am. Chem. Soc.* **2002**, *124*, 2485.
(148) Uragami, Y.; Senda, T.; Sugimoto, K.; Sato, N.; Nagarajan, V.; Masai, E.; Fukuda, M.; Mitsui, Y. *J. Inorg. Biochem.* **2001**, *83*, 269.
(149) Sato, N.; Uragami, Y.; Nishizaki, t.; Takahashi, Y.; Sazaki, G.; Sugimoto, K.; Nonaka, T.; Masai, E.; Fukuda, M.; Senda, T. *J. Mol. Biol.* **2002**, *321*, 621.
(150) Shu, L.; Chiou, Y.-M.; Orville, A. M.; Miller, M. A.; Lipscomb, J. D.; Que, L., Jr. *Biochemistry* **1995**, *34*, 6649.
(151) Reynolds, M. F.; Costas, M.; Ito, M.; Jo, D.-H.; Tipton, A. A.; Whiting, A. K.; Que, L., Jr. *J. Biol. Inorg. Chem.* **2003**, *8*, 263.
(152) Wang, Y. Z.; Lipscomb, J. D. *Protein Expression* **1997**, *10*, 1.
(153) Lah, M. S.; Dixon, M. M.; Pattridge, K. A.; Stallings, W. C.; Fee, J. A.; Ludwig, M. L. *Biochemistry* **1995**, *34*, 1646.
(154) Vance, C. K.; Miller, A.-F. *J. Am. Chem. Soc.* **1998**, *120*, 461.
(155) Vance, C. K.; Miller, A.-F. *Biochemistry* **2001**, *40*, 13079.
(156) Tyson, C. A. *J. Biol. Chem.* **1975**, *250*, 1765.
(157) Miller, M. A.; Lipscomb, J. D. *J. Biol. Chem.* **1996**, *271*, 5524.
(158) Funabiki, T.; Mizoguchi, A.; Sugimoto, T.; Yoshida, S. *Chem. Lett.* **1983**, 917.
(159) Funabiki, T.; Tada, S.; Yoshioka, T.; Takano, M.; Yoshida, S. *J. Chem. Soc., Chem. Commun.* **1986**, 1699.
(160) Funabiki, T.; Konishi, T.; Kobayashi, S.; Mizoguchi, A.; Takano, M.; Yoshida, S. *Chem. Lett.* **1987**, *719−722*.
(161) Funabiki, T.; Kojima, H.; Kaneko, M.; Inoue, T.; Yoshioka, T.; Tanaka, T.; Yoshida, S. *Chem. Lett.* **1991**, 2143.
(162) Funabiki, T.; Yoneda, I.; Ishikawa, M.; Ujiie, M.; Nagai, Y.; Yoshida, S. *J. Chem. Soc., Chem. Commun.* **1994**, 1453.
(163) Funabiki, T.; Ishikawa, M.; Nagai, Y.; Yorita, J.; Yoshida, S. *J. Chem. Soc., Chem. Commun.* **1994**, 1951.
(164) Lin, G.; Reid, G.; Bugg, T. D. H. *Chem. Commun.* **2000**, 1119.
(165) Jo, D.-H.; Que, L., Jr. *Angew. Chem., Int. Ed.* **2000**, *39*, 4284.

(166) Lim, J. H.; Park, T. H.; Lee, H.-J.; Lee, K.-B.; Jang, H. G. *Bull. Korean Chem. Soc.* **1999**, *20*, 1428.
(167) Arciero, D. M.; Lipscomb, J. D.; Huynh, B. H.; Kent, T. A.; Münck, E. *J. Biol. Chem.* **1983**, *258*, 14981.
(168) Senda, T.; Sugiyama, K.; Narita, H.; Yamamoto, T.; Kimbara, K.; Fukuda, M.; Sato, M.; Yano, K.; Mitsui, Y. *J. Mol. Biol.* **1996**, *255*, 735.
(169) Spence, E. L.; Langley, G. J.; Bugg, T. D. H. *J. Am. Chem. Soc.* **1996**, *118*, 8336.
(170) Eley, K. L.; Crowley, P. J.; Bugg, T. D. H. *J. Org. Chem.* **2001**, *66*, 2091.
(171) Goodman, R. M.; Kishi, Y. *J. Am. Chem. Soc.* **1998**, *120*, 9392
(172) Goodman, R. M.; Kishi, Y. *J. Org. Chem.* **1994**, *59*, 5125.
(173) Cullis, P. M.; Arnold, J. R. P.; Clarke, M.; Howell, R.; De Mira, M.; Naylor, M.; Nicholls, D. *J. Chem. Soc., Chem. Commun.* **1987**, 1088.
(174) Corey, E. J.; Su, W.-G.; Mehrotra, M. M. *Tetrahedron Lett.* **1984**, *25*, 5123.
(175) Corey, E. J.; Mehrotra, M. M. *Tetrahedron Lett.* **1983**, *24*, 4921.
(176) Nishinaga, A.; Nakamura, K.; Shimizu, T.; Matsuura, T. *Tetrahedron Lett.* **1979**, *20*, 2165.
(177) Winfield, D. J.; Al-Mahrizy, Z.; Gravestock, M.; Bugg, T. D. H. *J. Chem. Soc., Perkin Trans. 1* **2000**, 3277.
(178) Deeth, R. J.; Bugg, T. D. H. *J. Biol. Inorg. Chem.* **2003**, *8*, 409.
(179) Groce, S. L.; Lipscomb, J. D. *J. Am. Chem. Soc.* **2003**, *125*, 11780.
(180) Schofield, C. J.; Zhang, Z. *Curr. Op. Struct. Biol.* **1999**, *9*, 722.
(181) Prescott, A. G.; Lloyd, M. D. *Nat. Prod. Rep.* **2000**, *17*, 367.
(182) Hanauske-Abel, H. M.; Popowicz, A. M. *Curr. Med. Chem.* **2003**, *10*, 1005.
(183) Fukumori, F.; Hausinger, R. P. *J. Biol. Chem.* **1993**, *268*, 24311.
(184) Hegg, E. L.; Whiting, A. K.; Saari, R. E.; McCracken, J.; Hausinger, R. P.; Que, L., Jr. *Biochemistry* **1999**, *38*, 16714.
(185) Falnes, P. Ø.; Johansen, R. F.; Seeberg, E. *Nature* **2002**, *419*, 178.
(186) Trewick, S. C.; Henshaw, T. F.; Hausinger, R. P.; Lindahl, T.; Sedgwick, B. *Nature* **2002**, *419*, 174.
(187) Aas, P. A.; Otterlei, M.; Falnes, P. Ø.; Vågbø, C. B.; Skorpen, F.; Akbari, M.; Sundheim, O.; Bjørås, M.; Slupphaug, G.; Seeberg, E.; Krokan, H. E. *Nature* **2003**, *421*, 859.
(188) Salowe, S. P.; Marsh, E. N.; Townsend, C. A. *Biochemistry* **1990**, *29*, 6499.
(189) Baldwin, J. E.; Abraham, E. *Nat. Prod. Rep.* **1988**, *5*, 129.
(190) Baldwin, J. E.; Adlington, R. M.; Crouch, N. P.; Schofield, C. J.; Turner, N. J.; Aplin, R. T. *Tetrahedron* **1991**, *47*, 9881.
(191) van der Ploeg, J. R.; Weiss, M. A.; Saller, E.; Nashimoto, H.; Saito, N.; Kertesz, M.; Leisinger, T. *J. Bacteriol.* **1996**, *178*, 5438.
(192) White, A. K.; Metcalf, W. W. *J. Biol. Chem.* **2002**, *277*, 38262.
(193) Lindblad, B.; Lindstedt, G.; Lindstedt, S. *J. Am. Chem. Soc.* **1970**, *92*, 7446.
(194) Ivan, M.; Kondo, K.; Yang, H.; Kim, W.; Valiando, J.; Ohh, M.; Salic, A.; Asara, J. M.; Lane, W. S.; Kaelin, W. G., Jr. *Science* **2001**, *292*, 464.
(195) Jaakkola, P.; Mole, D. R.; Tian, Y.-M.; Wilson, M. I.; Gielbert, J.; Gaskell, S. J.; von Kriegsheim, A.; Hebestreit, H. F.; Mukherji, M.; Schofield, C. J.; Maxwell, P. H.; Pugh, C. W.; Ratcliffe, P. J. *Science* **2001**, *292*, 468.
(196) Lando, D.; Peet, D. J.; Whelan, D. A.; Gorman, J. J.; Whitelaw, M. L. *Science* **2002**, *295*, 858.
(197) Semenza, G. L. *Annu. Rev. Cell Dev. Biol.* **1999**, *15*, 551.
(198) Kung, A. L.; Wang, S.; Klco, J. M.; Kaelin, W. G., Jr.; Livingston, D. M. *Nat. Med.* **2000**, *6*, 1335.
(199) Clement, P. M. J.; Hanauske-Abel, H. M.; Wolff, E. C.; Kleinman, H. K.; Park, M. H. *Int. J. Cancer* **2002**, *100*, 491.
(200) Hogan, D. A.; Smith, S. R.; Saari, A. A.; McCracken, J.; Hausinger, R. P. *J. Biol. Chem.* **2000**, *275*, 12400.
(201) Lukacin, R.; Britsch, L. *Eur. J. Biochem.* **1997**, *249*, 748.
(202) Armstrong, R. N. *Biochemistry* **2000**, *39*, 13625.
(203) Babbitt, P. C.; Gerlt, J. A. *J. Biol. Chem.* **1997**, *272*, 30591.
(204) Choroba, O. W.; Williams, D. H.; Spencer, J. B. *J. Am. Chem. Soc.* **2000**, *122*, 5389.
(205) Sabourin, P. J.; Bieber, L. L. *J. Biol. Chem.* **1982**, *257*, 7468.
(206) Hanauske-Abel, H. M.; Günzler, V. *J. Theor. Biol.* **1982**, *94*, 421.
(207) Cosper, N. J.; Stålhandske, C. M. V.; Saari, R. E.; Hausinger, R. P.; Scott, R. A. *J. Biol. Inorg. Chem.* **1999**, *4*, 122.
(208) Lloyd, M. D.; Lee, H.-J.; Harlos, K.; Zhang, Z.-H.; Baldwin, J. E.; Schofield, C. J.; Charnock, J. M.; Garner, C. D.; Hara, T.; van Scheltinga, A. C. T.; Valegård, K.; Viklund, J. A. C.; Hajdu, J.; Andersson, I.; Danielsson, Å.; Bhikhabhai, R. *J. Mol. Biol.* **1999**, *287*, 943.
(209) Pavel, E. G.; Kitajima, N.; Solomon, E. I. *J. Am. Chem. Soc.* **1998**, *120*, 3949.
(210) Tuderman, L.; Myllylä, R.; Kivirikko, K. I. *Eur. J. Biochem.* **1977**, *80*, 341.
(211) Myllylä, R.; Tuderman, L.; Kivirikko, K. I. *Eur. J. Biochem.* **1977**, *80*, 349.
(212) Holme, E. *Biochemistry* **1975**, *14*, 4999.
(213) Puistola, U.; Turpeenniemi-Hujanen, T. M.; Myllylä, R.; Kivirikko, K. I. *Biochim. Biophy. Acta* **1980**, *611*, 51.
(214) De Carolis, E.; De Luca, V. *J. Biol. Chem.* **1993**, *268*, 5504.
(215) Rundgren, M. *J. Biol. Chem.* **1977**, *252*, 5094.
(216) Johnson-Winters, K.; Purpero, V. M.; Kavana, M.; Nelson, T.; Moran, G. R. *Biochemistry* **2003**, *42*, 2072.
(217) Ryle, M. J.; Padmakumar, R.; Hausinger, R. P. *Biochemistry* **1999**, *38*, 15278.
(218) Pavel, E. G.; Zhou, J.; Busby, R. W.; Gunsior, M.; Townsend, C. A.; Solomon, E. I. *J. Am. Chem. Soc.* **1998**, *120*, 743.
(219) Zhou, J.; Gunsior, M.; Bachmann, B. O.; Townsend, C. A.; Solomon, E. I. *J. Am. Chem. Soc.* **1998**, *120*, 13539.
(220) Zhou, J.; Kelly, W. L.; Backmann, B. O.; Gunsior, M.; Townsend, C. A.; Solomon, E. I. *J. Am. Chem. Soc.* **2001**, *123*, 7388.
(221) Zhang, Z.; Ren, J.-s.; Harlos, K.; McKinnon, C. H.; Clifton, I. J.; Schofield, C. J. *FEBS Lett.* **2002**, *517*, 7.
(222) San Filippo, J., Jr.; Chern, C.; Valentine, J. S. *J. Org. Chem.* **1976**, *41*, 1077.
(223) Myllylä, R.; Schubotz, L. M.; Weser, U.; Kivirikko, K. I. *Biochem. Biophys. Res. Commun.* **1979**, *89*, 98.
(224) Holme, E.; Lindstedt, S.; Nordin, I. *Biochem. Biophys. Res. Commun.* **1982**, *107*, 518.
(225) Wehbie, R. S.; Punekar, N. S.; Lardy, H. A. *Biochemistry* **1988**, *27*, 2222.
(226) Myllylä, R.; Majamaa, K.; Günzler, V.; Hanauske-Abel, H. M.; Kivirikko, K. I. *J. Biol. Chem.* **1984**, *259*, 5403.
(227) Counts, D. F.; Cardinale, G. J.; Udenfriend, S. *Proc. Natl. Acad. Sci. U.S.A.* **1978**, *75*, 2145.
(228) Jefford, C. W.; Cadby, P. A. *Experientia* **1981**, *37*, 1134.
(229) Price, J. C.; Barr, E. W.; Tirupati, B.; Bollinger, J. M., Jr.; Krebs, C. *Biochemistry* **2003**, *42*, 7497.
(230) Münck, E. In *Physical Methods in Bioinorganic Chemistry. Spectroscopy and Magnetism*; Que, L., Jr., Ed.; University Science Books: Sausalito, CA, 2000; pp 287−319.
(231) Price, J. C.; Barr, E. W.; Glass, T. E.; Krebs, C.; Bollinger, J. M., Jr. *J. Am. Chem. Soc.* **2003**, *125*, 13008.
(232) Pascal, R. A., Jr.; Oliver, M. A.; Chen, Y.-C. J. *Biochemistry* **1985**, *24*, 3158.
(233) Thornburg, L. D.; Lai, M.-T.; Wishnok, J. S.; Stubbe, J. *Biochemistry* **1993**, *32*, 14023.
(234) Baldwin, J. E.; Adlington, R. M.; Crouch, N. P.; Pereira, I. A. C. *Tetrahedron* **1993**, *49*, 7499.
(235) Baldwin, J. E.; Adlington, R. M.; Crouch, N. P.; Pereira, I. A. C.; Aplin, R. T.; Robinson, C. *J. Chem. Soc., Chem. Commun.* **1993**, 105.
(236) Baldwin, J. E.; Adlington, R. M.; Schofield, C. J.; Sobey, W. J.; Wood, M. E. *J. Chem. Soc., Chem. Commun.* **1989**, 1012.
(237) Lloyd, M. D.; Merritt, K. D.; Lee, V.; Sewell, T. J.; Wha-Son, B.; Baldwin, J. E.; Schofield, C. J.; Elson, S. W.; Baggaley, K. H.; Nicholson, N. H. *Tetrahedron* **1999**, *55*, 10201.
(238) Kikuchi, Y.; Susuki, Y.; Tamiya, N. *Biochem. J.* **1983**, *213*, 507.
(239) Holme, E.; Lindstedt, G.; Lindstedt, S.; Tofft, M. *J. Biol. Chem.* **1971**, *246*, 3314.
(240) Wu, M.; Begley, T. P.; Myllyharju, J.; Kivirikko, K. I. *Bioorg. Chem.* **2000**, *28*, 261.
(241) McNeill, L. A.; Hewitson, K. S.; Gleadle, J. M.; Horsfall, L. E.; Oldham, N. J.; Maxwell, P. H.; Pugh, C. W.; Ratcliffe, P. J.; Schofield, C. J. *Bioorg. Med. Chem. Lett.* **2002**, *12*, 1547.
(242) Hewitson, K. S.; McNeill, L. A.; Riordan, M. V.; Tian, Y.-M.; Bullock, A. N.; Welford, R. W.; Elkins, J. M.; Oldham, N. J.; Bhattacharya, S.; Gleadle, J. M.; Ratcliffe, P. J.; Pugh, C. W.; Schofield, C. J. *J. Biol. Chem.* **2002**, *277*, 26351.
(243) Groves, J. T.; Han, Y.-Z. In *Cytochrome P450: Structure, Mechanism, and Biochemistry*, 2nd ed.; Ortiz de Montellano, P. R., Ed.; Plenum Press: New York, 1995; pp 3−48.
(244) Poulos, T. L.; Finzel, B. C.; Howard, A. J. *J. Mol. Biol.* **1987**, *195*, 687.
(245) Iwata-Reuyl, D.; Basak, A.; Townsend, C. A. *J. Am. Chem. Soc.* **1999**, *121*, 11356.
(246) Ziering, D. L.; Pascal, R. A., Jr. *J. Am. Chem. Soc.* **1990**, *112*, 834.
(247) Baldwin, J. E.; Adlington, R. M.; Crouch, N. P.; Keeping, J. W.; Leppard, S. W.; Pitlik, J.; Schofield, C. J.; Sobey, W. J.; Wood, M. E. *J. Chem. Soc., Chem. Commun.* **1991**, 768.
(248) Wu, M.; Moon, H.-S.; Begley, T. P. *J. Am. Chem. Soc.* **1999**, *121*, 587.
(249) De Carolis, E.; De Luca, V. *J. Biol. Chem.* **1993**, *268*, 5504.
(250) Lee, H.-J.; Lloyd, M. D.; Harlos, K.; Clifton, I. J.; Baldwin, J. E.; Schofield, C. J. *J. Mol. Biol.* **2001**, *308*, 937.
(251) Ryle, M. J.; Liu, A.; Muthukumaran, R. B.; Ho, R. Y. N.; Koehntop, K. D.; McCracken, J.; Que, L., Jr.; Hausinger, R. P. *Biochemistry* **2003**, *42*, 1854.
(252) Ryle, M. J.; Koehntop, K. D.; Liu, A.; Que, L., Jr.; Hausinger, R. P. *Proc. Natl. Acad. Sci. U.S.A.* **2003**, *100*, 3790.
(253) Hikichi, S.; Ogihara, T.; Fujisawa, K.; Kitajima, N.; Akita, M.; Moro-Oka, Y. *Inorg. Chem.* **1997**, *36*, 4539.
(254) Ha, E. H.; Ho, R. Y. N.; Kosiel, J. F.; Valentine, J. S. *Inorg. Chem.* **1995**, *34*, 2265.
(255) Liu, A.; Ho, R. Y. N.; Que, L., Jr.; Ryle, M. J.; Phinney, B. S.; Hausinger, R. P. *J. Am. Chem. Soc.* **2001**, *123*, 5126.
(256) Bradley, F. C.; Lindstedt, S.; Lipscomb, J. D.; Que, L., Jr.; Roe, A. L.; Rundgren, M. *J. Biol. Chem.* **1986**, *261*, 11693.

(257) Schenk, W. A. *Angew. Chem., Int. Ed.* **2000**, *39*, 3409.
(258) Roach, P. L.; Clifton, I. J.; Fülöp, V.; Harlos, K.; Barton, G. J.; Hajdu, J.; Andersson, I.; Schofield, C. J.; Baldwin, J. E. *Nature* **1995**, *375*, 700.
(259) Roach, P. L.; Clifton, I. J.; Hensgens, C. M. H.; Shibata, N.; Long, A. J.; Strange, R. W.; Hasnain, S. S.; Schofield, C. J.; Baldwin, J. E.; Hajdu, J. *Eur. J. Biochem.* **1996**, *242*, 736.
(260) Randall, C. R.; Zang, Y.; True, A. E.; Que, L., Jr.; Charnock, J. M.; Garner, C. D.; Fujishima, Y.; Schofield, C. J.; Baldwin, J. E. *Biochemistry* **1993**, *32*, 6664.
(261) Orville, A. M.; Chen, V. J.; Kriauciunas, A.; Harpel, M. R.; Fox, B. G.; Münck, E.; Lipscomb, J. D. *Biochemistry* **1992**, *31*, 4602.
(262) Roach, P. L.; Clifton, I. J.; Hensgens, C. M. H.; Shibata, N.; Schofield, C. J.; Hajdu, J.; Baldwin, J. E. *Nature* **1997**, *387*, 827.
(263) Baldwin, J. E.; Bradley, M. *Chem. Rev.* **1990**, *90*, 1079.
(264) Burzlaff, N. I.; Rutledge, P. J.; Clifton, I. J.; Hensgens, C. M. H.; Pickford, M.; Adlington, R. M.; Roach, P. L.; Baldwin, J. E. *Nature* **1999**, *401*, 721.
(265) Ogle, J. M.; Clifton, I. J.; Rutledge, P. J.; Elkins, J. M.; Burzlaff, N. I.; Adlington, R. M.; Roach, P. L.; Baldwin, J. E. *Chem. Biol.* **2001**, *8*, 1231.
(266) Baldwin, J. E.; Adlington, R. M.; Bradley, M.; Pitt, A. R.; Turner, N. J. *J. Chem. Soc., Chem. Commun.* **1989**, 978.
(267) Baldwin, J. E.; Adlington, R. M.; Domayne-Hayman, B. P.; Knight, G.; Ting, H.-H. *J. Chem. Soc., Chem. Commun.* **1987**, 1661.
(268) Wirstam, M.; Siegbahn, P. E. M. *J. Am. Chem. Soc.* **2000**, *122*, 8539.
(269) John, P. *Physiol. Plantarum* **1997**, *100*, 583.
(270) Pirrung, M. C. *Acc. Chem. Res.* **1999**, *32*, 711.
(271) Adams, D. O.; Yang, S. F. *Proc. Natl. Acad. Sci. U.S.A.* **1979**, *76*, 170.
(272) Yang, S. F.; Hoffman, N. E. *Annu. Rev. Plant Physiol.* **1984**, *35*, 155.
(273) McGarvey, D. J.; Christoffersen, R. E. *J. Biol. Chem.* **1992**, *267*, 5964.
(274) Zhang, Z.; Schofield, C. J.; Baldwin, J. E.; Thomas, P.; John, P. *Biochem. J.* **1995**, *307*, 77.
(275) Borovok, I.; Landman, O.; Kreisberg-Zakarin, R.; Aharonowitz, Y.; Cohen, G. *Biochemistry* **1996**, *35*, 1981.
(276) Tan, D. S. H.; Sim, T.-S. *J. Biol. Chem.* **1996**, *271*, 889.
(277) McRae, D. G.; Coker, J. A.; Legge, R. L.; Thomson, J. E. *Plant Physiol.* **1983**, *1983*, 784.
(278) Barlow, J. N.; Zhang, Z.; John, P.; Baldwin, J. E.; Schofield, C. J. *Biochemistry* **1997**, *36*, 3563.
(279) Zhang, Z.; Barlow, J. N.; Baldwin, J. E.; Schofield, C. J. *Biochemistry* **1997**, *36*, 15999.
(280) McRae, D. G.; Baker, J. E.; Thompson, J. E. *Plant Cell Physiol.* **1982**, *23*, 375.
(281) Pirrung, M. C.; Cao, J.; Chen, J. *Chem. Biol.* **1998**, *5*, 49.
(282) Brunhuber, N. M. W.; Mort, J. L.; Christoffersen, R. E.; Reich, N. O. *Biochemistry* **2000**, *39*, 10730.
(283) Thrower, J. S.; Blalock, R., III; Klinman, J. P. *Biochemistry* **2001**, *40*, 9717.
(284) Zhou, J.; Rocklin, A. M.; Lipscomb, J. D.; Que, L., Jr.; Solomon, E. I. *J. Am. Chem. Soc.* **2002**, *124*, 4602.
(285) Rocklin, A. M.; Kato, K.; Liu, H.-w.; Que, L., Jr.; Lipscomb, J. D. *J. Biol. Inorg. Chem.* **2004**, *9*, in press (DOI: 10.1007/s00775-003-0510-3).
(286) Rocklin, A. M.; Tierney, D. L.; Kofman, V.; Brunhuber, N. M. W.; Hoffman, B. M.; Christofferson, R. E.; Reich, N. O.; Lipscomb, J. D.; Que, L., Jr. *Proc. Natl. Acad. Sci. U.S.A.* **1999**, *96*, 7905.
(287) Kappock, T. J.; Caradonna, J. P. *Chem. Rev.* **1996**, *96*, 2659.
(288) Flatmark, T.; Stevens, R. C. *Chem. Rev.* **1999**, *99*, 2137.
(289) Fitzpatrick, P. F. *Annu. Rev. Biochem.* **1999**, *68*, 355.
(290) Klinman, J. P. *J. Biol. Inorg. Chem.* **2001**, *6*, 1.
(291) Kappock, T. J.; Harkins, P. C.; Friedenberg, S.; Caradonna, J. P. *J. Biol. Chem.* **1995**, *270*, 30532.
(292) Miranda, F. F.; Teigen, K.; Thórólfsson, M.; Svebak, R. M.; Knappskog, P. M.; Flatmark, T.; Martínez, A. *J. Biol. Chem.* **2002**, *277*, 40937.
(293) Moran, G. R.; Daubner, S. C.; Fitzpatrick, P. F. *J. Biol. Chem.* **1998**, *273*, 12259.
(294) Chen, D.; Frey, P. A. *J. Biol. Chem.* **1998**, *273*, 25594.
(295) Volner, A.; Zoidakis, J.; Abu-Omar, M. M. *J. Biol. Inorg. Chem.* **2003**, *8*, 121.
(296) Shiman, R.; Gray, D. W.; Hill, M. A. *J. Biol. Chem.* **1994**, *269*, 24637.
(297) Fitzpatrick, P. F. *Biochemistry* **1991**, *30*, 3658.
(298) Erlandsen, H.; Fusetti, F.; Martinez, A.; Hough, E.; Flatmark, T.; Stevens, R. C. *Nat. Struct. Biol.* **1997**, *4*, 995.
(299) Goodwill, K. E.; Sabatier, C.; Stevens, R. C. *Biochemistry* **1998**, *37*, 13437.
(300) Andersen, O. A.; Flatmark, T.; Hough, E. *J. Mol. Biol.* **2001**, *314*, 266.
(301) Andersen, O. A.; Flatmark, T.; Hough, E. *J. Mol. Biol.* **2002**, *320*, 1095.
(302) Andersen, O. A.; Stokka, A. J.; Flatmark, T.; Hough, E. *J. Mol. Biol.* **2003**, *333*, 747.
(303) Dix, T. A.; Bollag, G. E.; Domanico, P. L.; Benkovic, S. J. *Biochemistry* **1985**, *24*, 2955.
(304) McKinney, J.; Teigen, K.; Frøystein, N. Å.; Salaün, C.; Knappskog, P. M.; Haavik, J.; Martínez, A. *Biochemistry* **2001**, *40*, 15591.
(305) Maass, A.; Scholz, J.; Moser, A. *Eur. J. Biochem.* **2003**, *270*, 1065.
(306) Daubner, S. C.; Fitzpatrick, P. F. *Biochemistry* **1999**, *38*, 4448.
(307) Loeb, K. E.; Westre, T. E.; Kappock, J. J.; Mitié, N.; Glasfeld, E.; Caradonna, J. P.; Hedman, B.; Hodgson, K. O.; Solomon, E. I. *J. Am. Chem. Soc.* **1997**, *119*, 1901.
(308) Kemsley, J. N.; Mitic, N.; Zaleski, K. L.; Caradonna, J. P.; Solomon, E. I. *J. Am. Chem. Soc.* **1999**, *121*, 1528.
(309) Davis, M. D.; Kaufman, S. *J. Biol. Chem.* **1989**, *264*, 8585.
(310) Daly, J. W.; Levitt, M.; Guroff, G.; Udenfriend, S. *Arch. Biochem. Biophys.* **1968**, *126*, 593.
(311) Siegmund, H. U.; Kaufman, S. *J. Biol. Chem.* **1991**, *266*, 2903.
(312) Sono, M.; Roach, M. P.; Coulter, E. D.; Dawson, J. H. *Chem. Rev.* **1996**, *96*, 2841.
(313) Francisco, W. A.; Tian, G.; Fitzpatrick, P. F.; Klinman, J. P. *J. Am. Chem. Soc.* **1998**, *120*, 4057.
(314) Bassan, A.; Blomberg, M. R. A.; Siegbahn, P. E. M. *Chem. Eur. J.* **2003**, *9*, 106.
(315) Massey, V. *J. Biol. Chem.* **1994**, *269*, 22459.
(316) Kemsley, J. N.; Wasinger, E. C.; Datta, S.; Mitic, N.; Acharya, T.; Hedman, B.; Caradonna, J. P.; Hodgson, K. O.; Solomon, E. I. *J. Am. Chem. Soc.* **2003**, *125*, 5677.
(317) Lehnert, N.; Fujisawa, K.; Solomon, E. I. *Inorg. Chem.* **2003**, *42*, 469.
(318) Bassan, A.; Blomberg, M. R. A.; Siegbahn, P. E. M. *Chem. Eur. J.* **2003**, *9*, 4055.
(319) Hillas, P. J.; Fitzpatrick, P. F. *Biochemistry* **1996**, *35*, 6969.
(320) Fitzpatrick, P. F. *Biochemistry* **1991**, *30*, 6386.
(321) Moran, G. R.; Derecskei-Kovacs, A.; Hillas, P. J.; Fitzpatrick, P. F. *J. Am. Chem. Soc.* **2000**, *122*, 4535.
(322) Guroff, G.; Daly, J. W.; Jerina, D. M.; Renson, J.; Witkop, B.; Udenfriend, S. *Science* **1967**, *157*, 1524.
(323) Fitzpatrick, P. F. *J. Am. Chem. Soc.* **1994**, *116*, 1133.
(324) Merz, J. H.; Waters, W. A. *J. Chem. Soc.* **1949**, 2427.
(325) Lindsay Smith, J. R.; Norman, R. O. C. *J. Chem. Soc.* **1963**, 2897.
(326) Walling, C. J., R. A. *J. Am. Chem. Soc.* **1975**, *97*, 363.
(327) Kurata, T.; Watanabe, Y.; Katoh, M.; Sawaki, Y. *J. Am. Chem. Soc.* **1988**, *110*, 7472.
(328) Udenfriend, S.; Clark, C. T.; Axelrod, J.; Brodie, B. B. *J. Biol. Chem.* **1954**, *208*, 731.
(329) Sawyer, D. T.; Sobkowiak, A.; Matsushita, T. *Acc. Chem. Res.* **1996**, *29*, 409.
(330) Hage, J. P.; Sawyer, D. T. *J. Am. Chem. Soc.* **1995**, *117*, 5617.
(331) Kitajima, N.; Ito, M.; Fukui, H.; Moro-oka, Y. *J. Am. Chem. Soc.* **1993**, *115*, 9335.
(332) Ménage, S.; Galey, J.-B.; Hussler, G.; Seité, M.; Fontecave, M. *Angew. Chem., Int. Ed. Engl.* **1996**, *35*, 2353.
(333) Ménage, S.; Galey, J.-B.; Dumats, J.; Hussler, G.; Seité, M.; Luneau, I. G.; Chottard, G.; Fontecave, M. *J. Am. Chem. Soc.* **1998**, *120*, 13370.
(334) Mekmouche, Y.; Ménage, S.; Toia-Duboc, C.; Fontecave, M.; Galey, J.-B.; Lebrun, C.; Pecaut, J. *Angew. Chem., Int. Ed.* **2001**, *40*, 949.
(335) Lange, S. J.; Miyake, H.; Que, L., Jr. *J. Am. Chem. Soc.* **1999**, *121*, 6330.
(336) Jensen, M. P.; Lange, S. J.; Mehn, M. P.; Que, E. L.; Que, L., Jr. *J. Am. Chem. Soc.* **2003**, *125*, 2113.
(337) Arends, I. W. C. E.; Ingold, K. U.; Wayner, D. D. M. *J. Am. Chem. Soc.* **1995**, *117*, 4710.
(338) Ingold, K. U.; MacFaul, P. A. In *Biomimetic Oxidations Catalyzed by Transition Metal Complexes*; Meunier, B., Ed.; Imperial College Press: London, 2000; pp 45−89.
(339) Jensen, M. P.; Mehn, M. P.; Que, L., Jr. *Angew. Chem., Int. Ed.* **2003**, *42*, 4357.
(340) MacFaul, P. A.; Ingold, K. U.; Wayner, D. D. M.; Que, L., Jr. *J. Am. Chem. Soc.* **1997**, *119*, 10594.
(341) Foster, T. L.; Caradonna, J. P. *J. Am. Chem. Soc.* **2003**, *125*, 3678.
(342) Zang, Y.; Kim, J.; Dong, Y.; Wilkinson, E. C.; Appelman, E. H.; Que, L., Jr. *J. Am. Chem. Soc.* **1997**, *119*, 4197.
(343) Gibson, D. T.; Parales, R. E. *Curr. Opin. Biotechnol.* **2000**, *11*, 236.
(344) Lau, P. C. K.; De Lozenzo, V. *Environ. Sci. Biotechnol.* **1999**, 124A.
(345) Timmins, K. N.; Pieper, D. H. *Trends Biotechnol.* **1999**, *17*, 201.
(346) Ensley, B. D.; Ratzkin, B. J.; Osslund, T. D.; Simon, M. J.; Wackett, L. P.; Gibson, D. T. *Science* **1983**, *222*, 167.
(347) Boyd, D. R.; Sheldrake, G. N. *Nat. Prod. Rep.* **1998**, *15*, 309.
(348) Hudlicky, T.; Tian, X.; Königsberger, K.; Maurya, R.; Rouden, J.; Fan, B. *J. Am. Chem. Soc.* **1996**, *118*, 10752.
(349) Hudlicky, T.; Gonzalez, D.; Gibson, D. T. *Aldrichimica Acta* **1999**, *32*, 35.
(350) Resnick, S. M.; Gibson, D. T. *J. Indust. Microbiol.* **1996**, *17*, 438.
(351) Lee, K.; Gibson, D. T. *J. Bacteriol.* **1996**, *289*, 3353.

(352) Lange, C. C.; Wackett, L. P. *J. Bacteriol.* **1997**, *179*, 3858.
(353) Gibson, D. T.; Resnick, S. M.; Lee, K.; Brand, J. M.; Torok, D. S.; Wackett, L. P.; Schocken, M. J.; Haigler, B. E. *J. Bacteriol.* **1995**, *177*, 2615.
(354) Carredano, E.; Karlsson, A.; Kauppi, B.; Choudhury, D.; Parales, R. E.; Parales, J. V.; Lee, K.; Gibson, D. T.; Eklund, H.; Ramaswamy, S. *J. Mol. Biol.* **2000**, *296*, 701.
(355) Karlsson, A.; Parales, J. V.; Parales, R. E.; Gibson, D. T.; Eklund, H.; Ramaswamy, S. *Science* **2003**, *299*, 1039.
(356) Cline, J. F.; Hoffman, B. M.; Mims, W. B.; LaHaie, E.; Ballou, D. P.; Fee, J. A. *J. Biol. Chem.* **1985**, *260*, 3251.
(357) Gurbiel, R. J.; Batie, C. J.; Sivaraja, M.; True, A. E.; Fee, J. A.; Hoffman, B. M.; Ballou, D. P. *Biochemistry* **1989**, *28*, 4861
(358) Tsang, H. T.; Batie, C. J.; Ballou, D. P.; Penner-Hahn, J. E. *Biochemistry* **1989**, *28*, 7233.
(359) Kuila, D.; Schoonover, J. R.; Dyer, R. B.; Batie, C. J.; Ballou, D. P.; Fee, J. A.; Woodruff, W. H. *Biochim. Biophys. Acta* **1992**, *1140*, 175.
(360) Pavel, E. G.; Martins, L. J.; Ellis, W. R., Jr.; Solomon, E. I. *Chem. Biol.* **1994**, *1*, 173.
(361) Wolfe, M. D.; Parales, J. V.; Gibson, D. T.; Lipscomb, J. D. *J. Biol. Chem.* **2001**, *276*, 1945.
(362) Yang, T.-C.; Wolfe, M. D.; Neibergall, M. B.; Mekmouche, Y.; Lipscomb, J. D.; Hoffman, B. M. *J. Am. Chem. Soc.* **2003**, *125*, 2034.
(363) Yang, T. C.; Wolfe, M. D.; Neibergall, M. B.; Mekmouche, Y.; Lipscomb, J. D.; Hoffman, B. M. *J. Am. Chem. Soc.* **2003**, *125*, 7056.
(364) Roelfes, G.; Vrajmisu, V.; Chen, K.; Ho, R. Y. N.; Rohde, J.-U.; Zondervan, C.; la Crois, R. M.; Schudde, E. P.; Lutz, M.; Spek, A. L.; Hage, R.; Feringa, B. L.; Münck, E.; Que, L., Jr. *Inorg. Chem.* **2003**, *42*, 2639.
(365) Chishiro, T.; Shimazaki, Y.; Tani, F.; Tachi, Y.; Naruta, Y.; Karasawa, S.; Hayami, S.; Maeda, Y. *Angew. Chem., Int. Ed.* **2003**, *42*, 2788.
(366) Batie, C. J.; LaHai, E.; Ballou, D. P. *J. Biol. Chem.* **1987**, *262*, 1510.
(367) Ballou, D.; Batie, C. *Prog. Clin. Biol. Res.* **1988**, *274*, 211.
(368) Wolfe, M. D.; Altier, D. J.; Stubna, A.; Popescu, C. V.; Münck, E.; Lipscomb, J. D. *Biochemistry* **2002**, *41*, 9611.
(369) Lee, K. *J. Bacteriol.* **1999**, *181*, 2719.
(370) Wolfe, M. D.; Lipscomb, J. D. *J. Biol. Chem.* **2003**, *278*, 829.
(371) Neese, F.; Solomon, E. I. *J. Am. Chem. Soc.* **1998**, *120*, 12829.
(372) Ho, R. Y. N.; Roelfes, G.; Hermant, R.; Hage, R.; Feringa, B. L.; Que, L., Jr. *Chem. Commun.* **1999**, 2161.
(373) Roelfes, G.; Lubben, M.; Hage, R.; Que, L., Jr.; Feringa, B. L. *Chem. Eur. J.* **2000**, *6*, 2152.
(374) Schröder, M. *Chem. Rev.* **1980**, *80*, 187.
(375) Shing, T. K. M.; Tam, E. K. W.; Tai, V. W.-F.; Chung, I. H. F.; Jiang, Q. *Chem. Eur. J.* **1996**, *2*, 50.
(376) Lee, D. G.; Chen, T. *J. Am. Chem. Soc.* **1989**, *111*, 7534
(377) Wackett, L. P.; Kwart, L. D.; Gibson, D. T. *Biochemistry* **1988**, *27*, 1360.
(378) Chen, K.; Que, L., Jr. *Angew. Chem., Int. Ed.* **1999**, *38*, 2227.
(379) Ryu, J. Y.; Kim, J.; Costas, M.; Chen, K.; Nam, W.; Que, L., Jr. *Chem. Commun.* **2002**, 1288.
(380) Fujita, M.; Costas, M.; Que, J., L. *J. Am. Chem. Soc.* **2003**, *125*, 9912.
(381) Costas, M.; Tipton, A. K.; Chen, K.; Jo, D.-H.; Que, L., Jr. *J. Am. Chem. Soc.* **2001**, *123*, 6722.
(382) Kim, C.; Chen, K.; Kim, J.; Que, L., Jr. *J. Am. Chem. Soc.* **1997**, *119*, 5964.
(383) Ho, R. Y. N.; Roelfes, G.; Feringa, B. L.; Que, L., Jr. *J. Am. Chem. Soc.* **1999**, *121*, 264.
(384) Roelfes, G.; Lubben, M.; Chen, K.; Ho, R. Y. N.; Meetsma, A.; Genseberger, S.; Hermant, R. M.; Hage, R.; Mandal, S. K.; Young, V. G., Jr.; Zang, Y.; Kooijman, H.; Spek, A. L.; Que, L., Jr.; Feringa, B. L. *Inorg. Chem.* **1999**, *38*, 1929.
(385) Bassan, A.; Blomberg, M. R. A.; Siegbahn, P. E. M.; Que, L., Jr. *J. Am. Chem. Soc.* **2002**, *124*, 11056.
(386) Wertz, D. L.; Valentine, J. S. *Struct. Bonding* **2000**, *97*, 38.
(387) Wada, A.; Ogo, S.; Nagatomo, S.; Kitagawa, T.; Watanabe, Y.; Jitsukawa, K.; Masuda, H. *Inorg. Chem.* **2002**, *41*, 616.
(388) Chen, K.; Que, L., Jr. *J. Am. Chem. Soc.* **2001**, *123*, 6327.
(389) Barton, D. H. R.; Doller, D. *Acc. Chem. Res.* **1992**, *25*, 504.
(390) Barton, D. H. R.; Hu, B.; Taylor, D. K.; Wahl, R. U. R. *J. Chem. Soc., Perkin Trans.* **1996**, 1031.
(391) Barton, D. H. R. *Chem. Soc. Rev.* **1996**, *25*, 237.
(392) Barton, D. H. R. *Tetrahedron* **1998**, *54*, 5805.
(393) Sawyer, D. T. *Coord. Chem. Rev.* **1997**, *165*, 297.
(394) Vincent, J. B.; Huffman, J. C.; Christou, G.; Li, Q.; Nanny, M. A.; Henrickson, D. N.; Fong, R. H.; Fish, R. H. *J. Am. Chem. Soc.* **1988**, *110*, 6898.
(395) Fish, R. H.; Oberhausen, K. J.; Chen, S.; Richardson, J. F.; Pierce, W.; Buchanan, R. M. *Catal. Lett.* **1993**, *18*, 357.
(396) Rabion, A.; Buchanan, R. M.; Seris, J.-L.; Fish, R. H. *J. Mol. Catal. A: Chemical* **1997**, *116*, 43.
(397) Neimann, K.; Neumann, R.; Rabion, A.; Buchanan, R. M.; Fish, R. H. *Inorg. Chem.* **1999**, *38*, 3575.
(398) Leising, R. A.; Norman, R. E.; Que, L., Jr. *Inorg. Chem.* **1990**, *29*, 2553.
(399) Leising, R. A.; Kim, J.; Pérez, M. A.; Que, L., Jr. *J. Am. Chem. Soc.* **1993**, *115*, 9524.
(400) Ménage, S.; Vincent, J.-M.; Lambeaux, C.; Chottard, G.; Grand, A.; Fontecave, M. *Inorg. Chem.* **1993**, *32*, 4766.
(401) Ménage, S.; Vincent, J.-M.; Lambeaux, C.; Fontecave, M. *J. Mol. Catal. A: Chem.* **1996**, *113*, 61.
(402) Kim, J.; Harrison, R. G.; Kim, C.; Que, L., Jr. *J. Am. Chem. Soc.* **1996**, *118*, 4373.
(403) Nguyen, C.; Guajardo, R. J.; Mascharak, P. K. *Inorg. Chem.* **1996**, *35*, 6273.
(404) Ménage, S.; Wilkinson, E. C.; Que, L., Jr.; Fontecave, M. *Angew. Chem., Int. Ed. Engl.* **1995**, *34*, 203.
(405) Kim, J.; Larka, E.; Wilkinson, E. C.; Que, L., Jr. *Angew. Chem., Int. Ed. Engl.* **1995**, *34*, 2048.
(406) MacFaul, P. A.; Arends, I. W. C. E.; Ingold, K. I.; Wayner, D. D. M. *J. Chem. Soc., Perkin Trans. 2* **1997**, 135.
(407) Costas, M.; Chen, K.; Que, L., Jr. *Coord. Chem. Rev.* **2000**, *200−202*, 517.
(408) Kulikova, V. S.; Gritsenko, O. N.; Shteinman, A. A. *Mendeleev Commun.* **1996**, 119.
(409) Duboc-Toia, C.; Ménage, S.; Lambeaux, C.; Fontecave, M. *Tetrahedron Lett.* **1997**, *38*, 3727.
(410) Chen, K.; Que, L., Jr. *Chem. Commun.* **1999**, 1375.
(411) Duboc-Toia, C.; Ménage, S.; Ho, R. Y. N.; Que, L., Jr.; Lambeaux, C.; Fontecave, M. *Inorg. Chem.* **1999**, *38*, 1261.
(412) Mekmouche, Y.; Duboc-Toia, C.; Ménage, S.; Lambeaux, C.; Fontecave, M. *J. Mol. Catal. A: Chem.* **2000**, *156*, 85.
(413) Hummel, H.; Mekmouche, Y.; Duboc-Toia, C.; Ho, R. Y. N.; Que, L., Jr.; Schünemann, V.; Thomas, F.; Trautwein, A.; Lebrun, C.; Fontecave, M.; Ménage, S. *Angew. Chem., Int. Ed.* **2002**, *41*, 617.
(414) Mekmouche, Y.; Hummel, H.; Ho, R. Y. N.; Que, L., Jr.; Schünemann, V.; Thomas, F.; Trautwein, A. X.; Lebrun, C.; Gorgy, K.; Leprêtre, J.-C.; Collomb, M.-N.; Deronzier, A.; Fontecave, M.; Ménage, S. *Chem. Eur. J.* **2002**, *8*, 1196.
(415) Kodera, M.; Taniike, Y.; Itoh, M.; Tanahashi, Y.; Shimakoshi, H.; Kano, K.; Hirota, S.; Iijima, S.; Ohba, M.; Okawa, H. *Inorg. Chem.* **2001**, *40*, 4821.
(416) Kodera, M.; Shimakoshi, H.; Nishimura, M.; Okawa, H.; Iijima, S.; Kano, K. *Inorg. Chem.* **1996**, *35*, 4967.
(417) Dubois, G.; Murphy, A.; Stack, T. D. P. *Org. Lett.* **2003**, *5*, 2469.
(418) White, M. C.; Doyle, A. G.; Jacobsen, E. N. *J. Am. Chem. Soc.* **2001**, *123*, 7194.
(419) Sam, J. W.; Tang, X.-J.; Peisach, J. *J. Am. Chem. Soc.* **1994**, *116*, 5250.
(420) Stubbe, J.; Kozarich, J. W. *Chem. Rev.* **1987**, *87*, 1107.
(421) Burger, R. M. *Struct. Bonding* **2000**, *97*, 287.
(422) Neese, F.; Zaleski, J. M.; Zaleski, K. L.; Solomon, E. I. *J. Am. Chem. Soc.* **2000**, *122*, 11703.
(423) Sugiyama, M.; Kumagai, T.; Hayashida, M.; Maruyama, M.; Matoba, Y. *J. Biol. Chem.* **2002**, *277*, 2311.
(424) Wu, W.; Vanderwall, D. E.; Turner, C. J.; Kozarich, J. W.; Stubbe, J. *J. Am. Chem. Soc.* **1996**, *118*, 1281.
(425) Wu, W.; Vanderwall, D. E.; Lui, S. M.; Tang, X.-J.; Turner, C. J.; Kozarich, J. W.; Stubbe, J. *J. Am. Chem. Soc.* **1996**, *118*, 1268.
(426) Lui, S. M.; Vanderwall, D. E.; Wu, W.; Tang, X.-J.; Turner, C. J.; Kozarch, J. W.; Stubbe, J. *J. Am. Chem. Soc.* **1997**, *119*, 9603.
(427) Loeb, K. E.; Zaleski, J. M.; Westre, T. E.; Guajardo, R. J.; Mascharak, P. K.; Hedman, B.; Hodgson, K. O.; Solomon, E. I. *J. Am. Chem. Soc.* **1995**, *117*, 4545.
(428) Loeb, K. E.; Zaleski, J. M.; Hess, C. D.; Hecht, S. M.; Solomon, E. I. *J. Am. Chem. Soc.* **1998**, *120*, 1249.
(429) Burger, R. M.; Kent, T. A.; Horwitz, S. B.; Münck, E.; Peisach, J. *J. Biol. Chem.* **1983**, *258*, 1559.
(430) Westre, T. E.; Loeb, K. E.; Zaleski, J. M.; Hedman, B.; Hodgson, K. O.; Solomon, E. I. *J. Am. Chem. Soc.* **1995**, *117*, 1309.
(431) Lehnert, N.; Neese, F.; Ho, R. Y. N.; Que, L., Jr.; Solomon, E. I. *J. Am. Chem. Soc.* **2002**, *124*, 10810.
(432) Guajardo, R. J.; Hudson, S. E.; Brown, S. J.; Mascharak, P. K. *J. Am. Chem. Soc.* **1993**, *115*, 7971.
(433) Guajardo, R. J.; Chavez, F.; Farinas, E. T.; Mascharak, P. K. *J. Am. Chem. Soc.* **1995**, *117*, 3883.
(434) Rowland, J. M.; Olmstead, M. M.; Mascharak, P. K. *Inorg. Chem.* **2001**, *40*, 2810.
(435) Girerd, J.-J.; Banse, F.; Simaan, A. J. *Struct. Bonding* **2000**, *97*, 143.
(436) Lubben, M.; Meetsma, A.; Wilkinson, E. C.; Feringa, B.; Que, L., Jr. *Angew. Chem., Int. Ed. Engl.* **1995**, *34*, 1512.
(437) Bernal, I.; Jensen, I. M.; Jensen, K. B.; McKenzie, C. J.; Toftlund, H.; Tuchagues, J. P. *J. Chem. Soc., Dalton Trans.* **1995**, 3667.
(438) Sobolev, A. P.; Babushkin, D. E.; Talsi, E. P. *Mendeleev Commun.* **1996**, 33.
(439) Simaan, A. J.; Banse, F.; Mialane, P.; Boussac, A.; Un, S.; Kargar-Grisel, T.; Bouchoux, G.; Girerd, J.-J. *Eur. J. Inorg. Chem.* **1999**, 993.
(440) Simaan, A. J.; Döpner, S.; Banse, F.; Bourcier, S.; Bouchoux, G.; Boussac, A.; Hildebrandt, P.; Girerd, J.-J. *Eur. J. Inorg. Chem.* **2000**, 1627.

(441) Simaan, A. J.; Banse, F.; Girerd, J.-J.; Wieghardt, K.; Bill, E. *Inorg. Chem.* **2001**, *40*, 6538.
(442) Hazell, A.; McKenzie, C. J.; Nielsen, L. P.; Schindler, S.; Weitzer, M. *J. Chem. Soc., Dalton Trans.* **2002**, 310.
(443) Jensen, K. B.; McKenzie, C. J.; Pedersen, J. Z. *Inorg. Chem.* **2001**, *40*, 5066.
(444) Horner, O.; Jeandey, C.; Oddou, J.-L.; Bonville, P.; McKenzie, C. J.; Latour, J.-M. *Eur. J. Inorg. Chem.* **2002**, 3278.
(445) Shearer, J.; Scarrow, R. C.; Kovacs, J. A. *J. Am. Chem. Soc.* **2002**, *124*, 11709.
(446) Balland, V.; Banse, F.; Anxolabéhère-Mallart, E.; Nierlich, M.; Girerd, J.-J. *Eur. J. Inorg. Chem.* **2003**, 2529.
(447) Balland, V.; Banse, F.; Anxolabéhère-Mallart, E.; Ghiladi, M.; Mattioli, T. A.; Philouze, C.; Blondin, G.; Girerd, J.-J. *Inorg. Chem.* **2003**, *42*, 2470.
(448) Lehnert, N.; Ho, R. Y. N.; Que, L., Jr.; Solomon, E. I. *J. Am. Chem. Soc.* **2001**, *123*, 8271.
(449) Brunold, T. C.; Tamura, N.; Kitajima, M.; Moro-oka, Y.; Solomon, E. I. *J. Am. Chem. Soc.* **1998**, *120*, 5674.
(450) Hashimoto, K.; Nagatomo, S.; Fujiinami, S.; Furutachi, H.; Ogo, S.; Suzuki, M.; Uehara, A.; Maeda, Y.; Watanabe, Y.; Kitagawa, T. *Angew. Chem., Int. Ed.* **2002**, *41*, 1202.
(451) Shiemke, A. J.; Loehr, T. M.; Sanders-Loehr, J. *J. Am. Chem. Soc.* **1984**, *106*, 4951.
(452) Okamura, M. Y.; Klotz, I. M.; Johnson, C. E.; Winter, M. R. C.; Williams, R. J. P. *Biochemistry* **1969**, *8*, 1951.
(453) Mizoguchi, T. J.; Kuzelka, J.; Spingler, B.; DuBois, J. L.; Davydov, R. M.; Hedman, B.; Hodgson, K. O.; Lippard, S. J. *Inorg. Chem.* **2001**, *40*, 4662.
(454) Kim, K.; Lippard, S. J. *J. Am. Chem. Soc.* **1996**, *118*, 4914.
(455) Ménage, S.; Brennan, B. A.; Juarez-Garcia, C.; Münck, E.; Que, L., Jr. *J. Am. Chem. Soc.* **1990**, *112*, 6423.
(456) Dong, Y.; Zang, Y.; Shu, L.; Wilkinson, E. C.; Que, L., Jr.; Kauffmann, K.; Münck, E. *J. Am. Chem. Soc.* **1997**, *119*, 12683.
(457) MacMurdo, V. L.; Zheng, H.; Que, L., Jr. *Inorg. Chem.* **2000**, *39*, 2254.
(458) Dong, Y.; Ménage, S.; Brennan, B. A.; Elgren, T. E.; Jang, H. G.; Pearce, L. L.; Que, L., Jr. *J. Am. Chem. Soc.* **1993**, *115*, 1851.
(459) Ookubo, T.; Sugimoto, H.; Nagayama, T.; Masuda, H.; Sato, T.; Tanaka, K.; Maeda, Y.; Okawa, H.; Hayashi, Y.; Uehara, A.; Suzuki, M. *J. Am. Chem. Soc.* **1996**, *118*, 701.
(460) Burstyn, J. N.; Roe, J. A.; Miksztal, A. R.; Shaevitz, B. A.; Lang, G.; Valentine, J. S. *J. Am. Chem. Soc.* **1988**, *110*, 1382.
(461) Horner, O.; Jeandey, C.; Oddou, J.-L.; Bonville, P.; Latour, J.-M. *Eur. J. Inorg. Chem.* **2002**, 1186.
(462) Jensen, K. B.; McKenzie, C. J.; Nielsen, L. P.; Pedersen, J. Z.; Svendsen, H. M. *Chem. Commun.* **1999**, 1313.
(463) Harris, D. L.; Loew, G. H. *J. Am. Chem. Soc.* **1998**, *120*, 8941.
(464) VanAtta, R. B.; Strouse, C. E.; Hanson, L. K.; Valentine, J. S. *J. Am. Chem. Soc.* **1987**, *109*, 1425.
(465) Dong, Y.; Yan, S.; Young, V. G., Jr.; Que, L., Jr. *Angew. Chem., Int. Ed. Engl.* **1996**, *35*, 618.
(466) Bukowski, M. R.; Zhu, S.; Brennessel, W. W.; Koehntop, K. D.; Que, L., Jr. *J. Biol. Inorg. Chem.* **2004**, *9*, 39.
(467) Tyeklár, Z.; Jacobson, R. R.; Wei, N.; Murthy, N. N.; Zubieta, J.; Karlin, K. D. *J. Am. Chem. Soc.* **1993**, *115*, 2677.
(468) Kojima, T.; Leising, R. A.; Yan, S.; Que, L., Jr. *J. Am. Chem. Soc.* **1993**, *115*, 11328.
(469) Miyake, H.; Chen, K.; Lange, S. J.; Que, L., Jr. *Inorg. Chem.* **2001**, *40*, 3534.
(470) Murugesan, N.; Hecht, S. M. *J. Am. Chem. Soc.* **1985**, *107*, 493.
(471) Absalon, M. J.; Wu, W.; Kozarich, J. W.; Stubbe, J. *J. Am. Chem. Soc.* **1995**, *34*, 2076.
(472) Wallar, B. J.; Lipscomb, J. D. *Chem. Rev.* **1996**, *96*, 2625.
(473) Collins, T. J.; Kostka, K. L.; Münck, E.; Uffelman, E. S. *J. Am. Chem. Soc.* **1990**, *112*, 5637.
(474) Kostka, K. L.; Fox, B. G.; Hendrich, M. P.; Collins, T. J.; Richard, C. E. F.; Wright, L. J.; Münck, E. *J. Am. Chem. Soc.* **1993**, *115*, 6746.
(475) Collins, T. J. *Acc. Chem. Res.* **1994**, *27*, 279.
(476) Cummins, C. C.; Schrock, R. R. *Inorg. Chem.* **1994**, *33*, 395.
(477) MacBeth, C. E.; Golombek, A. P.; Young, V. G., Jr.; Yang, C.; Kuczera, K.; Hendrich, M. P.; Borovik, A. S. *Science* **2000**, *289*, 938.
(478) MacBeth, C. E.; Hammes, B. S.; Young, V. G., Jr.; Borovik, A. S. *Inorg. Chem.* **2001**, *40*, 4733.
(479) Gupta, R.; Borovik, A. S. *J. Am. Chem. Soc.* **2003**, *125*, 13234.
(480) Jüstel, T.; Weyhermüller, T.; Wieghardt, K.; Bill, E.; Lengen, M.; Trautwein, A. X.; Hildebrandt, P. *Angew. Chem., Int. Ed. Engl.* **1995**, *34*, 669.
(481) Jüstel, T.; Michael Müller; Weyhermüller, T.; Kressl, C.; Bill, E.; Hildebrandt, P.; Lengen, M.; Grodzicki, M.; Trautwein, A. X.; Nuber, B.; Wieghardt, K. *Chem. Eur. J.* **1999**, *5*, 793.
(482) Meyer, K.; Bill, E.; Mienert, B.; Weyhermüller, T.; Wieghardt, K. *J. Am. Chem. Soc.* **1999**, *121*, 4859.
(483) Grapperhaus, C. A.; Mienert, B.; Bill, E.; Weyhermüller, T.; Wieghardt, K. *Inorg. Chem.* **2000**, *39*, 5306.
(484) Dutta, S. K.; Beckmann, U.; Bill, E.; Weyhermüller, T.; Wieghardt, K. *Inorg. Chem.* **2000**, *39*, 3355.
(485) Dong, Y.; Fujii, H.; Hendrich, M. P.; Leising, R. A.; Pan, G.; Randall, C. R.; Wilkinson, E. C.; Zang, Y.; Que, L., Jr.; Fox, B. G.; Kauffmann, K.; Münck, E. *J. Am. Chem. Soc.* **1995**, *117*, 2778.
(486) Dong, Y.; Que, L., Jr.; Kauffmann, K.; Münck, E. *J. Am. Chem. Soc.* **1995**, *117*, 11377.
(487) Que, L., Jr.; Dong, Y. *Acc. Chem. Res.* **1996**, *29*, 190.
(488) Zheng, H.; Yoo, S. J.; Münck, E.; Que, L., Jr. *J. Am. Chem. Soc.* **2000**, *122*, 3789.
(489) Hsu, H.-F.; Dong, Y.; Shu, L.; Young, V. G., Jr.; Que, L., Jr. *J. Am. Chem. Soc.* **1999**, *121*, 5230.
(490) Lee, D.; Pierce, B.; Krebs, C.; Hendrich, M. P.; Huynh, B. H.; Lippard, S. J. *J. Am. Chem. Soc.* **2002**, *124*, 3993.
(491) Slep, L. D.; Mijovilovich, A.; Meyer-Klaucke, W.; Weyhermüller, T.; Bill, E.; Bothe, E.; Neese, F.; Wieghardt, K. *J. Am. Chem. Soc.* **2003**, *125*, 15554.
(492) Rohde, J.-U.; In, J. H.; Lim, M. H.; Brennessel, W. W.; Bukowski, M. R.; Stubna, A.; Münck, E.; Nam, W.; Que, L., Jr. *Science* **2003**, *299*, 1037.
(493) Penner-Hahn, J. E.; Eble, K. S.; McMurry, T. J.; Renner, M.; Balch, A. L.; Groves, J. T.; Dawson, J. H.; Hodgson, K. O. *J. Am. Chem. Soc.* **1986**, *108*, 7819.
(494) Chance, M.; Powers, L.; Kumar, C.; Chance, B. *Biochemistry* **1986**, *25*, 1266.
(495) Wolter, T.; Meyer-Klaucke, W.; Müther, M.; Mandon, D.; Winkler, H.; Trautwein, A. X.; Weiss, R. *J. Inorg. Biochem.* **2000**, *78*, 117.
(496) Kitagawa, T.; Mizutani, Y. *Coord. Chem. Rev.* **1994**, *135/136*, 685.
(497) Lim, M. H.; Rohde, J.-U.; Stubna, A.; Bukowski, M. R.; Costas, M.; Ho, R. Y. N.; Münck, E.; Nam, W.; Que, L., Jr. *Proc. Natl. Acad. Sci. U.S.A.* **2003**, *100*, 3665.
(498) Kaizer, J.; Costas, M.; Que, L., Jr. *Angew. Chem., Int. Ed.* **2003**, *42*, 3671.
(499) Costas, M.; Kaizer, J.; Jensen, M. P.; Rohde, J.-U.; Stubna, A.; Münck, E.; Que, L., Jr. *J. Am. Chem. Soc.* **2004**, submitted.
(500) Kaizer, J.; Klinker, E. J.; Oh, N. Y.; Rohde, J.-U.; Song, W. J.; Stubna, A.; Kim, J.; Münck, E.; Nam, W.; Que, L., Jr. *J. Am. Chem. Soc.* **2004**, *126*, 472.
(501) Balland, V.; Charlot, M.-F.; Banse, F.; Girerd, J.-J.; Mattioli, T. A.; Bill, E.; Bartoli, J.-F.; Battioni, P.; Mansuy, D. *Eur. J. Inorg. Chem.* **2004**, 301.
(502) Decker, A.; Rohde, J.-U.; Que, L., Jr.; Solomon, E. I., *J. Am. Chem. Soc.*, submitted.
(503) Costas, M.; Rohde, J.-U.; Stubna, A.; Ho, R. Y. N.; Quaroni, L.; Münck, E.; Que, L., Jr. *J. Am. Chem. Soc.* **2001**, *123*, 12931.
(504) Debrunner, P. G. In *Iron Porphyrins*; Lever, B., Gray, H. B., Eds.; VCH: New York, 1989; Vol. III, pp 137−234.
(505) Schulz, C. E.; Rutter, R.; Sage, J. T.; Debrunner, P. G.; Hager, L. P. *Biochemistry* **1984**, *23*, 4743.
(506) Sturgeon, B. E.; Burdi, D.; Chen, S.; Huynh, B.-H.; Edmondson, D. E.; Stubbe, J.; Hoffman, B. M. *J. Am. Chem. Soc.* **1996**, *118*, 7551.
(507) Liu, K. E.; Valentine, A. M.; Wang, D.; Huynh, B. H.; Edmondson, D. E.; Salifoglou, A.; Lippard, S. J. *J. Am. Chem. Soc.* **1995**, *117*, 10174.
(508) Valentine, A. M.; Tavares, P.; Pereira, A. S.; Davydov, R.; Krebs, C.; Hoffman, B. M.; Edmondson, E. E.; Huynh, B. H.; Lippard, S. J. *J. Am. Chem. Soc.* **1998**, *120*, 2190.
(509) Lee, S.-K.; Fox, B. G.; Froland, W. A.; Lipscomb, J. D.; Münck, E. *J. Am. Chem. Soc.* **1993**, *115*, 6450.
(510) Roe, A. L.; Schneider, D. J.; Mayer, R.; Pyrz, J. W.; Widom, J.; Que, L., Jr. *J. Am. Chem. Soc.* **1984**, *106*, 1676.
(511) Randall, C. R.; Shu, L.; Chiou, Y.-M.; Hagen, K. S.; Ito, M.; Kitajima, N.; Lachicotte, R. J.; Zang, Y.; Que, L., Jr. *Inorg. Chem.* **1995**, *34*, 1036.
(512) Westre, T. E.; Kennepohl, P.; DeWitt, J. G.; Hedman, B.; Hodgson, K. O.; Solomon, E. I. *J. Am. Chem. Soc.* **1997**, *119*, 6297.
(513) Nam, W.; Choi, S. K.; Lim, M. H.; Rohde, J.-U.; Kim, I.; Kim, J.; Kim, C.; Que, L., Jr. *Angew. Chem., Int. Ed.* **2003**, *42*, 109.
(514) Skulan, A. J.; Hanson, M. A.; Hsu, H.-f.; Que, L., Jr.; Solomon, E. I. *J. Am. Chem. Soc.* **2003**, *125*, 7344.
(515) Skulan, A. J.; Hanson, M. A.; Hsu, H.-f.; Dong, Y.; Que, L., Jr.; Solomon, E. I. *Inorg. Chem.* **2003**, *42*, 6489.
(516) Shu, L.; Nesheim, J. C.; Kauffmann, K.; Münck, E.; Lipscomb, J. D.; Que, L., Jr. *Science* **1997**, *275*, 515.
(517) Davidson, E. R., Ed. *Chem. Rev.* **2000**, *100*, 351.

CR020628N